Aus dem Biomedizinischen Centrum der Ludwig-Maximilians-Universität München
und dem Institut für Biochemie der FAU Erlangen-Nürnberg

Dissertation
zum Erwerb des Doctor of Philosophy (Ph.D.) an der
Medizinischen Fakultät der
Ludwig-Maximilians-Universität zu München

Molecular dissection of pericyte-to-neuron reprogramming reveals cellular identity safeguarding mechanisms

vorgelegt von:

Benjamin Albert Lohrer

aus:

Vilshofen, Deutschland

Jahr:

2022

Mit Genehmigung der Medizinischen Fakultät der
Ludwig-Maximilians-Universität zu München

First evaluator:	Prof. Dr. rer. nat. Marisa Karow
Second evaluator:	Prof. Dr. rer. nat. Moritz Rossner
Third evaluator:	Prof. Dr. med. Jochen Herms
Fourth evaluator:	Prof. Dr. rer. nat. Magdalena Götz
Dean:	Prof. Dr. med. Thomas Gudermann
Date of oral defense:	November 28th 2022

TABLE OF CONTENTS

ABSTRACT

Neurodegenerative diseases, strokes, and injuries affect millions of people worldwide and current treatment options are insufficient. Since death of neurons in the brain is a common feature of all these disorders, a potential therapy could replace the lost neurons by newly generated ones to restore brain function. Natural adult neurogenesis in humans has been proven inadequate to deal with a major loss of brain cells. Therefore, for many years, transplantation of fetal tissue or stem cell-derived neural progenitors have been the focus of investigations regarding new treatments. More recently, new methods and insights have rendered brain-resident cells a promising means of an alternative therapeutic approach. While cellular identity was believed to be irreversible once differentiated for a long time, this view has changed gradually over the last decades. Among other cells, it has been shown for human brain pericytes that retroviral expression of the transcription factors (TFs) Ascl1 and Sox2 (AS) is sufficient to generate functional induced neurons (iNs) by direct reprogramming, and that this process is accompanied by a neural stem cell (NSC)-like state.

While it is clear now that even a terminal cellular identity can be changed, the exact mechanisms remain elusive. Therefore, in this study we aimed at (i) identifying barriers and molecular mechanisms involved in cellular identity conversion from somatic cells into induced neurons, (ii) improving the efficiency of pericyte-to-neuron reprogramming, and (iii) directing the reprogramming process towards the desired cell types.

By single cell RNA sequencing, we generated a high-resolution dataset of cells during pericyte-to-iN conversion. Using RNA velocity analysis, we were able to predict the progression of cells towards the neuronal fate and could identify blocker and facilitator genes that obstruct or enable cells to pass past a designated decision point. Among the facilitator genes, we identified several chromatin remodelers and cytoskeleton genes, and revealed a temporal heterogeneity regarding their expression pattern. Interestingly, we show that the blocker genes are part of a cellular identity safeguarding mechanism triggered by AS reprogramming. We demonstrate that the metabolic transition from glycolysis to oxidative phosphorylation is an essential barrier cells must overcome to

transit from a pericyte towards a neuronal identity. Our findings suggest that any failure to meet metabolic requirements results in cells being either unable to change their identity or adopting a confused fate.

To impact on the NSC-like state, we used either modulation of NOTCH signaling or TGF-β signaling by inhibition of the γ-secretase or dual SMAD inhibition, respectively, via small molecules. Strikingly, both treatments counteracted pericyte identity safeguarding mechanisms and significantly lowered reprogramming barriers. Consequently, our results show a strong increase in the number of generated iNs. Interestingly, we demonstrate that TGF-β signaling inhibition is more potent in lowering these metabolic barriers than NOTCH signaling inhibition, re-routing cells onto an entirely different route towards neurons. Additionally, TGF-β signaling inhibition almost completely suppresses the generation of undesired off-target cells without a clear identity, likely due to antioxidant regulon activity, which supports the metabolic transition.

Remarkably, we illustrate that despite different treatments, iNs are transcriptionally similar and that both neuronal subtypes can be mapped to developing human brain regions. Finally, we used a different approach and reprogrammed pericytes into TUBB3+ cells using Neurog2/Sox2 (NS). We show that NS generated cells have a distinct transcriptomic identity from AS generated ones: While they are more likely to lose their original identity, the NS-generated iNs exhibit more progenitor-like properties, pointing at the different reprogramming capacities of proneural TFs.

Altogether, this thesis emphasizes not only that cellular identity even in terminally differentiated cells can still be altered without returning to a pluripotent state. It further illustrates several previously unknown mechanisms during direct pericyte-to-iN reprogramming and opens new ways to improve its efficiency. Every new insight into cross-lineage cellular identity conversion paves the way for future neuronal replacement therapies.

1 Introduction

1.1 Brain diseases and injuries require cellular restoration

Neurological disorders are the world's largest cause of disability (G. B. D. Neurological Disorders Collaborator Group, 2017). Among others, the Global Burden of Diseases, Injuries, and Risk Factors Study (GBD) 2016 on neurological disorders counted more than 13 million new incidents of strokes and more than 27 million traumatic brain injuries worldwide per year, it also lists more than 49 million patients globally that are currently affected by neurodegenerative diseases (43 million patients with Alzheimer's disease (AD) and other dementias, more than 6 million patients with Parkinson's disease (PD), more than 300,000 patients with motor neuron diseases) (G. B. D. Neurology Collaborators, 2019). Although these neurological disorders are vastly different in their causes, their course of progression, and their lethality rate, they have one thing in common: They all involve the death of neurons in the human brain.

For decades, this has been widely thought to be an irreversible process. It was believed that brain repair, if at all, happens mainly via postmitotic mechanisms, like synaptic reorganization, axon terminal sprouting and modulation of neurotransmitter-receptor expression (Lie et al., 2004). Already in the 1960s, however, evidence was found that neurons are being newly generated in the brains of adult mammals (Altman, 1962). Later, adult neurogenesis has also been found in humans, even though only in very restricted areas like the hippocampus (Eriksson et al., 1998; Spalding et al., 2013), striatum (Ernst et al., 2014), subventricular zone (SVZ) and a rostral migratory stream (RMS)-like pathway in the adult human brain (Curtis et al., 2007; Wang et al., 2011). These findings have been questioned later regarding their methodology (Paredes et al., 2018) and other studies were not able to find evidence for existence of neurogenesis in the adult human brain (Sorrells et al., 2018). While this is the subject of an ongoing scientific debate, it seems reasonable to believe that the neurogenesis rates and sites of cell generation would not be sufficient to replace lost neurons after strokes, injuries, and neurodegenerative diseases in a way to restitute lost brain functions.

1.2 Brain repair strategies

When the adult human brain itself is largely unable to regenerate lost neurons, this calls for the development of human brain repair strategies. One therapeutic approach focuses on supporting the extracellular environment with trophic or anti-inflammatory factors, since both acute injuries and chronic neurodegenerative diseases present with inflammatory reactions which include changes in the blood-brain barrier and extracellular matrix in the affected brain regions (Barker et al., 2018). It has been shown in a mouse model of AD that antibodies to extracellular matrix components are able to restore memory function by blocking axon growth inhibitors (Yang et al., 2017). While animal models of neurodegenerative diseases treated with different trophic factors have shown significant improvements, this effect could not be shown in clinical trials so far (Bartus & Johnson, 2017a, 2017b). As soon as a certain number of neurons are lost, however, the effect of trophic or anti-inflammatory factors is inadequate to restore brain function. Instead, only neuronal replacement could help these patients. There are two different approaches for cell replacement in the adult brain: Transplantation of exogenous cells or recruitment of new neurons from endogenous neurogenic niches (Barker et al., 2018).

Transplantation of cells to lesioned sites represents a promising approach especially for those conditions where cell death is restricted to clearly delineated regions of the brain and/or cell types. Both is the case in PD, where a majority of the motor symptoms are caused by progressing cell death of midbrain dopaminergic neurons in the substantia nigra (Kalia & Lang, 2015). Already in the 1970's, researchers have shown that motor abnormalities in PD model rats could be significantly reduced after grafting fetal substantia nigra tissue (Perlow et al., 1979). Importantly, it has been indicated that already a small number of transplanted cells is sufficient to restore basic functions (Björklund Lars et al., 2002). Many clinical studies since then have used developing midbrain dopaminergic cells from human fetal tissue, of which some have shown significant improvement for patients, while others could not restore normal brain function and were even associated with major side effects (Barker et al., 2013; Barker et al., 2015). One major issue with transplanted fetal tissue is that the cell populations are very heterogeneous and unwanted neuronal subtypes might be transplanted, causing side effects (Barker et al., 2018).

More recent advances in stem cell research have enabled the generation of disease-relevant human neural progenitors and neurons patterned towards a certain fate (Steinbeck & Studer, 2015), reducing side effects caused by non-homogenous cell populations. Transplanted human embryonic stem cell (hESC) or human induced pluripotent stem cell (hiPSC)-derived ventral midbrain dopaminergic neurons were shown to survive, expand and function in both a rat and a primate model of PD, reversing motor deficits (Kikuchi et al., 2017; Kirkeby et al., 2012). Clinical trials to investigate transplantation of hESC-derived midbrain dopaminergic neuronal progenitors in human patients are forthcoming (Piao et al., 2021). However, even in initially successful treatments, transplanted cells can get affected by PD themselves (Kurowska et al., 2011; Li et al., 2008), which could be overcome by genetic modifications to the donor cells before transplantation (Barker et al., 2018). Stem cell based therapies are also being investigated in the treatment of strokes (Wei et al., 2017). Transplantation or intravenous injection of human mesenchymal stem cells for stroke patients improved some functional measures and showed no major side effects (Bang et al., 2005; Honmou et al., 2011), but other trials could not find any beneficial effects of the treatment on functional restoration (Prasad et al., 2014).

Since stem cell based therapies are often associated with side effects like immune reactions, rejection of the transplanted cells, and tumor formation (Wei et al., 2017), other therapeutic approaches are coming into focus, which do not rely on stem cells.

1.3 Changing cellular identities

As pointed out earlier, adult neurogenesis has been found in the human brain (Frisén, 2016). Therefore, using active neurogenic areas in the adult brain to produce new neurons for neighboring brain regions seems to be an obvious approach (Barker et al., 2018). However, most of the neurons generated endogenously in animal models upon induced brain injury (Arvidsson et al., 2002; Nakatomi et al., 2002) do not have the correct subtype identity needed for repair (Barker et al., 2018). Waddington proposed that a cell's identity from the beginning of embryogenesis on is like a marble rolling down a hill, passing several bifurcations where it can go either one way or the other, just like a cell coming from pluripotency that gets primed towards a certain germ layer, becomes a

specialized progenitor and finally a mature differentiated cell (Waddington, 1957) (**Figure 1**). In Waddington's model, this was a unidirectional process. However, over the last decades, it has turned out that cellular identities can actually be forcibly changed.

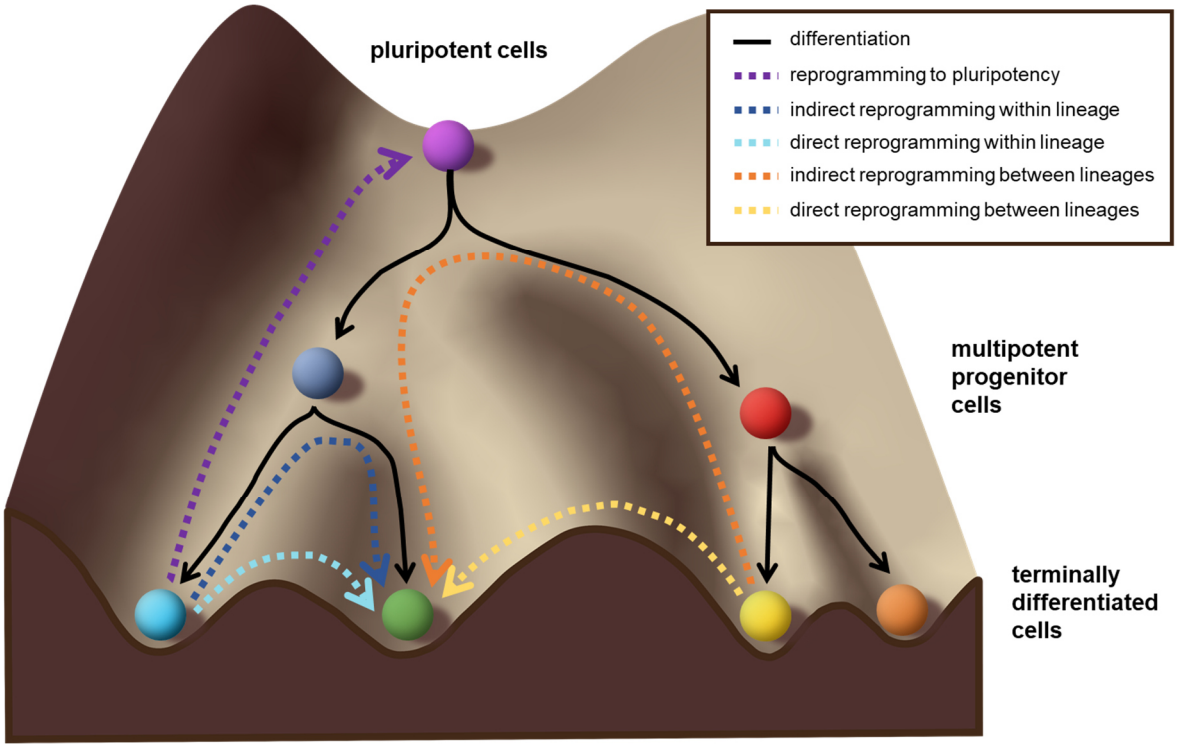

Figure 1 | Waddington's landscape model and cellular identity changes. Cellular identities were long believed to behave like a marble rolling down a hill: It starts from a pluripotent state (symbolized by the marble on top of the hill that still has the possibility to end up in any of the valleys at the bottom). During the differentiation process already small modulations in gene regulatory networks can change the cellular lineage (symbolized by bifurcations, where already small forces to the left or right puh the marble towards a different route). At every bifurcation, the number of potential outcomes is getting more and more restricted, it is impossible for the cell to return to an earlier state (and for the marble to roll back up the hill). Nowadays it is known that cellular identities are much more plastic: Even if cells are fully differentiated (like the marbles in the valleys at the bottom of the hill), their identity can still be changed. It has been shown that by modulating their gene regulatory networks by forced expression of transcription factors, cells can be reprogrammed back to pluripotency (Takahashi et al., 2007; Takahashi & Yamanaka, 2006), or can be, directly (without a progenitor state, e.g. from hepatocytes to neuronal cells (Marro et al., 2011) or from astrocytes into neurons (Heinrich et al., 2010)) or indirectly (including a progenitor state, e.g. from fibroblasts into hepatocytes (Xie et al., 2019) or from astrocytes into different neural cell types (Corti et al., 2012)), converted into various differentiated cell types, outside of or within the original lineage of the starting cell. Adapted from Waddington (1957).

Already in the 1950's, it was shown that the epigenomic identity of differentiated nuclei can be reprogrammed back to pluripotency (Briggs & King, 1952). A striking breakthrough followed in the 1990's with the successful generation of mammal offspring from a differentiated cell after nuclear transfer to an enucleated unfertilized egg (Wilmut

et al., 1997). These findings indicated that some factors that maintain the identity of ES cells might also be able to regain pluripotency in differentiated cells. Based on this idea, only a few years later, it was shown that also adult mouse cells can be reprogrammed back to pluripotency by forced expression of the transcription factors Oct3/4, Sox2, c-Myc, and Klf4 (Takahashi & Yamanaka, 2006). Takahashi and Yamanaka (2006) called these cells induced pluripotent stem cells (iPSCs) and, shortly later, were able to generate human iPSCs from adult human dermal fibroblast (Takahashi et al., 2007). Their striking discovery has made it possible to generate iPSCs from any genetic background, laying the foundation for custom-tailored therapies with stem cells derived directly from the patients' own cells.

hESCs had been used to generate neural progenitors and after transplantation into newborn mouse brains these cells differentiated region-specifically into the three lineages astrocytes, oligodendrocytes, and neurons (Reubinoff et al., 2001; Zhang et al., 2001). With the emergence of iPSCs, also these were successfully converted into different neuronal subtypes (Chambers et al., 2009; Sun et al., 2016).

Although iPSCs with the same genome as the patient should make immune reactions and rejection of the cells a thing of the past, the cells still need to be transplanted to the lesion sites. Also, reverting cells to pluripotency before differentiation might increase the risk of tumor formation (Lee et al., 2013). This is a caveat that needs to be considered and that may be avoided by using postmitotic cells as target cells.

1.3.1 Direct lineage reprogramming

A new opportunity rose with the discovery that reversion to pluripotency is not necessary to trans-differentiate cells; within the neural lineage, this was shown already in 2002, when murine postnatal astrocytes were successfully converted into neurons by retroviral expression of Pax6 (Heins et al., 2002). Later, the same group showed that retroviral expression of Neurog2 or Ascl1 (earlier Mash1), both basic helix loop helix (bHLH) transcription factors, is sufficient to generate functional neurons from murine astrocytes (Berninger et al., 2007) and that this reprogramming process can occur in the absence of mitosis (Heinrich et al., 2010).

Only in 2010, it was shown that also terminally differentiated cells of other, non-neural lineages, like murine fibroblasts, could be directly reprogrammed into functional neurons using the three factors Ascl1, Brn2 (Pou3f2) and Myt1l (Vierbuchen et al., 2010). (Vierbuchen et al., 2010) called these cells induced neuronal (iN) cells, which expressed neuronal markers, were able to form synapses and generate action potentials. Shortly later, the same group was able to show that these three factors combined with NeuroD1 can also convert both fetal and postnatal human fibroblasts into functional iN cells (Pang et al., 2011). This discovery for the first time enabled the generation of patient-specific neuronal cells without the need to reprogram cells back to pluripotency and therefore reducing the risk for tumor formation. Shortly later, other groups showed that with different sets of transcription factors, fibroblasts could be reprogrammed into motor neurons (Son et al., 2011), GABAergic neurons (Colasante et al., 2015), serotonergic neurons (Vadodaria et al., 2016) and dopaminergic neurons (Caiazzo et al., 2011), all without undergoing a proliferative progenitor state. By now, many different cell types have been shown to be convertible into functional iNs (Vasan et al., 2021), such as hepatocytes (Marro et al., 2011), cardiomyocytes (Chuang et al., 2017), adipocyte progenitors (Yang et al., 2013), and non-neural cochlear cells (Nishimura et al., 2014). All these results demonstrate that cell identities can be shifted between different lineages. Especially fibroblasts as a starting population are quite easily accessible, however for brain repair strategies a cell type already residing within the brain would be more useful. Besides astrocytes, pericytes have been shown to accumulate particularly at lesion sites in the brain (Göritz et al., 2011; Nivet et al., 2013). Therefore, it was a striking discovery that pericytes can be directly reprogrammed into induced neurons by forced expression of the two transcription factors Ascl1 and Sox2 (Karow et al., 2012). Notably, this cell type derived from the human cortex during surgeries could be cultured *in vitro* (Karow et al., 2012), making it a promising target for further studies on direct reprogramming.

1.3.2 Pericytes

According to Armulik et al. (2011), pericytes have originally been discovered by Eberth (1871), and described shortly later by the French researcher Charles-Marie Benjamin Rouget as “contractile cells surrounding the endothelial cells of small blood

vessels" (Rouget, 1873). The term 'pericyte' is generally ascribed to Zimmermann (1923), after the Greek words for 'surrounding cell'. The exact definition of pericytes is complex. There is no unique molecular marker and no unique location that refers only to pericytes; therefore, identification of pericytes is based on several criteria including marker expression, cell location, and morphology (Armulik et al., 2011). Pericyte morphology is marked by strong primary processes along the endothelial tube, spanning multiple endothelial cells, with thin secondary processes, partially ensheathing the tube (Armulik et al., 2011).

As Armulik et al. (2011) describe in their review, several markers are used to distinguish pericytes from other perivascular cells, all of which are also expressed in other cell types: PDGFRβ (Lindahl et al., 1997; Winkler et al., 2010) as the probably most widely used marker, CD13 (ANPEP) (Dermietzel & Krause, 1991; Kunz et al., 1994), NG2 (Huang et al., 2010; Ozerdem et al., 2001; Ruiter et al., 1993), desmin (Nehls et al., 1992), and αSMA – the latter only in case of inflammation (Nehls & Drenckhahn, 1993). Other proteins like RGS5 (Cho et al., 2003; Mitchell et al., 2008) and CD146 (MCAM) (Li et al., 2003; Middleton et al., 2005) have also been reported as pericyte markers.

Generally, ratios of pericytes to endothelial cells are given as 1:1 for the central nervous system (CNS), while other tissues have lower ratios of 1:10 or 1:100; however, these numbers rely on very few, restricted observations (Shepro & Morel, 1993).

1.3.2.1 Developmental origins of pericytes

For a long time, it was not completely understood where brain pericytes originate from and how they are recruited to the vasculature, and still there are open questions. While pericytes in general where previously believed to be of mesodermal origin (Hungerford & Little, 1999; Rucker et al., 2000), lineage tracing studies have indicated that pericytes of the CNS are mostly neural crest-derived (Simon et al., 2012; Trost et al., 2013). However, newer studies suggest that in early phases of CNS vascular development, macrophage-like cells from the blood adhere to the brain vessels and after cell division transdifferentiate into pericytes, forming a subpopulation of pericytes with hematopoietic origin (Yamamoto et al., 2017).

1.3.2.2 Pericyte functions

With their ability to contract, pericytes are believed to contribute to regional blood flow control in the brain (Fernández-Klett et al., 2010; Peppiatt et al., 2006), even though this has not been shown *in vivo* (Armulik et al., 2011; Attwell et al., 2010). Pericytes further play an important role in the formation of the blood-brain barrier (BBB) during embryogenesis (Daneman et al., 2010) and for BBB stabilization (Armulik et al., 2010; Bell et al., 2010; Daneman et al., 2010). Pericyte loss has been shown to lead to progressive neurodegeneration (Bell et al., 2010). More recent evidence has suggested that pericytes also show immune-regulating properties, such as the expression of and response to inflammatory factors as well as antigen presentation and even phagocytic activity (Jansson et al., 2014; Rustenhoven et al., 2017). Moreover, some observations indicate neural stem and progenitor cell (NSC) properties of adult CNS pericytes from microvessels *in vitro* (Dore-Duffy et al., 2006). In an ischemic/hypoxic environment, pericytes have been shown to acquire stem cell activity and to differentiate into neural, vascular (Nakagomi et al., 2015) and microglial identities (Özen et al., 2014). Pericytes have further been shown to be involved in spinal cord scar formation (Göritz et al., 2011).

1.3.3 Direct pericyte-to-neuron reprogramming

While the cultured cells from human cortices in Karow et al. (2012) expressed the pericyte markers PDGFRB, NG2, SMA, CD146 and CD13, they did not show expression of TUBB3, ASCL1 or SOX2. After retroviral expression of Ascl1, which had been shown earlier to be a major factor in neuronal reprogramming of other cell types like astroglia and fibroblasts (Berninger et al., 2007; Caiazzo et al., 2011; Vierbuchen et al., 2010), some cells started to express TUBB3 as demonstrated immunohistochemically, but without a neuronal morphology and processes (Karow et al., 2012). Only upon additional expression of Sox2, which had been shown to be upregulated during reprogramming earlier (Heinrich et al., 2010) and which alone did not induce TUBB3 expression, a major fraction of cells (28% ± 5% SEM) started to exhibit neuronal morphology in addition to TUBB3 expression (Karow et al., 2012). By live imaging, Karow et al. (2012) further proved that almost all cells converted directly from PDGFRB$^+$ cells to TUBB3$^+$ cells, without any cell division. At

the same time, more than a third of the Ascl1/Sox2-transduced cells underwent cell death, indicating a potential cell fate conflict (Karow et al., 2012).

1.3.4 NSC-like state during direct pericyte-to-neuron reprogramming

In a follow-up study, by using single-cell RNA sequencing, Karow et al. (2018) revealed a heterogeneity in the pericyte starting population that might partially account for the variable competence of pericytes to be reprogrammed by Ascl1 and Sox2. Most notably, it turned out that during the trajectory from pericytes to iNs, even in the absence of cell division, cells adopt an NSC-like state that is marked by transient transcription of several genes known to be expressed in neural stem cells or progenitor cells during forebrain embryonic development, although lacking neural stem cell markers like *MSI1* (Musashi) or *NES* (Nestin) (Karow et al., 2018). This intermediate state is particularly interesting since it was unexpected in a direct conversion process.

1.4 Mechanisms of (forced) neurogenesis

All mentioned reprogramming approaches use a combination of different transcription factors (TFs). This is based on the logic that TFs involved in natural neurogenesis can also initiate a similar cascade of molecular changes in direct reprogramming, leading to an identity change towards the desired cell type.

1.4.1 The proneural genes Ascl1 and Neurog2

It had been shown initially in Drosophila that a small group of bHLH TFs, encoded by the so-called proneural genes, is both required and sufficient for neural lineage initiation from the ectoderm (Bertrand et al., 2002; Jan & Jan, 1994; Jiménez & Modolell, 1993). An evolutionary conserved neurogenic function was also shown for some of their related genes in vertebrates (Bertrand et al., 2002; Guillemot, 1999; Lee, 1997). While some bHLH genes in vertebrates are only necessary for neuronal fate specification or differentiation, others, like *Ascl1* and *Neurog2* have been shown to exert a vital function in

neurogenesis (Bertrand et al., 2002). In the embryonic forebrain, Ascl1 is predominantly expressed in basal ganglia, where GABAergic neurons originate, while Neurog2 expression is found in the cortex, contributing to glutamatergic identity acquisition; this pattern is mostly mutually exclusive (Osório et al., 2010).

Knockout of *Ascl1* causes major defects in neurogenesis, as shown exemplary for the olfactory sensory epithelium and the ventral telencephalon (Casarosa et al., 1999; Cau et al., 2002; Guillemot et al., 1993; Horton et al., 1999). Despite its GABAergic lineage expression during embryogenesis (Osório et al., 2010; Parras et al., 2002), the exact reprogramming outcomes of Ascl1 are highly context dependent and have surprisingly been shown to yield both GABAergic (Berninger et al., 2007) and glutamatergic neurons (Chanda et al., 2014; Vierbuchen et al., 2010).

Neurog2 was shown to be required for the formation of cranial sensory ganglia and for the correct expression of neural progenitor genes as well as other features of neurogenesis (Fode et al., 1998; Scardigli et al., 2001). While the main fate of Neurog2-reprogrammed cells is that of glutamatergic iNs (Berninger et al., 2007; Heinrich et al., 2010; Vierbuchen et al., 2010), there are also studies showing GABAergic iNs after Neurog2-induced cellular conversion (Chouchane et al., 2017; Florio et al., 2012).

In addition to their proneural function, both Ascl1 and Neurog2 serve divergent functions during neuronal subtype specification (Parras et al., 2002). While many TF combinations in direct reprogramming contain Ascl1, this was shown to be replaceable by Neurog2 in some combinations, indicating that a generic transcriptional program exists besides subtype-specific transcriptional networks (Tsunemoto et al., 2018). Within the neural lineage, cells can be reprogrammed to iNs by just either Ascl1 or Neurog2 (Heinrich et al., 2011). The same is true for ESCs and iPSCs (Zhang et al., 2013), whereas differentiated cells are usually converted to iNs in combination with additional TFs (Aydin et al., 2019). However, it has been shown that the initial transcriptional programs of Ascl1 and Neurog2 share only a small subset of target genes (Masserdotti et al., 2015). Aydin et al. (2019) revealed that Ascl1 and Neurog2 bind to different sets of genomic sites in a similar context, resulting in different regulatory landscapes, which affect downstream TFs' activity.

1.4.2 Cellular plasticity and molecular barriers in direct reprogramming

With the discovery of natural *in vivo* reprogramming of originally ectodermal cranial neural crest cells (CNCCs) into mesenchymal cells (Zalc et al., 2021), it was proven that cellular plasticity is not an artificial concept. Cellular identities can be changed, but a cell's original identity may still continue to have an effect on its new identity. Strikingly, even after successful conversion of astrocytes to neurons, regional specificity is maintained to a major extent (Herrero-Navarro et al., 2021). The differentiation into neuronal subtypes further seems to be dependent on the cellular position within the brain (Mattugini et al., 2019). This is surprising, since the cellular environment during direct reprogramming is different from the one during embryonic development, but it is very promising for potential therapeutic approaches that rely on region-specific neuronal cell types. However, the fact that even after forced expression of proneural genes in combination with other TFs, not all cells reprogram, shows that there are additional barriers that need to be overcome for a cell to erase the old identity and acquire a new fate.

1.4.2.1 Chromatin accessibility

Cellular differentiation usually is accompanied by global chromatin reorganization (Bonev et al., 2017). Therefore, one important factor in reprogramming is the chromatin context, in particular at the target sites of the TFs; it needs to be accessible and allow binding of the TFs (Wapinski et al., 2013). Ascl1 is capable of binding to previously closed chromatin sites and is therefore oftentimes considered a pioneer TF (Wapinski et al., 2013). Neurog2 can as well exhibit pioneer factor functions when combined with small molecules (Smith et al., 2016). Most TFs however, are unable to open the chromatin at the target binding sites themselves; epigenetic regulators therefore have a gatekeeping function to chromatin accessibility, preventing binding of TFs that would change the cell lineage (Vasan et al., 2021). Pluripotency factors like Sox2 and Oct4 increase the chromatin accessibility, with Sox2 being the more potent factor (Malik et al., 2019).

1.4.2.2 Safeguarding mechanisms for cellular identity

Chromatin accessibility can be restricted by large repressive protein complexes, like the RE1-silencing transcription factor (REST) complex, that prevents differentiation in neural stem cells (Laugesen & Helin, 2014) and reprogramming in fibroblasts (Drouin-Ouellet et al., 2017). The repressor REST has also been shown to reduce reprogramming efficiency by preventing binding of Neurog2 to the promoter of *NeuroD4*, another proneural gene (Masserdotti et al., 2015). Once a decision is reached within the cell to reprogram to iNs, other safeguarding mechanisms start to act in favor of the new fate. Myt1l was shown to repress many somatic fates, but not the neuronal one (Mall et al., 2017). Interestingly, forced overexpression of Myt1l was sufficient to convert pericytes into cholinergic neurons, while increasing the levels of Ascl1, Brn2, and Neurog2 (Liang et al., 2018).

1.4.2.3 Switch in energy metabolism

All cells need to produce energy to survive. However, energy demands are highly dependent on their cell type. The main metabolic process is glycolysis, which is fast and generates other useful molecules, whereas oxidative phosphorylation (OxPhos), has a much higher efficiency but also produces reactive oxygen species (ROS) as a side product potentially resulting in oxidative stress (Falk et al., 2021). Hypoxia triggers stabilization of the HIF-1α protein, leading to a switch from oxidative to glycolytic metabolism (Candelario et al., 2013). In general, the extent to which cells use one or the other metabolic process is different for each cell type: While cells like fibroblasts (McKay et al., 1983), pericytes (Nwadozi et al., 2020) and glia (Tsacopoulos & Magistretti, 1996) have lower energy demands and use mostly glycolysis, cell types like muscle cells and neurons substantially depend on OxPhos (Falk et al., 2021). Also NSCs still rely mostly on glycolysis (Candelario et al., 2013), which means that during differentiation into neurons the cells' metabolism also needs to change from glycolysis to OxPhos (Maffezzini et al., 2020; Zheng et al., 2016). Therefore, also successful lineage reprogramming of non-neuronal cells into iNs requires a switch of the metabolic program (Gascón et al., 2016; Kim et al., 2018) and this process can be enhanced by HIF-1α inhibition (Herdy et al., 2019). It has been shown that there is a decision point at which cells either successfully convert into their target identity or, if

they don't meet the metabolic requirements to proceed, they return to the starting identity (Biddy et al., 2018), proceed towards an alternative fate (Falk et al., 2021) or undergo cell death (Gascón et al., 2016; Karow et al., 2012). The latter can be vastly reduced by lowering the oxidative stress caused by ROS (reactive oxygen species) (Gascón et al., 2016). Another part of the metabolic transition is the change of mitochondria, which provide energy to the cell – they adapt both their proteome and their morphology (Russo et al., 2021). Expression of antioxidant genes has been shown to improve lineage conversion from astrocytes to iNs (Russo et al., 2021).

1.4.3 Modulation of signaling pathways in direct reprogramming

During development of the nervous system, genes act in a well-organized temporal manner. Several conserved pathways are involved in this differentiation process. In direct reprogramming to iNs, particular gene regulatory networks therefore are of great interest as they might enable modulation of the process.

1.4.3.1 NOTCH signaling

Ascl1 and Neurog2 are both found in NSCs during neurogenesis, where they are expressed in a dynamic manner (Britz et al., 2006; Shimojo et al., 2008). They induce expression of several Notch ligands such as Dll1 (Castro et al., 2006), Dll3 (Henke et al., 2009) and Jag1 (Lindsell et al., 1995) which – at the start of the Notch signaling cascade (**Figure 2**) – in a process termed lateral inhibition bind to the Notch receptors on neighboring cells. Once a ligand binds to a Notch receptor, the Notch intracellular domain (NICD) is cleaved first by the metalloprotease ADAM10 (van Tetering et al., 2009), then by γ-secretase (De Strooper et al., 1999), subsequently translocates to the nucleus and together with the TF RBPJ and mastermind-like proteins (MAML) forms a complex, leading to transcription of downstream genes (Fryer et al., 2002). bHLH TFs are known to be major targets of Notch signaling (Artavanis-Tsakonas et al., 1999). Very prominent target genes are several members of the *Hes* (hairy and enhancer of split) family, such as *Hes1*, *Hes5*, and *Hes7* (Bessho et al., 2001; Jouve et al., 2000; Ohtsuka et al., 1999), as well as all members of the *Hey* (Hairy/enhancer-of-split related with YRPW motif protein) family,

Hey1/*Hey2* (Leimeister et al., 1999), all coding for bHLH TFs. Further target genes are *Ascl1* and *Neurog2* themselves, which generates a feedback loop to proneural gene expression through the repressor function of Hes1 and Hes5 (Kageyama et al., 2020; Kageyama et al., 2007; Kageyama et al., 2008). Thereby, the dynamics of Ascl1/Neurog2 expression are also directly regulated by Notch signaling (Kageyama et al., 2020; Kageyama et al., 2008, 2009). *Hes1* and other Notch targets are silenced by Myt1l, which explains molecular mechanisms of this safeguarding factor (Mall et al., 2017).

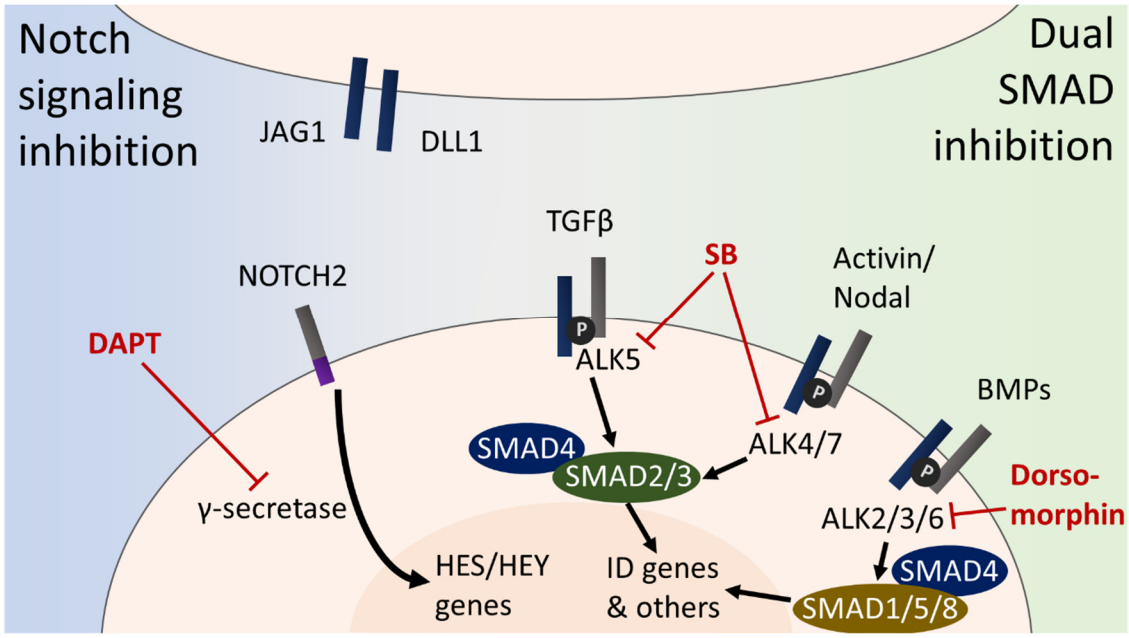

Figure 2 | Inhibition of NOTCH signaling & dual SMAD inhibition (adapted from Karow et al. (2018)). Neurogenesis involves inhibition of two major gene regulatory networks, Notch signaling and TGF-β/BMP signaling. Notch signaling cascade: Ligands like JAG1 and DLL1 bind to NOTCH receptors on other cells' surfaces, NOTCH intracellular domain (NICD) is cleaved and translocates to the nucleus, where it regulates gene expression, mainly of HES/HEY genes. The small molecule DAPT inhibits the γ-secretase, which prevents cleavage of the NICD and thereby all downstream gene regulatory action. TGF-β/BMP signaling cascade: Several ligands of the subfamilies TGF-β, Activin/Nodal or BMP can bind to their respective receptors of the activin receptor-like kinase (ALK) family, thereby enabling phosphorylation and activation of SMAD transcription factors, which form hetero-oligomers with SMAD4 and then regulate gene activity in the nucleus. Dual SMAD inhibition is achieved by the small molecules SB (SB431542) and Dorsomorphin, which inhibit ALK4/5/7 and ALK2/3/6, respectively. Thereby the expression of downstream target genes is modulated.

1.4.3.2 TGF-β/BMP signaling

During embryogenesis, neural induction results mainly from the inhibition of the transforming growth factor-beta (TGF-β)/bone morphogenetic protein (BMP) pathway (**Figure 2**) (Muñoz-Sanjuán & Brivanlou, 2002; Stern, 2006; Weinstein & Hemmati-Brivanlou, 1999). This is an evolutionary very conserved regulatory network within the

animal kingdom (Huminiecki et al., 2009). The pathway starts when ligands bind to receptors on the cell surface, with ligands belonging to either the TGFβ subfamily, the Activin-Nodal subfamily, the large BMP subfamily, or the fourth subfamily of all other, more distant ligands (Mueller & Nickel, 2012). The receptors are complexes of Ser/Thr protein kinases - always two type I components, which propagate the signal, and two type II components, exhibiting an activator role (Massagué, 2012). In humans, there are seven type I receptors: TGFBR1 (activin receptor-like kinase 5; ALK5), which binds only to TGFβ; ACVR1B (ALK4) and ACVR1C (ALK7), which bind to Activin and Nodal; ACVR1 (ALK2), BMPR1A (ALK3) and BMPR1B (ALK6), which bind to BMPs (Luecken et al., 2020; Massagué, 2012; Moustakas & Heldin, 2009; Shi & Massagué, 2003). ACVRL1 (ALK1) mainly binds to BMPs but also to TGFβ, in case of high TGFβ concentrations (Pardali et al., 2010). Additionally, five type II receptors can be found in humans: TGFBR2, which binds only to TGFβ; Activin receptor type 2A (ACVR2A) and ACVR2B, which bind to Activin, Nodal and BMPs; BMPR2, which binds to BMPs; and AMHR2, which binds to Anti-Müllerian hormone (AMH) (Massagué, 2012; Moustakas & Heldin, 2009; Shi & Massagué, 2003). The type I receptors get phosphorylated by the type II receptors and then in turn phosphorylate and thereby activate SMAD proteins (Mueller & Nickel, 2012). While type I receptors triggered by BMPs mainly activate SMAD1, SMAD5 and SMAD8, type I receptors triggered by TGFβ, Activin and Nodal mainly activate SMAD2 and SMAD3 (Massagué, 2012; Mueller & Nickel, 2012). Upon activation, SMAD TFs hetero-oligomerize with SMAD4, then translocate into the nucleus, where they act as transcriptional activators or repressors (Mueller & Nickel, 2012). Whether TGF-β/BMP signaling upregulates or downregulates its target genes, differs depending on the gene and the cellular context (Massagué, 2012). Among the genes regulated by TGF-β/BMP signaling is the inhibitor of differentiation (*Id*) protein family with its four members *Id1*, *Id2*, *Id3*, and *Id4* – all bHLH TFs, which are expressed in dynamic patterns in the developing neuroblasts (Yokota, 2001). Transient induction of *Id1* leads to increased degradation of Ascl1 (Viñals et al., 2004).

1.4.3.3 Modulation of NOTCH and TGF-β/BMP signaling and their effects on pericyte-to-iN reprogramming

Both Notch and TGF-β/BMP signaling can be interfered using small molecules. The Notch pathway is modulated by DAPT (N-[N-(3,5-difluorophenacetyl)-l-alanyl]-S-

phenylglycine t-butyl ester), which inhibits the γ-secretase, preventing the cleavage of Notch and thereby translocation of NICD to the nucleus (Geling et al., 2002). The TGF-β/BMP pathway regulatory network can be modulated by inhibitors of SMAD signaling, e.g. by SB431542 and Noggin, leading to conversion of hES cells to a neuronal fate (Chambers et al., 2009). Also, Dorsomorphin induces rapid and high-efficiency neural conversion in both human ESCs and iPSCs (Zhou et al., 2010). Dual SMAD inhibition of both ALK4/5/7 on the one hand and ALK2/3/6 on the other hand via SB431542 and Dorsomorphin, respectively, was shown to promote neural differentiation from hiPSCs and hESCs (Kim et al., 2010).

To investigate if the direct pericyte-to-iN reprogramming process can be affected by modulation of NOTCH and TGF-β/BMP signaling during the NSC-like state, Karow et al. (2018) used DAPT or dual SMAD inhibition, respectively, and demonstrated that both treatments significantly increased the numbers of TUBB3+ cells. Counteracting on dual SMAD inhibition by NODAL or BMP4 had the opposite effect and decreased the number of iNs (Karow et al., 2018), proofing the importance of this signaling pathway. Additionally, Karow et al. (2018) observed that the BMP inhibitor Dorsomorphin enhanced neuronal maturation, with iNs exhibiting higher morphological complexity and soma size, more mature electrophysiological properties as well as increased expression of genes involved in synapse formation and synaptic function. The molecular mechanisms of these improvements in iN numbers and iN maturation upon NOTCH or TGF-β/BMP signaling modulation, however, have remained elusive so far.

1.5 Aims of this study

Direct lineage reprogramming of human brain pericytes into iNs represents a promising new therapeutic approach to regenerate lost brain cells and, hopefully, function. Therefore, the main goal of this study was to deepen our understanding of this process of forced cellular identity change and to be able to modulate it regarding its efficiency and specificity.

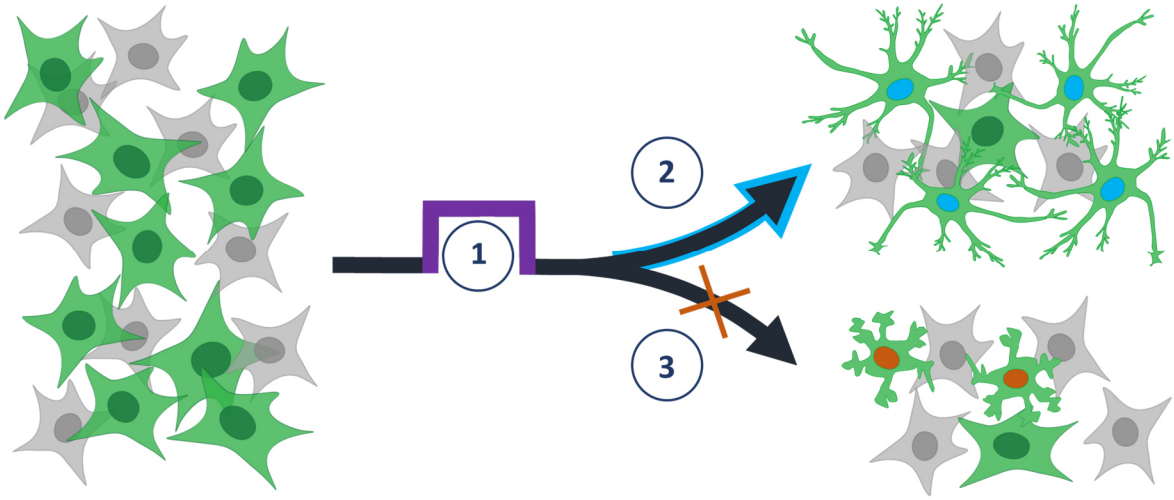

Figure 3 | Aims of this study. (**1**) To identify barriers to cellular identity conversion. (**2**) To improve the efficiency of pericyte-to-neuron reprogramming. (**3**) To direct the reprogramming process towards the desired cell types.

Firstly, as we know that only a minority fraction of pericytes become iNs upon retroviral expression of Ascl1 and Sox2 (Karow et al., 2012), we aimed to identify molecular reprogramming barriers by investigating transcriptomic differences between those cells that are successfully getting reprogrammed and those that fail to do so (**Figure 3**).

Secondly, having identified reprogramming hurdles, this would enable us to purposefully modulate the signaling pathways during the NSC-like state to improve reprogramming efficiency (**Figure 3**). As Karow et al. (2018) have shown that different neuronal subtypes can be generated with direct reprogramming, we will also assess the effect of signaling modulation on the reprogramming outcome.

Finally, as Karow et al. (2018) have revealed that AS reprogramming generates both iNs and off-target populations, we intended to steer cell fate towards our desired cell types during the reprogramming process (**Figure 3**).

2 Material and Methods

2.1 Primary human pericytes

Human primary pericytes were obtained from cerebral cortex tissue donated by adult patients of different ages, male and female, who had to undergo surgical interventions due to non-traumatic, non-malignant brain lesions. The specimens were taken from healthy tissue in the access channel introduced by surgeons to reach the target region. Patients had given their written informed consent and the ethical committee of the Medical Faculty of the LMU Munich had approved the usage of patients' tissue in this study (Karow et al., 2018; Karow et al., 2012). The human brain pericyte culture used in this study is termed AHG54 and was obtained from the healthy surgery channel tissue from the cortex of a 26-year-old female undergoing cavernoma resection.

2.1.1 Generation of primary human pericyte cultures

Pericyte cultures were derived from brain tissue specimen according to the protocol described in previous studies of the laboratory (Karow et al., 2014). In short, the freshly obtained specimens were kept on ice in Hanks' balanced salt solution with $CaCl_2$ and $MgCl_2$ (HBSS) medium including HEPES (10 mM final concentration) during transportation. First, under sterile conditions in a laminar flow hood, the tissue was dissociated mechanically using a scalpel and then digested enzymatically using 3-6 ml TrypLE (Thermo Fisher) at 37 °C for 15-30 min. Next, one volume of prewarmed growth medium (DMEM high glucose with GlutaMAX, 20% heat-inactivated fetal calf serum (FCS), 1% penicillin/streptomycin, all Thermo Fisher) was added to stop the trypsin reaction and the suspension was gently triturated using first a 5 ml glass pipette, then a Pasteur pipette until it was homogeneous. The suspension was spun at 1000 rpm for 5 min and the pellet was resuspended in growth medium. The cells were then cultured in uncoated T75 culture flasks (one per 5-10mm specimen) using 10 ml of medium per flask at 37 °C in an incubator with 5% CO_2 and 5% O_2 (Galaxy 170R, New Brunswick).

2.1.2 Passaging and freezing

Half of the medium was changed twice per week and the cells were grown until confluency (1-2 weeks) and then split in a 1:3 ratio. Splitting was performed by adding 2 ml TrypLE (Thermo Fisher) per T75 culture flask at 37 °C for approximately 5 min, then stopping the trypsin reaction by addition of 4 ml prewarmed growth medium per T75 flask. The cell suspension was then triturated with a 5 ml glass pipette and subsequently spun at 1000 rpm for 5 min. The pellet was resuspended in growth medium and replated in new T75 culture flasks. After the first passage, medium was changed completely twice per week and cells were split every 1-2 weeks. After expansion, cells not immediately used in experiments were frozen in freezing medium (90% FCS, Thermo Fisher, 10% DMSO, Sigma-Aldrich).

2.2 Retroviral transduction

For lineage conversion with Ascl1 and Sox2 (AS), a retrovirus expressing pCAG-*Ascl1*-p2A-*Sox2*-IRES-*GFP* was used as described previously (Karow et al., 2018). Briefly, this enabled polycistronic expression of these two transcription factors; they were under control of an internal chicken beta-actin promoter with cytomegalovirus enhancer (CAG), linked via p2A, while a downstream *GFP* was separated by an internal ribosomal entry site (IRES). As a control, pCAG-IRES-*GFP* was used, expressing only GFP downstream of the IRES site (Karow et al., 2012).

Direct reprogramming using Neurog2 and Sox2 (NS) was performed using two separate retroviral constructs that were previously described, pCAG-*Sox2*-IRES-*GFP* (Karow et al., 2012) and pCAG-*Neurog2*-IRES-*DsRed* (Heinrich et al., 2010). The latter was also used as a control to evaluate the effects of Neurog2 in the absence of Sox2 (N only). All fluorescent reporter protein sequences were followed by a Woodchuck Hepatitis Virus (WHV) Posttranscriptional Regulatory Element (WPRE) which enhances transcription.

Primary pericyte cultures were cultured in growth medium on T75 cell culture flasks without additional coating or Poly-D-lysine coated glass coverslips in 24-well cell culture plates. After 24 h, retroviral transductions were performed using the viruses

mentioned above, by adding the virus stored in TBS-5 buffer (5% 1M Tris-HCl pH 7.8, 2.51% 1M NaCl, 1% 1M KCl, 0.5% 1M $MgCl_2$). For T75 flasks, 3 µl virus were added per flask, for 24-well cell culture plates, 0.5 µl virus were added per well. Upon addition, the plates were gently shaken to improve viral distribution. The growth medium was replaced by B27 differentiation medium (DMEM high glucose with GlutaMAX with 2% B27 supplement (Thermo Fisher)) 24 h after transductions to enhance differentiation.

2.3 Small molecule treatments after transduction

Small molecules were added on day 1, 3 and 5 after transduction. As recently described (Karow et al., 2018), the following final concentrations of small molecules were used: 10 µM for DAPT (N-[N-(3,5-Difluorophenacetyl)-L-alanyl]-S-phenylglycine t-butyl ester; StemCell Technologies); 10 µM (Inman et al., 2002; Laping et al., 2002) for SB431542 (StemCell Technologies) and 1 µM (Liu et al., 2013; Yu et al., 2008) for Dorsomorphin (Sigma-Aldrich). All small molecules were dissolved in DMSO. Therefore, as a control, pCAG-Ascl1-p2A-Sox2-IRES-GFP and pCAG-IRES-GFP expressing cultures that did not receive small molecule treatments were instead treated with 1:1000 DMSO on day 1, 3 and 5 after transduction. Cells were then grown at 37 °C in an incubator with 5% CO_2 and 5% O_2 without medium change until further experimental usage.

2.4 Immunocytochemical stainings

For fixation, primary pericytes grown on PDL-coated coverslips in 24-well culture plates were fixed 28 days after transduction by removing the medium and incubating them in 4% paraformaldehyde (PFA) in phosphate buffered saline (PBS) at room temperature for 15 min. They were washed three times with PBS and once with blocking solution (PBS with 0.25% Triton X-100 and 4% donkey serum, both Sigma-Aldrich), then incubated in blocking solution at room temperature for 1h. Subsequently, they were incubated with primary antibodies in antibody solution (PBS with 0.1% Triton X-100 and 4% donkey serum, both Sigma-Aldrich) overnight at 4°C. The antibody dilutions were as follows: chick anti-GFP (Aves; GFP-1020; 1:500), rat anti-RFP (Chromotek; 5F8; 1:500), mouse (IgG2b) anti-TUBB3 (Sigma-Aldrich; T8660; 1:300). They were then washed three times with PBS

and once with blocking solution and incubated with the appropriate fluorophore-coupled secondary antibodies as well as 1 µg/ml DAPI (4′,6-diamidino-2-phenylindole, Thermo Fisher) in antibody solution for 1 h at room temperature. Eventually, coverslips were mounted onto glass slides using Aqua Poly/Mount anti-fading mounting medium (Polysciences, Warrington, PA) and dried at room temperature shed from light.

2.5 Fluorescence imaging

Stained and mounted cells were imaged using an epifluorescence microscope (Axio Observer Z1, Carl Zeiss) or a laser-scanning confocal microscope (LSM710, Carl Zeiss) with appropriate filter sets, using a 25x objective and acquiring 5x5 tile images of each coverslip, saved in czi format using the ZEN software (Carl Zeiss). To assess reprogramming efficiency, TUBB3-positive cells and fluorescent reporter-positive cells in images were then manually counted via the ZEN software or semi-automatically counted using Fiji (Schindelin, 2012) and RStudio.

2.6 Fluorescence-activated cell sorting (FACS)

Primary pericytes from T75 cell culture flasks were sorted via flow cytometry on day 7 or day 14 after transduction for single-cell RNA sequencing. To detach cells from flasks, they were washed with PBS, incubated with 2 ml TrypLE per flask for ~5 min and then resuspended in 4 ml growth medium per flask. After centrifugation at 1000 rpm for 5 min and removal of the supernatant, cells were resuspended in 1.5-3 ml B27 differentiation medium, pooling identically treated cell suspensions. Cells were subsequently kept on ice until being sorted. At the flow cytometer FACSAria III (BD Bioscience), events were identified as cells by first gating them in forward scatter area and sideward scatter area, then gating them in forward scatter width and forward scatter area, excluding events with very low area or very high or low width that were likely cell debris or doublets. Finally, cells were sorted by gating them in the wavelength of their respective expressed fluorescent reporter protein (GFP and/or DsRed), subtracting autofluorescence by comparison to untransduced cells and setting gates accordingly. For each condition, the maximal available number of gated events were sorted (ranging from 40,000 to 693,000

events), and samples kept on ice. After manual recounting using a Neubauer chamber, they were directly used for 10x Genomics scRNA sequencing.

2.7 scRNA-seq library construction and sequencing

For single-cell RNA sequencing (scRNA-seq), the 10x Genomics Chromium Single Cell Kit was used, which enables the generation of a cDNA library with cell-individual barcodes, unique molecular identifiers (UMI) and individual indices for each sample. The samples were handled according to Chromium Single Cell 3' Reagent Kits v2 User Guide (Document Number CG00052 Rev E, 10x Genomics, 2018). In brief, for each condition, the maximal available number of sorted cells were used, or the maximum according to the 10x Genomics User Guide (17400 cells). Then the Chromium Chip A was loaded with a master mix and cells, the Chromium Controller was run, the generated Gel Bead-in-Emulsion (GEM) was subsequently transferred, and GEM-RT incubation performed. Next, the reaction was cleaned with Silane Dynabeads (Thermo Fisher), cDNA was amplified, and another clean-up step was performed with SPRIselect (Beckman Coulter). Quality control and quantification were then done using a Bioanalyzer with a High Sensitivity DNA analysis kit (Agilent). This was also used for all subsequent quality control and quantification steps. For library construction, cDNA was fragmented, end-repaired and A-tailed, then cleaned-up with SPRIselect (Beckman Coulter). Adaptors were then ligated, and clean-up was performed using SPRIselect (Beckman Coulter). Eventually, the unique sample index was attached by PCR, a double-sided size selection was done using SPRIselect (Beckman Coulter) and quality control and quantification were performed. Finally, all samples were pooled, quantified again, then 23 µl of the 10 nM pool were sent for sequencing to the Core Facility Next-Generation-Sequencing at the Helmholtz Center Munich. 20 µl of the sample pool were sequenced 100 bp paired-end on the same lane on an Illumina Novaseq 6000.

2.8 Preprocessing of scRNA-seq data

Following sequencing, basecalling and fastq file generation was performed by the Illumina Novaseq 6000. Then Dr. Sven Falk performed subsequent preprocessing steps on a Linux workstation using Cell Ranger (10x Genomics, version 4.0.0 – 6.0.2): The function

cellranger mkfastq was applied to demultiplex the data and generate fastq files, cellranger count was used to generate read counts per sample, cellranger mkref was used to modify the human genome (GRCh38 from Ensembl) by addition of the DNA sequences of GFP, DsRed, and WPRE, and cellranger aggr was utilized for normalization of sequencing depth variation between samples.

Table 1 | Cell numbers before and after preprocessing performed with Scanpy (Wolf et al., 2018).

dataset	before preprocessing	after preprocessing	
AS-all	*47,309*	total: *27,512*	thereof: GFP: *5382* AS d7: *2392* AS d14: *5867* AS+DAPT d7: *1722* AS+DAPT d14: *4448* AS+SB/DM d7: *1751* AS+SB/DM d14: *5950*
AS+NS	*58,668*	total: *34,872* total after N-only cell removal: *21,195*	thereof: GFP: *5686* AS d7: *2875* AS d14: *6518* NS d7: *2029* NS d14: *4087*

All subsequent analysis steps I performed using python (version 3.8.11) packages if not indicated otherwise. Further preprocessing of the dataset was performed with Scanpy (version 1.8.1) (Wolf et al., 2018), independently for all batches (d7 and d14). First, cells were restricted to those that expressed >=200 genes, genes were restricted to those expressed in >=3 cells. Second, mitochondrial genes were identified, and cells were filtered to exclude those with >=5% mitochondrial counts. Subsequently, cells were filtered for number of genes by counts (>1900 & <3400 for d7, >1900 & <3600 for d14) and total counts per cell (<13500 for both d7 and d14). Cell cycle parameters were assigned by Scanpy's tl.score_genes_cell_cycle function. The dataset was then normalized, log-transformed and highly variable genes were identified. Unwanted sources of variation were regressed out of the dataset; these were the total counts per cell, percentage of mitochondrial counts and the cell cycle scores for S phase and G2M phase. The data was scaled to unit variance. Doublets were identified independently for each single experiment using Scanpy's implementation of Scrublet (Wolock et al., 2019) and subsequently removed. Batches were concatenated and integrated using Scanpy's implementation of Batch Balanced k-Nearest-Neighbor (BBKNN) (Polański et al., 2020). A total of 27,512 cells and 25,522 genes were used for downstream analysis of the *AS* (Ascl1+Sox2)-*all* dataset (including AS, AS+DAPT, AS+SB/DM, each for d7 and d14, GFP control), while 34,872 cells

and 25,019 genes were used downstream for the *AS+NS* (Neurog2+Sox2) dataset (including AS and NS, N only, each for d7 and d14, GFP control) (**Table 1**).

2.9 Embedding and clustering of scRNA-seq datasets

2.9.1 2-dimensional embedding of scRNA-seq data

Principal components (PC) of the dataset were calculated, and different embeddings were performed: *AS-all* and *AS-only* & NS. Force-directed graph drawing was chosen as embedding method due to its preservation of the data's topology (Islam et al., 2011). The Python implementation of ForceAtlas2 (fa2) (Chippada, 2018; Jacomy et al., 2014) was used via Scanpy's tl.draw_graph function (Wolf et al., 2018) with different settings for each embedding that were targeted at achieving the best possible display for each partial dataset, with clear separation of the trajectories. These were the settings used for BBKNN before each embedding: n_pcs=20, annoy_n_trees=100, neighbors_within_batch=10, trim=100. Following the first embedding, Leiden clustering (Traag et al., 2019), which is an improved version of the previously widely used Louvain algorithm (Blondel et al., 2008), was used via Scanpy's implementation (version 0.8.7) with appropriate resolution to get meaningful clusters. If necessary, some clusters were subclustered to increase cluster resolution in regions of the embedding with a more diverse topology. Subsequently, a partition-based graph abstraction (PAGA) was calculated for each embedding, with edge weights representing confidence in the presence of connections (Wolf et al., 2019). After thresholding the confidence levels, this PAGA was then used via init_pos as precomputed initialization coordinates to compute another force directed graph using Scanpy's tl.draw_graph function (Wolf et al., 2018), where the different clusters were more clearly separated than in the previous embeddings. For *AS-all*, this embedding and its subsets were used to perform all subsequent analyses. For *AS+NS*, the embedding was used to identify NS-transduced cells that were falsely sorted as double positive during FACS; those NS cells that clustered with N only cells were therefore removed from the embedding together with both N only experiments. The remaining 21,195 cells (**Table 1**) were then re-embedded to optimally depict the dimensions of the

reduced dataset. This re-embedding was performed as described above and was then used to perform all subsequent analyses.

2.9.2 2-dimensional embedding of iN cells

To visualize the heterogeneity of iNs of the *AS-all* dataset and the *AS+NS* dataset, the clusters with high *TUBB3* expression (without the confused fate cluster) were processed as a new dataset with Scanpy (Wolf et al., 2018). PCs of the dataset were calculated, and neighbors were found using Scanpy's implementation of BBKNN (Polański et al., 2020), with 8 PCs used for the iN subset of the *AS-all* dataset, 10 PCs used for the iN subset of the *AS+NS* dataset, and 10 neighbors within batch for both datasets. Each iN subset was embedded using UMAP (McInnes et al., 2018) to get a better visual separation between cellular populations. After the first embedding, the embedding was clustered with the Leiden algorithm (Traag et al, 2019). A PAGA graph was calculated for each embedding, which was thresholded to remove the smallest connections between clusters and then used via init_pos as precomputed initialization coordinates to recompute the UMAP embedding using Scanpy's tl.umap function (Wolf et al., 2018), to improve the visual perception of different cell populations. These embeddings were used for visualization of gene expression in the iN cells. The Leiden clusters shown on the embedding are the ones originally calculated on each full dataset.

2.9.3 Cluster nomenclature and individual clustering of experiments

Clusters generated with the Leiden algorithm (Traag et al., 2019) during generation of the embeddings were named as follows: clusters were first assigned to the respective treatment/trajectory (for the *AS-all* dataset: 1 for AS, 2 for AS+DAPT, 3 for AS+SB/DM; for the *AS+NS* dataset: AS, NS or both) or a combination of trajectories (**Table 2**). Then the outcomes, namely confused fate (AS), alternative fate (NS), and different neuronal clusters with high *TUBB3* expression, were named. Neuronal subclusters (in the *AS-all* dataset) were further defined by the expression of markers *NEUROG2* (type 1) and *DLX2* (type 2).

Table 2 | Nomenclature of clusters according to predominant treatment/trajectory and position.

dataset	cluster type	predominant treatment/ trajectory of cluster	starting population (PDGFRB+)	trajectory		
				early	mid	target population (TUBB3+) or off-target identity
AS-all	clustered all treatments together	AS only	*Tra1_A1* *Tra1_A2* *Tra1_A3* *Tra1_A4* *Tra1_A5*			
		AS+DAPT	*Tra2_A1* *Tra2_A2*			
		AS+SB/DM	*Tra3_A1* *Tra3_A2*	*Tra3_B*	*Tra3_C*	*Tra3_early_neurons* *Tra3_neurons_type1*
		clusters combining cells of different treatments	*Tra1/2_AC* *Tra1/2_AB*	*Tra1/2_B*	*Tra1/2_C*	*Tra1/2_early_neurons* *Tra1/2_neurons_type1* *Tra1/2/3_neurons_type1* *Tra1/2/3_neurons_type2* *Tra1/2/3_confused_fate*
	clustered treatments individually	AS only	*AS_start_1* *AS_start_2* *AS_start_3* *AS_start_4* *AS_start_5*	*AS_tra_early*	*AS_tra_mid_1* *AS_tra_mid_2*	*AS_neurons_early* *AS_neurons_late* *AS_confused_fate*
		AS+DAPT	*DAPT_start_1* *DAPT_start_2* *DAPT_start_3* *DAPT_start_4*	*DAPT_tra_early*	*DAPT_tra_mid_1* *DAPT_tra_mid_2*	*DAPT_neurons_early* *DAPT_neurons_type_1* *DAPT_neurons_type_2* *DAPT_confused_fate*
		AS+SB/DM	*SBDM_start_1* *SBDM_start_2* *SBDM_start_3*	*SBDM_tra_early_1* *SBDM_tra_early_2*	*SBDM_tra_mid_1* *SBDM_tra_mid_2*	*SBDM_neurons_early* *SBDM_neurons_type_1* *SBDM_neurons_type_2* *SBDM_confused_fate*
AS+NS	clustered all treatments together	AS only		*Tra_AS_B1* *Tra_AS_B2*	*Tra_AS_C1* *Tra_AS_C2*	*Tra_AS_neurons_early* *Tra_AS_neurons_late* *Tra_AS_confused_fate*
		NS only		*Tra_NS_B1* *Tra_NS_B2*	*Tra_NS_C1* *Tra_NS_C2*	*Tra_NS_alternative_fate* *Tra_NS_neurons_early* *Tra_NS_neurons_late*
		clusters combining cells of both treatments	*Tra_AS_NS_A1* *Tra_AS_NS_A3* *Tra_AS_NS_A2* *Tra_AS_NS_A4* *Tra_AS_NS_A5*	*Tra_AS_NS_B*		

All other clusters were then named with the letters A, B, C according to their position on the trajectory, A being a cluster of the starting population with (in case of *AS-all* clusters including significant numbers of GFP control cells, and corresponding clusters

of other trajectories), B being a cluster in the early trajectory (clearly separated from the starting population but still with *PDGFRB* expression) and C being in the mid trajectory (before upregulation of *TUBB3*). Clusters meeting more than one of these criteria were assigned letter combinations. To differentiate between clusters that would have received identical names according to this nomenclature, numbers were added after the letters if necessary.

In addition to clustering of the whole embeddings, the treatments of the *AS-all* dataset were clustered individually. The nomenclature started with the name of the treatment (for the *AS-all* dataset); end points (neuronal clusters, confused fate, alternative fate) were defined as described above. All other clusters were defined as described above, with "start" indicating a cluster of the starting population, "early" indicating a cluster in the early trajectory, and "mid" indicating a cluster in the mid trajectory (**Table 2**). Again, adjacent clusters with otherwise identical criteria were given an additional number after the previous nomenclature.

2.10 Velocity-based analyses of scRNA-seq data

2.10.1 Single cell velocity

To "predict the future state of single cells on a timescale of hours" (Ma et al., 2020), first annotations of spliced/unspliced reads were obtained using velocyto (La Manno et al., 2018). Subsequently, scVelo (version 0.2.4) was used for velocity analysis and visualization (Bergen et al., 2020). For velocity computation, the datasets were filtered using scVelo's tl.filter_and_normalize function and only the 1000 most variable genes with at least 10 counts (spliced or unspliced) were kept. First- and second-order moments were computed per cell across its 30 nearest neighbors, using 20 PCs. Differential kinetics between the treatments' individual clusters were calculated using the tl.differential_kinetic_test function, which also recovers the splicing dynamics of all genes in the dataset, including modeling of transcription, splicing, and degradation rates. Subsequently, velocities were calculated with tl.velocity in dynamical mode, taking

differential kinetics into account, grouped by the treatment. scVelo was then used to calculate the velocity graph and the velocity embedding on the force-directed graph.

In the velocity embedding, each cell's direction is indicated with an arrow. To be able to compare the direction of these arrows with the direction of the trajectories from pericytes to neuronal and confused outcomes, the trajectories were manually drawn onto the embedding in Fiji (Schindelin, 2012). The acquired coordinates were processed in Python, where the trajectories were smoothened and then for each treatment separately, each cell's velocity arrow was compared to the closest point on the trajectory. By subtracting the angle of the arrow from the angle of the closest trajectory coordinate, for each cell the 'velocity angle' was calculated, with values ranging from 0° (meaning the cell is exactly following the trajectory) to +/-180 (meaning the cell is going exactly in reverse direction to the trajectory, in left or right direction). While angles towards neurons and confused fate had been calculated separately, they were then combined using the angle towards confused fate on the confused fate cluster. Then, velocity classes were defined by a cutoff of +/-30° - cells within that range were considered progressing, all others were non-progressing.

2.10.2 Latent time calculation

Based on the velocities obtained from the dynamical model, a cell-specific latent time was calculated on the dataset using default settings with the tl.latent_time function. This relies on combination of gene-specific latent timepoints of all genes with a likelihood fitness of at least 0.1 from the 1000 most variable genes with at least 10 counts. For comparison between treatments a scaled latent time was used, which was scaled to each treatment's or each TF combination's minima and maxima.

2.10.3 Identification of blockers and facilitators

To identify genes that are upregulated in progressing cells (facilitators) and genes that are upregulated in non-progressing cells (blockers), the decision point was identified in the *AS-only* cells of the *AS-all* embedding as follows: Latent time was used to bin cells in

20 bins, then, using only cells that had left the starting population, cell density along latent time was evaluated. In the latent time bin including the density peak as well as the two preceding ones, there was a steady increase of progressing cells, with d7 cells having a higher rate of progressing cells than d14 cells, indicating time-dependent dynamics of a decision point. Cells that managed to leave the density peak showed a further increase in the progressing cell rate in the three subsequent latent time bins. Therefore, to identify transcriptomic differences, the non-progressing cells of the three preceding latent time bins were compared to the progressing cells of the three subsequent latent time bins using differential expression (DE). Using Scanpy's tl.rank_genes_groups and tl.filter_rank_genes_groups functions, a t-test was applied with Benjamini-Hochberg correction and results were filtered to obtain only genes with a minimal log fold change of 1, a minimal in-group-expression fraction of 0.2, and a corrected p-value <0.05. To filter out genes that were only differentially expressed due to their position on the trajectory but not due to their velocity angle, the progressing cells of the three preceding latent time bins were compared to the non-progressing cells of the three subsequent latent time bins using DE and filtering as described above; the genes identified thereby were then respectively subtracted from the earlier identified lists. The genes remaining in the list that were upregulated in the progressing cells after the peak were termed facilitator genes, the genes remaining in the list that were upregulated in the non-progressing cells before or at the peak were termed blocker genes.

2.10.4 Directed single cell fate mapping

To identify terminal cell fates and different lineages from velocity data, CellRank (version 1.5.0) was used (Lange et al., 2022). Both initial states and terminal states were computed from the dynamical velocity using the CFLARE (Clustering and Filtering of Left and Right Eigenvectors) estimator, which models cell dynamics building a Markov chain via spectral heuristics. To account for noise in velocity vectors, cell-cell similarities were given a weight of 0.5. Since the eigengap heuristic that was used only yielded three terminal states for the *AS-all* dataset by default (starting population, confused fate, and early neurons), yet we wanted to resolve the heterogeneity in neuronal fates, we used the fixed number of six terminal states (previous ones plus neurons 1, neurons 2, mid trajectory). In

the *AS+NS* dataset, the default eigengap heuristic only offered one terminal state (NS neurons), therefore, to capture the AS neuron lineage, the fixed number of seven terminal states was used (both AS and NS neurons, plus starting population, AS mid trajectory, NS early neurons and two different NS alternative fates; however no AS confused state). For each dataset, default settings yielded only one initial state, which was the used to identify lineages and calculate absorption probabilities. Gene trends for these lineages were computed with CellRank (Lange et al., 2022), which uses Generalized Additive Models (GAMs) to fit gene expression levels and weighs cellular contributions by the absorption probabilities. They were plotted separately by treatment.

To identify cells of the AS/AS+DAPT mid trajectory with the highest probability to become confused ('confused root cells'), a threshold > 0.0075 was applied to absorption probabilities for confused fate.

2.11 Visualizing connections and connected cells by scores

To visualize which cells are connected the closest with clusters of interest of AS-transduced cells, a neighbor calculation with BBKNN (to again integrate d7 and d14 samples) was performed on this subset using 5 neighbors within each batch to reduce the maximum number of calculated connections. The sparse connectivities matrix returned from Scanpy's BBKNN implementation, which gives weights to the connections between all cells, was then restricted to only those connections involving cells of the cluster of interest. These remaining connections were used for visualization of the cluster of interest's connections. All connectivity weights associated with a particular cell were then added up to generate the connectivity score for this cell. The score was plotted on the embedding using a non-linear color scale to improve perception of small connection scores and using a scaled dot size in relation to the connection score.

2.12 Marker gene identification for clusters and treatments

To define marker genes that are expressed significantly (corrected p-value <0.05) different between clusters of the AS-transduced cells or between the bulks of the different treatments, DE analysis was performed using Wilcoxon rank-sum (Mann-Whitney-U) test with Benjamini-Hochberg correction. Each cluster's gene expression values were compared to all other clusters' expression as a reference. Subsequently, results were filtered for a minimal log fold change of 1, a minimal in-group-expression fraction of 0.2.

2.13 Mapping clusters of treatments by integration

To allow for a better comparison of the cells of the clusters on the AS+SB/DM trajectory to the AS clusters despite their different location on the embedding, we used Scanpy's asymmetric integration function *ingest*. Hereby, we used the AS trajectory and its clusters as a reference dataset to integrate AS+SB/DM into. According to Scanpy (Wolf et al., 2018), the tl.ingest function fits a PCA model on the reference dataset, then maps labels (here: clusters defined in AS) using a k-nearest neighbors algorithm (kNN) classifier and the UMAP package (McInnes et al., 2018) to map the embeddings. We then generated a Sankey diagram to visualize the cellular contributions of AS+SB/DM clusters mapped onto AS clusters. Prior to plotting, links between AS+SB/DM clusters and AS clusters with fewer than 3 cells were excluded to improve clarity. For comparison, the same mapping was performed for AS+DAPT.

2.14 Transcription factor activity prediction

Since scRNA-seq measures gene expression from RNA, TF activity cannot directly be assessed. However, through the expression of a TF's target genes, its activity can also be predicted from the transcriptome. Each TF and its transcriptional targets form a regulon. To predict regulon activity, the Python implementation of DoRothEA (version 1.0.5) was used, a package that utilizes a collection of regulons identified through various sources from literature and from databases of binding site motifs, ChIP-seq data, and gene

expression data (Garcia-Alonso et al., 2019; Holland et al., 2020). Only regulons of confidence levels A, B, and C for human data were used. For TF activity calculation on the log normalized expression data, the gene expression was centered by mean per cell and 100 random activities were simulated. To correct for large regulons, values were normalized by the number of edges, and to make them comparable across cells, values were scaled per feature. TFs with fewer than three target genes were not included. Regulon activity was calculated for the full datasets and, depending on the region of interest, on subsets. The implemented Wilcoxon rank-sum test was used to identify differentially active regulons between groups and regulons were filtered for adjusted p-value (by Benjamini-Hochberg correction) <0.05. Only regulons with a net mean activity change of >0.25 were included in heatmaps.

Network graphs were generated to show the mean change in TF activity together with their target genes for selected regulons. Target genes were tested for differential expression using a t-test with Benjamini-Hochberg correction and only genes with an adjusted p<0.05 were displayed in network graphs. To improve graph visualization, for the differentially expressed regulons of the starting population only significantly differentially expressed with a minimum absolute fold change of 0.75 and a minimum in group fraction of 0.2 were included; for the mid trajectory populations as well as confused root cells, all target genes with a minimum absolute fold change of 0.5 and a minimum in group fraction of 0.1 were included in the graph. Additionally, regulons with less than 2 differentially expressed target genes were removed from the graph.

2.15 Generation of overarching gene set scores

To show the combined expression of several genes at once, Scanpy's tl.score function was used with default settings (Wolf et al., 2018), which is an implementation of an approach originally developed for Seurat (Butler et al., 2018; Hao et al., 2021; Satija et al., 2015; Stuart et al., 2019). It uses the average expression of a given gene set and subtracts the average expression of a randomly sampled reference gene set (Wolf et al., 2018). Blocker and facilitator scores were generated from the identified blocker and facilitator genes (including identified subsets) (**Table 4**). Due to the heterogeneity of subsets of facilitator genes identified during our analysis of only AS-transduced cells, only

facilitator genes subsets 1 and 2 were used to generate the facilitator score on the full AS dataset including AS+DAPT and AS+SB/DM.

Glycolysis and Oxphos scores were derived from gene lists curated in the KEGG database (Kanehisa, 2019; Kanehisa et al., 2021; Kanehisa & Goto, 2000) for the terms KEGG_GLYCOLYSIS_GLUCONEOGENESIS (https://www.gsea-msigdb.org/gsea/msigdb/cards/KEGG_GLYCOLYSIS_GLUCONEOGENESIS) and KEGG_OXIDATIVE_PHOSPHORYLATION (https://www.gsea-msigdb.org/gsea/msigdb/cards/KEGG_OXIDATIVE_PHOSPHORYLATION), respectively (**Table 3**). From the HIF1A regulon activity calculated with DoRothEA, a HIF1A TF score was generated.

Table 3 | Gene sets used to generate glycolysis and OxPhos scores.

Glycolysis score gene set		OxPhos score gene set			
ACSS1	*G6PC2*	*ATP12A*	*ATP6V1C2*	*MT-ATP6*	*NDUFB7*
ACSS2	*GALM*	*ATP4A*	*ATP6V1D*	*MT-ATP8*	*NDUFB8*
ADH1A	*GAPDH*	*ATP4B*	*ATP6V1E1*	*MT-CO1*	*NDUFB9*
ADH1B	*GCK*	*ATP5F1A*	*ATP6V1E2*	*MT-CO2*	*NDUFC1*
ADH1C	*GPI*	*ATP5F1B*	*ATP6V1F*	*MT-CO3*	*NDUFC2*
ADH4	*HK1*	*ATP5F1C*	*ATP6V1G1*	*MT-CYB*	*NDUFS1*
ADH5	*HK2*	*ATP5F1D*	*ATP6V1G2*	*MT-ND1*	*NDUFS2*
ADH6	*HK3*	*ATP5F1E*	*ATP6V1G3*	*MT-ND2*	*NDUFS3*
ADH7	*LDHA*	*ATP5MC1*	*ATP6V1H*	*MT-ND3*	*NDUFS4*
AKR1A1	*LDHAL6A*	*ATP5MC1P5*	*COX10*	*MT-ND4*	*NDUFS5*
ALDH1A3	*LDHAL6B*	*ATP5MC2*	*COX11*	*MT-ND4L*	*NDUFS6*
ALDH1B1	*LDHB*	*ATP5MC3*	*COX15*	*MT-ND5*	*NDUFS7*
ALDH2	*LDHC*	*ATP5ME*	*COX17*	*MT-ND6*	*NDUFS8*
ALDH3A1	*PCK1*	*ATP5MF*	*COX4I1*	*NDUFA1*	*NDUFV1*
ALDH3A2	*PCK2*	*ATP5MG*	*COX4I2*	*NDUFA10*	*NDUFV2*
ALDH3B1	*PDHA1*	*ATP5PB*	*COX5A*	*NDUFA11*	*NDUFV3*
ALDH3B2	*PDHA2*	*ATP5PD*	*COX5B*	*NDUFA2*	*PPA1*
ALDH7A1	*PDHB*	*ATP5PF*	*COX6A1*	*NDUFA3*	*PPA2*
ALDH9A1	*PFKL*	*ATP5PO*	*COX6A2*	*NDUFA4*	*SDHA*
ALDOA	*PFKM*	*ATP6AP1*	*COX6B1*	*NDUFA4L2*	*SDHB*
ALDOB	*PFKP*	*ATP6V0A1*	*COX6B2*	*NDUFA5*	*SDHC*
ALDOC	*PGAM1*	*ATP6V0A2*	*COX6C*	*NDUFA6*	*SDHD*
BPGM	*PGAM2*	*ATP6V0A4*	*COX6CP3*	*NDUFA7*	*TCIRG1*
DLAT	*PGAM4*	*ATP6V0B*	*COX7A1*	*NDUFA8*	*UQCR10*
DLD	*PGK1*	*ATP6V0C*	*COX7A2*	*NDUFA9*	*UQCR10P1*
ENO1	*PGK2*	*ATP6V0D1*	*COX7A2L*	*NDUFAB1*	*UQCR11*
ENO2	*PGM1*	*ATP6V0D2*	*COX7B*	*NDUFB1*	*UQCRB*
ENO3	*PGM2*	*ATP6V0E1*	*COX7B2*	*NDUFB10*	*UQCRC1*
FBP1	*PKLR*	*ATP6V0E2*	*COX7C*	*NDUFB2*	*UQCRC2*
FBP2	*PKM*	*ATP6V1A*	*COX8A*	*NDUFB3*	*UQCRFS1*
G6PC	*TPI1*	*ATP6V1B1*	*COX8C*	*NDUFB4*	*UQCRH*
		ATP6V1B2	*CYC1*	*NDUFB5*	*UQCRHL*
		ATP6V1C1	*LHPP*	*NDUFB6*	*UQCRQ*

2.16 Mapping neuronal transcriptome to human brain structures

To compare the generated neuronal cells with human brain structures, Voxhunt (version 1.0.1) was used (Fleck et al., 2021). This particularly enables to map single cell data to bulk RNA-sequencing data from microdissected human developing brain structures (BrainSpan). To use this R (version 4.1.1) package, Scanpy's Anndata objects were manually converted into Seurat (Butler et al., 2018; Hao et al., 2021; Satija et al., 2015; Stuart et al., 2019) objects. Regional marker genes were defined via DE feature selection on *in situ* hybridization (ISH) data from the Allen Developing Mouse Brain Atlas (Fleck, 2020), selecting the top 10 unique marker genes per brain structure at developmental stage E11. These features were then used to map neuronal clusters of our dataset as pseudobulk to microdissected human developing brain structures of stages pcw 10 - pcw 24 from BrainSpan data and construct a similarity map. Finally, the similarity map was exported to Python and plotted as a heatmap, ordered by marker expression similarities, which are indicated by a hierarchically clustered dendrogram.

3 Results

3.1 Investigation of molecular mechanisms in direct pericyte-to-neuron conversion

3.1.1 Direct conversion of human brain pericytes into induced neurons

To investigate the molecular mechanisms involved in direct reprogramming of human brain pericytes into induced neurons, we generated a new culture primary of human brain pericytes and after expansion used the retrovirus expressing Ascl1/Sox2 with a GFP reporter previously used in Karow et al. (2018). Since it has been shown by Karow et al. (2018) that cell sampling at d7 and d14 is sufficient to capture the main phases of the reprogramming trajectory, cells were FAC sorted 7 and 14 days, respectively, after AS-transduction to select only successfully transduced cells. Sorted cells were collected and subsequently underwent high-throughput droplet microfluidic scRNA-seq (10x Genomics) (**Figure 4A**). A fraction of 10-15% of transduced cells successfully converted into induced neurons. In comparison to the flat pericytes, the iNs exhibited a clear neuronal morphology with a small soma and several, more or less branched processes (**Figure 4B**). The gating settings for FAC sorting were selected in a conservative way to ensure that no debris, but only single cells that had been transduced, were used for further analyses (**Figure 4C**).

After filtering the transcriptomic data of multiplets and dead/damaged cells, and insufficient read counts, a total of 13,641 cells (GFP control: 5382 cells, AS d7: 2392 cells, AS d14: 5867 cells) were included in the analysis (**Table 1**). To reconstruct the reprogramming trajectory from pericytes to iNs, cells were embedded in 2-dimensional space using a force directed graph, which is known to retain the data's topology (Islam et al., 2011). The embedding showed an apparent reprogramming trajectory from the starting population consisting of both GFP-transduced and AS-transduced cells towards transcriptomically distinct populations of only AS-transduced cells (**Figure 5A**).

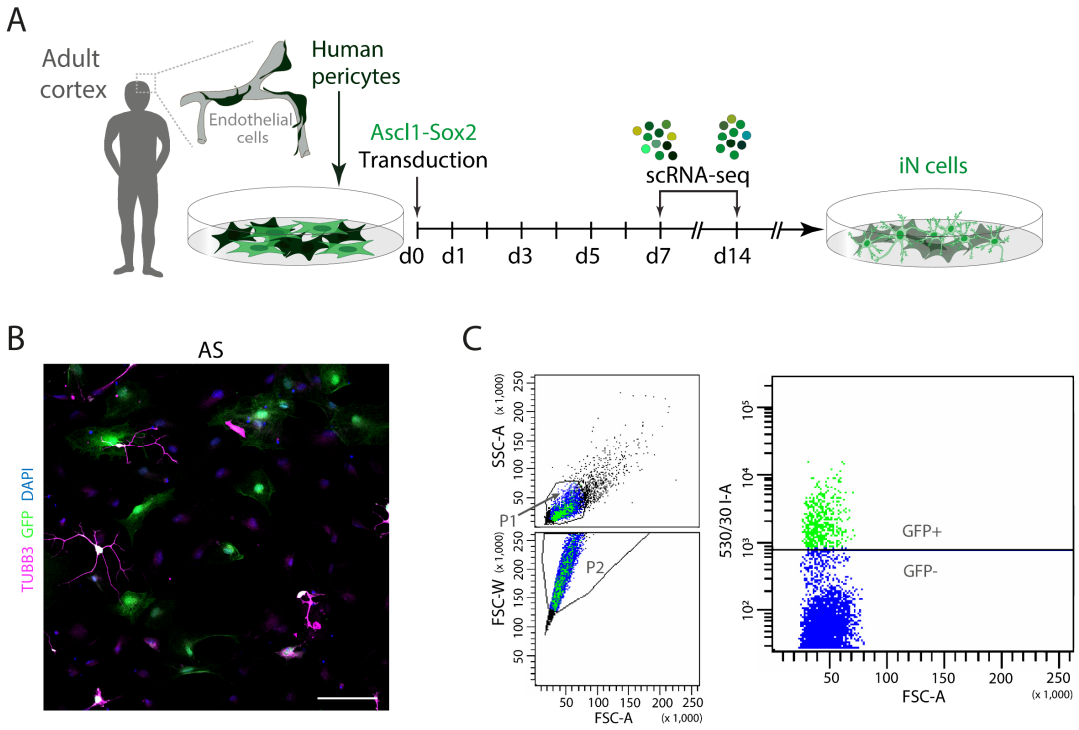

Figure 4 | Successful transduction and reprogramming of human brain pericytes. (**A**) Schematic of the experimental design: Cultured brain pericytes derived from the brain of an adult human patient were retrovirally transduced to express Ascl1 and Sox2 (AS) with GFP as an expression control. On d7 and d14 after transduction, cells were FAC sorted for GFP expression and GFP+ cells were used for single cell transcriptome analysis using the 10x Genomics platform. (**B**) Representative image of successfully reprogrammed pericytes after immunostaining 28 days after transduction: neuronal cells (*TUBB3*, magenta), AS-transduced cells (*GFP*, green) and nuclei (DAPI, blue) are visible. Scale bar, 50 µm. (**C**) Representative images of the FACS gating used to select the cells for scRNA-seq. To exclude cell debris and doublets, events were gated in the forward scatter (area) and sideward scatter (area) (gate P1) as well as in the forward scatter (area) and forward scatter (width) (gate P2). Finally, reporter protein positive cells were selected (GFP+).

Visualization of the cells' neighbors confirmed a continuous trajectory instead of disjointed populations (**Figure 5A**), indicating reprogramming to be a stochastic process. Noticeably, while the embedding of starting population remained quite homogenous apart from a small protrusion, the cells on the trajectory displayed a more diverse topology and bifurcated into two clearly separated populations, a main one as well as a smaller one, with only few cells reaching the end of the trajectory. As evident from the expression of *PDGFRB* (a marker for pericytes), the pericyte identity was still present in the starting population (**Figure 5B**). The AS-transduced cells distant from the starting population started to express the neuronal marker *TUBB3* (**Figure 5C**).

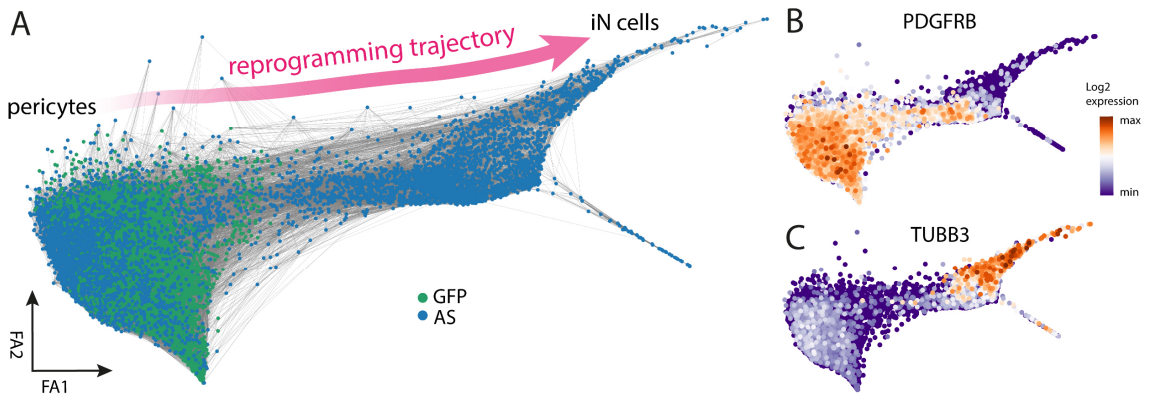

Figure 5 | Reconstruction of the reprogramming trajectory of AS-transduced cells. (**A**) Transcriptome data was analyzed using Scanpy (Wolf et al., 2018). Force directed graph was used to visualize 8259 AS-transduced cells (blue) (d7: 2392 cells, d14: 5867 cells) and 5382 GFP-transduced control cells (green) in a 2-dimensional embedding. Each dot represents one cell, and their order represents their similarity. GFP cells co-embed with AS-transduced cells on the left, suggesting this to be the reprogramming starting population. Grey lines between the cells indicate the 20 closest neighbors of each cell over all dimensions used in the embedding. (**B**) *PDGFRB* as a pericyte marker is confirmed to be expressed mostly in the starting population and to decline along the trajectory. (**C**) *TUBB3* as a neuronal marker is shown to be upregulated during the trajectory.

3.1.2 Incorporation of transcriptional dynamics to predict future cellular states

Although we could successfully convert pericytes into iNs, a majority of cells did not express TUBB3, as shown by Karow et al. (2012). From the generated embedding however, it was unclear if *TUBB3*- cells will become *TUBB3*+ later on. To get beyond the static view of transcriptomics, which just shows the current cellular state, we therefore took advantage of the recently emerged concept of RNA velocity (La Manno et al., 2018): As mRNA is transcribed, at first it contains both exonic and intronic sequences, then splicing, the excision of introns from the mRNA, leads to the final mRNA (**Figure 6A**). Since transcription, splicing (and degradation) of the mRNA occur with different rates and non-simultaneously, the ratio between unspliced and spliced reads of a gene yields information about the transcriptional dynamics (**Figure 6B**). Whether genes expressed are currently in induction or repression phase, allows for prediction of the cellular identity several hours in the future – this is harnessed by scVelo (Bergen et al., 2020). We applied scVelo to our dataset and observed that the cellular identities are highly dynamic (**Figure 6C**). In fact, when comparing the individual cells' transcriptional dynamics on the embedding, we could show that while the starting population was almost not progressing at all, the cells that had left the starting population consisted of both progressing and non-progressing cells

(**Figure 6D**). Interestingly, both at the beginning of the trajectory, right after the starting population, as well as at the tip of the main trajectory, many cells seemed to revert to an earlier state (**Figure 6C, D**).

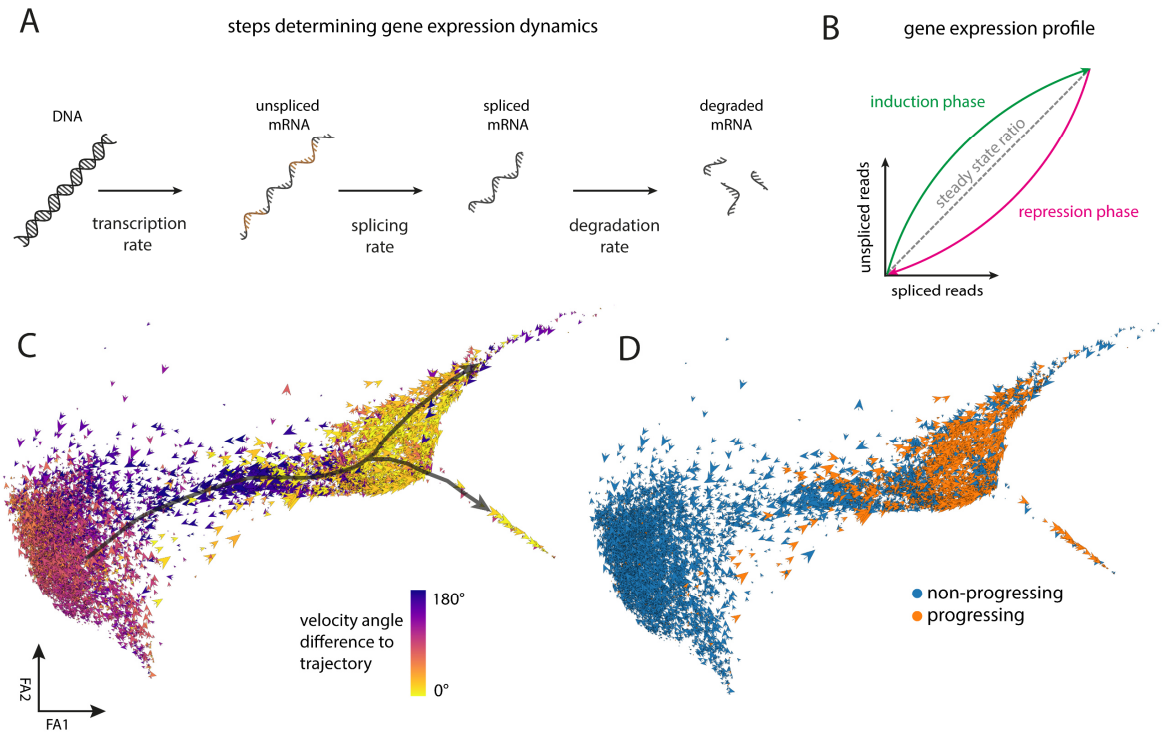

Figure 6 | RNA velocity shows individual cellular dynamics in AS-transduced cells. (**A**) Order of steps responsible for gene expression dynamics (based on La Manno et al. (2018)). All turnover rates depend on the gene and the cellular context. (**B**) Schematic of gene expression dynamics that can be inferred from the ratio of unspliced to spliced reads, including phases of gene induction and repression as well as a steady state (based on La Manno et al. (2018)). Reads can be identified as unspliced if they include intronic sequences. (**C**) The embedding with velocities calculated by scVelo (Bergen et al., 2020). Arrow directions indicate an individual cell's predicted fate based on the most dynamically expressed genes. Arrow size indicates the speed of an individual cell's identity change. The individual cells' velocity directions are compared to the previously identified reprogramming trajectory (dark grey arrows) and indicated via color scale ranging from 0° difference (the same direction as the reprogramming trajectory) to 180° difference (the opposite direction of the reprogramming trajectory). This reveals that most starting population cells are not progressing towards the trajectory, while on the trajectory, many cells are progressing towards the trajectory ends but some are reverting to earlier states. (**D**) Individual cells' velocities can be categorized based on the velocity angle difference towards the trajectory into progressing cells (orange; less than 30° deviation from the trajectory) and non-progressing cells (blue; more than 30° deviation from the trajectory). This visualization shows that non-progressing cells can be found all along the trajectory.

3.1.3 Identification of a decision point for cellular progression

The velocity data contained information about the directionality of the reprogramming process, which could be harnessed to obtain a gene-shared latent time for

each cell. This allowed for a pseudotemporal ordering of the cells according to their transcriptomic state in the reprogramming process. As expected, the cells in the starting population and the early trajectory exhibited the lowest latent time and followed a latent time gradient towards the iN population (**Figure 7A**).

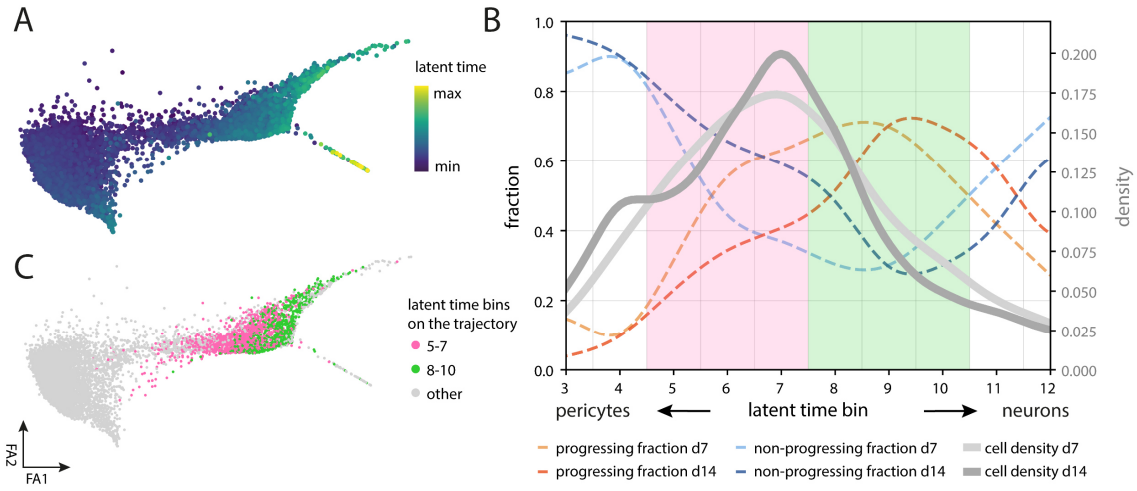

Figure 7 | Density and progression dynamics reveal decision point on trajectory. (**A**) Representation of the AS-transduced cells' latent time. Based on velocity-inferred directionalities, transition probabilities between single cell identities are derived and a latent time is calculated depicting a cell's transcriptomic state along the trajectory. The earliest latent time point (min=0) represents the origin within the trajectory (dark blue), while the latest latent time point (max=1) represents the destinations (green->yellow). (**B**) Identification of a cellular decision point. Visualization of the density of the cells along latent time (grey lines, right axis) and the fraction of progressing (dashed orange lines, left axis) and non-progressing (dashed blue lines, left axis) cells along latent time. Both density and progressing/non-progressing fractions are visualized separated by day (d7 vs. d14, the first indicated by lighter color). All cells outside of the starting population were binned into 20 equal bins along latent time, e.g. each bin contains 1/20 of the time. A decision point of progression on the trajectory from pericytes (left side) and neurons (right side) was identified by taking into account both the density peak and the fractions of progressing/non-progressing cells: Density is increasing until its peak in latent time bin 7, indicating cells being accumulating here, then decreasing again, indicating that some cells manage to leave the accumulation. The fraction of progressing cells starts to increase from latent time bin 5 and only decreases again in latent time bin 9 (d7) and 10 (d14). Thereby, the decision point was identified between the two phases of increasing accumulation and progression (latent time bins 5-7; magenta) and continuous high progression afterwards (latent time bins 8-10; green). (**C**) Cells on the trajectory in the latent time bins of interest shown on the embedding: decision is taken between latent time bins 5-7 (before density peak; magenta) and latent time bins 8-10 (after density peak; green).

We anticipated the existence of a decision point on the trajectory, at which cells with a certain transcriptional profile progressed further on the trajectory, while others did not. When looking at the distribution of cells along latent time, cellular density clearly peaked at latent time bin 7 (≙latent time 0.30-0.35), after approximately one third of the velocity-derived trajectory timeline (**Figure 7B**). This suggested a large fraction of cells

getting stuck at this point and that only cells expressing the right set of genes could progress. This was also supported by the comparison between days: While d7 and d14 AS-transduced cells shared the same density peak, d14 cells peaked higher, indicating a greater proportion of cells being stuck after longer experimental time. Consideration of the fractions of progressing and non-progressing cells along latent time shed more light on where the decision was taken: Already before the cellular accumulation, cells were increasingly progressing, starting at latent time bin 5 with only about one quarter of cells progressing. This increase in the fraction of progressing cells continued until latent time bin 9 (d7) and latent time bin 10 (d14) with almost three quarters of cell progressing. Interestingly, comparison between the two experimental timepoints showed more progressing cells at an earlier latent time for d7 cells, but less progressing cells at a later latent time. Altogether, two phases of the decision were identified within the latent time span exhibiting increasing progression: before (or at) the density peak (latent time bins 5-7 (≙latent time 0.20-0.35) and after the density peak (latent time bins 8-10 (≙latent time 0.35-0.50). The embedding revealed that the transition between these phases of decision took place in the middle of the trajectory (**Figure 7C**).

3.1.4 Identification of genes facilitating or blocking progression

Following the obvious assumption that the transcriptomic profiles of progressing cells were different from the profiles of non-progressing cells, we sought to identify the gene sets that define this difference. We therefore used differential expression (DE) analysis between progressing cells that had passed the decision point as well as non-progressing cells that had not done so, obtaining lists of significantly differentially expressed genes. As both populations of cells were only partly overlapping on the embedding, however, parts of the differential expression might be attributed to the differences in transcriptomics, not distinct cellular dynamics. Therefore, to exclude purely positional effects, we performed another DE analysis between non-progressing cells after the decision point and progressing cells before the decision point, obtaining these gene sets as a control. The original lists of genes were then filtered to remove any genes that also occurred in the control lists. This procedure eventually yielded a list of 108

"facilitator" genes that were upregulated in progressing cells at the decision point, and a list of 125 "blocker" genes that were upregulated in non-progressing cells at the decision point (**Table 4**).

Table 4 | Blocker and facilitator genes identified around the density peak.

blocker genes				facilitator genes			
				subset 1		subset 2	subset 3
ACTN1	*CYTOR*	*LUM*	*S100A13*	*ABAT*	*PPM1K*	*BTG1*	*AL049838.1*
ADIRF	*EDN1*	*LY96*	*S100A4*	*ABHD12*	*PRXL2A*	*FNDC5*	*ALDH1A1*
AKR1C3	*EHD2*	*METTL7B*	*S100A6*	*AC010642.2*	*PYROXD2*	*GADD45G*	*AP2A2*
ARL4D	*ELN*	*MFAP2*	*SCD*	*ALDH4A1*	*RBFOX2*	*GPM6B*	*ARMH4*
BGN	*EMP2*	*MGLL*	*SELENOP*	*ARFGEF1*	*RGMB*	*HES6*	*CAV2*
BST1	*EMP3*	*MGP*	*SEMA5A*	*BCL7A*	*RGS2*	*LINC01198*	*CDRT1*
CARMN	*ENDOD1*	*MGST1*	*SFRP4*	*C1QTNF2*	*RNF165*	*MAP1B*	*CEMIP2*
CAVIN3	*ENG*	*MIR4435-2HG*	*SGCD*	*CCNG2*	*SERPINF1*	*MARCKSL1*	*COL2A1*
CCDC80	*ERCC6*	*MT1E*	*SLC16A3*	*CENPV*	*SIRT2*	*MFNG*	*COX6A2*
CCL2	*EVA1A*	*MT2A*	*SLC20A2*	*CILK1*	*SPPL2B*	*MIAT*	*CXorf38*
CCN2	*FBLN1*	*NDUFA4L2*	*SLC29A1*	*CPSF4*	*SRGAP3*	*OS9*	*CYFIP2*
CCND1	*FBLN2*	*NID1*	*SORBS2*	*DLL1*	*SYNE2*	*PHLDA1*	*GNG2*
CD248	*FOXS1*	*NPR3*	*SORBS3*	*DPYSL3*	*TGIF1*	*RASD1*	*GPR155*
CD302	*FRZB*	*NQO1*	*SPARC*	*ERVK3-1*	*TP53BP1*	*RASSF4*	*LINC00968*
CD44	*FXYD5*	*NT5E*	*SPARCL1*	*FGF7*	*TPD52L1*	*RGS16*	*LUC7L2*
CDC42EP1	*GADD45B*	*NTRK2*	*SRPX2*	*GFOD2*	*TRIT1*	*RPAIN*	*LYRM7*
CDH11	*GLT8D2*	*NTRK3*	*STC2*	*GLRB*	*TST*	*SERPING1*	*NGF*
CEMIP	*GNG11*	*NUPR1*	*SYNGR1*	*HPS1*	*TUBB2A*	*SOX4*	*OSBPL11*
CFD	*HES1*	*P4HA2*	*TCN2*	*ING1*	*ZBTB18*	*STMN1*	*PAMR1*
CHST15	*ID3*	*PCOLCE*	*TENT5A*	*JAM3*	*ZNF436-AS1*	*TAGLN3*	*PRDM2*
CLDN11	*IFITM2*	*PDE1C*	*TFPI*	*KDM6B*	*ZNF521*	*TPM3*	*PRUNE2*
COL11A1	*IGFBP7*	*PDGFB*	*TIMP1*	*KIT*	*ZSWIM6*	*TPPP3*	*PTPN1*
COL18A1	*IL34*	*PDGFRA*	*TIMP4*	*LRRC8D*		*TUBA1A*	*PTPN21*
COL1A1	*INHBA*	*PDGFRB*	*TMEM189*	*LRRN1*		*TUBB2B*	*RFLNB*
COL3A1	*ISLR*	*PHGDH*	*TRIB2*	*MAP1A*		*TUBB3*	*SEMA3D*
COPZ2	*ITGBL1*	*PLAC9*	*TSPAN18*	*MINPP1*			*SLC15A3*
CRYAB	*ITI–H5*	*PLTP*	*UGDH*	*MYCL*			*SRGAP1*
CTHRC1	*KANK2*	*PRRX1*	*VCAN*	*NIN*			*SUN1*
CTSC	*LAMA4*	*PRSS12*	*ZFP36L1*	*PACC1*			*TMEM132A*
CTSK	*LGALS3*	*PTN*	*ZFP36L2*	*PAK1*			*TMEM178B*
CXCL1	*LITAF*	*RAMP1*		*PDGFC*			*TRIM16*
CXCL6	*LMO7*	*RGS5*		*PDP1*			*WWC2*
CYP1B1	*LOX*	*RRAS*		*PLXNA2*			

Despite their similar expression profile (**Figure 8A**), the blocker genes belong to a variety of biological processes. Among the blocker genes were the pericyte markers

PDGFRB and *RGS5*, suggesting that cells need to lose their pericyte identity to proceed towards neurons. The list also contained the mitochondrial protein-coding gene *MGST1* that has been shown to be downregulated in neurons compared to astrocytes (Russo et al., 2021), as well as the chromatin remodeler *ERCC6*. Several genes (*SPARCL1*, *NTRK2*, *ELN*, *CRYAB*) identified by Karow et al. (2018) as "switch genes" due to their transient expression during reprogramming were also found among the blocker genes, indicating that their downregulation as part of the "switch" is a precondition for further progression. Finally, the blocker gene list also comprised the NOTCH target *HES1*, and the TGFβ signaling pathway members *INHBA* and *ID3*, regulatory networks that play an important role during neuronal development.

By contrast, the facilitator genes differed more in their expression profiles between cells (**Figure 8A**). Three subsets of genes could be identified. With *PAK1*, *KDM6B*, and *CENPV*, subset 1 contained three genes involved in chromatin remodeling, which is an essential factor in the regulation of gene expression. In addition, subset 1 comprised genes dealing with cytoskeletal changes like *TUBB2A* and *MAP1A*, the neurotrophic factor *SERPINF1* and the NOTCH ligand-coding gene *DLL1*. Subset 2 included among others the NOTCH target *HES6* and NOTCH signaling modulator *MFNG*, as well as further genes involved in neuronal cytoskeleton formation such as *TUBB3*, *TUBB2B* and *MAP1B*. Subset 3 contained genes like *COX6A*, coding for an enzyme of the mitochondrial respiratory chain, and *SEMA3D*, which is involved in axon guidance (Liu & Halloran, 2005).

Notably, the expression profile of all facilitator genes was so distinct from that of all blocker genes that they remained separated as two blocks in the hierarchical clustering (**Figure 8A**). Even when cells were ordered by transcriptomic similarities, their velocity angle was considerably smaller in cells with high facilitator and low blocker gene expression; these cells were on track to become neurons. Moreover, cells with high facilitator and low blocker gene expression showed a later latent time, indicating these cells to be further progressed on the reprogramming trajectory. Interestingly, cells with high facilitator and low blocker gene expression also seemed to exhibit a higher velocity length, indicating a faster reprogramming process.

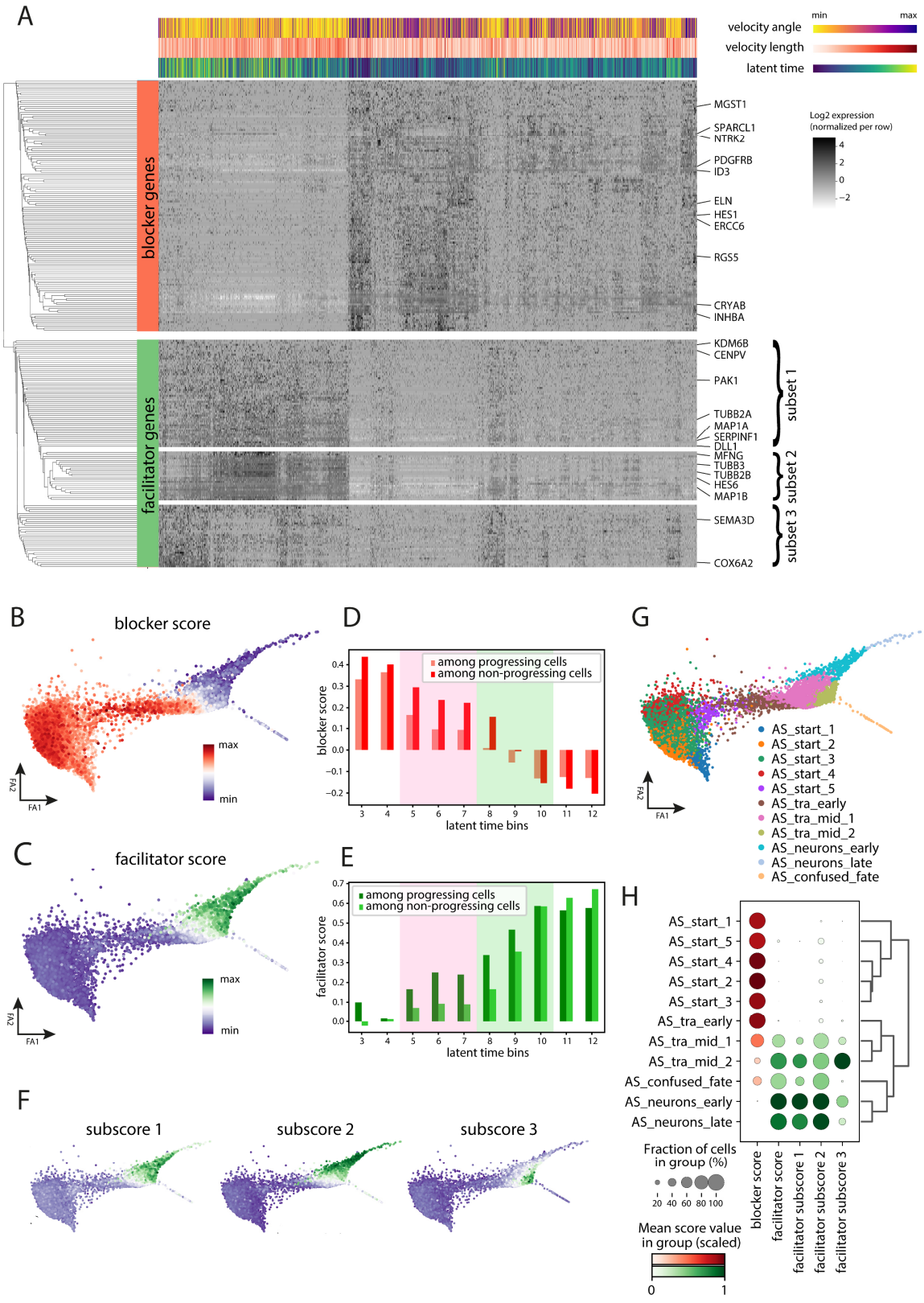

Figure 8 | Blocker and facilitator genes are expressed in an opposing manner along the trajectory. (**A**) Hierarchically clustered heatmap of all blocker (125) and facilitator (108) genes (rows) and all cells in latent time bins 5-10 (columns) of AS-transduced cells. Gene expression (Log2) is shown normalized per row. Genes are

ordered by expression similarities depicted in a hierarchically clustered dendrogram (similarity distance shown by length of branches). Only selected genes are indicated. Cells are ordered by similarities in their facilitator and blocker gene expression profiles. For each cell, the bars on top of the heatmap display the velocity angle (yellow: small velocity angle, cellular dynamics follows the reprogramming trajectory; dark blue: large velocity angle, cellular dynamics oppose the reprogramming trajectory), the velocity length (white: small velocity arrow, no cellular dynamics; dark red: large velocity arrow, highly dynamical transcriptomics), and latent time (dark blue: early in latent time, green->yellow: late in latent time). Facilitator genes can be distributed into three subsets based on their expression profiles. (**B**) Blocker and (**C**) facilitator score visualized on the embedding. Scores were calculated as the average expression of the respective gene set normalized using a randomly sampled reference gene set. (**D**) Blocker and (**E**) facilitator score levels among progressing and non-progressing cells along latent time bins. Latent time bins before (magenta background) and after (green background) the decision point are indicated. (**F**) Facilitator subscores, calculated from the respective facilitator gene subsets, visualized on the embedding. (**G**) Leiden clustering of the embedding, with 11 clusters each containing transcriptionally similar cells. (**H**) Dot plot of blocker and facilitator scores including facilitator subscores for all clusters. Brightness indicates the score level, scaled to each score's maximum expression over all clusters. Dot size depicts the fraction of cells that have a positive score. Dendrogram shows the transcriptional similarities between the clusters.

To get a generalized view on the expression of both facilitator and blocker genes in our dataset, we generated scores of their average expression for all cells. Blocker and facilitator score appeared to be inversely proportional to each other, with similar expression in the mid trajectory (**Figure 8B, C**). Strikingly, this revealed an important difference between the two populations distant from the starting population: While the highly *TUBB3*+ upper population in the main trajectory also had a high facilitator score and low blocker score, the lower, rather disconnected population exhibited intermediate levels of both blocker and facilitator score, denoting that the latter population was not progressing towards iNs and remained in a rather 'confused' state.

Remarkably, progressing cells showed a lower blocker score than non-progressing cells already before the decision point (**Figure 8D**). Similarly, the facilitator score of progressing cells was continuously higher than the score of non-progressing cells during the whole decision point in latent time (**Figure 8E**). These findings supported the velocity difference as the determining factor in the identification of facilitator and blocker genes.

To further investigate the three identified facilitator gene subsets, we generated individual expression scores (**Figure 8F**). While subscore 1 and 3 seemed to be only transiently expressed, subscore 2 remained on a high level until the end of the trajectory. Whereas the distribution of subscore 1 and 2 on the embedding appeared rather similar, subscore 3 was mainly expressed in a small indentation along the trajectory.

To identify subpopulations in our dataset, we used Leiden clustering (Traag et al., 2019), identifying 11 clusters (**Figure 8G, Table 2**). The five starting clusters were identified by their colocalization with GFP-transduced cells, the neuronal clusters by their high *TUBB3* expression. The less *TUBB3*+ cluster that was disconnected from the main trajectory with mixed blocker and facilitator scores we termed 'confused fate'. On the trajectory, an 'early' cluster as well as two 'mid' clusters were found, AS_tra_mid_2 colocalizing with the high subscore 3 expression.

Using this the identified clusters enabled us to get a more systematic view on the blocker score, the facilitator score as well as its subscores (**Figure 8H**). The blocker score remained high in the starting population and the early trajectory, then rapidly decreased from AS_tra_mid_1 to AS_tra_mid_2 and disappeared completely in late neurons but not in confused fate. The facilitator score expression was vastly driven by subscores 1 and 2, while subscore 3 was mostly found in AS_tra_mid_2, and to a particularly lower extent in AS_tra_mid_2 and neurons. This led us to see only subscores 1 and 2 as "true" facilitator scores. Interestingly, despite the proximity on the embedding of AS_tra_mid_2 and confused fate, subscore 3 was almost not expressed in confused fate, indicating that these populations are more different. This was also supported by the finding that these clusters were separated by several nodes in the hierarchically clustered dendrogram (**Figure 8H**).

3.1.5 Characterizing subpopulations along the trajectory

We then went on investigating transcriptomic differences between the experimental clusters as specified in **Figure 8G**. DE analysis showed the most differentially expressed genes for each cluster (**Figure 9A**). Notably, in particular in the starting clusters, many genes did not appear to be exclusively expressed in a single cluster but rather in several or even all starting clusters, with decreasing levels from starting population to the early and mid trajectory, e.g. the collagen-coding gene *COL1A1* and the extracellular matrix protein-coding gene *FN1* (fibronectin). Interestingly, among the genes differentially expressed in the AS_start_5 cluster, which was the closest starting population cluster to the early trajectory, the TGFβ signaling target genes *ID1* and *ID3* were upregulated. The early trajectory was defined among others by the expression of two members of the *S100* gene family, involved in the regulation of cell cycle progression and differentiation, which we

also identified as blocker genes. The AS_tra_mid_1 cluster was characterized among other genes by *SLC12A2*, which is involved in maintaining proper ionic balance and cell volume, suggesting also morphological changes occurring at this point. *RBP1*, which is involved in regulation of the vitamin A metabolism that is vital to nervous system generation (Toresson et al., 1999), was observed to be upregulated from cluster AS_start_5 on, reaching its maximum in late neurons. *RBP1* levels were comparably lower in the AS_tra_mid_2 cluster, which was defined among other genes by *ASAH1*, which is involved in fatty acid metabolism. The histone-coding gene *H3-3A* was increasing in expression from start to neuron and confused clusters. Early neurons expressed elevated levels of *MAP1B*, responsible for microtubule assembly in neurogenesis. While early and late neurons were similar in their marker gene expression, cells of the confused fate cluster were characterized by expression of the cell adhesion protein-coding gene *LGALS3* and the metabolism gene *GDE1*, which were absent in the neuronal clusters.

After this unbiased approach, we specifically looked for known cellular identity markers (**Figure 9B**). We could show that the pericyte marker *RGS5* was widely expressed in the starting population and disappeared in the early trajectory, similar to *ANPEP*, the gene coding for the pericyte marker *CD13*. The pericyte marker *CD146* (*MCAM*) was expressed only in a minor fraction of cells on the starting population and early trajectory. *LEPR*, which was found to be expressed in pericytes less amenable to AS-mediated conversion into iNs by Karow et al. (2018), was expressed in a part of the starting populations as well as a part of the mid trajectory. Confirming the neuronal identity of the target population, the neurogenic factors *ASCL1* (not the ectopically expressed *Ascl1*) and *NEUROD4* were found in few cells between early and late neurons, whereas the other important neurogenic factor *NEUROG2* was more widely expressed throughout neurons, while none of these genes were found in confused fate. *PROX1*, a key player in neurogenesis which is regulated by NOTCH signaling (Kaltezioti et al., 2010), was found highly expressed in the neuronal clusters.

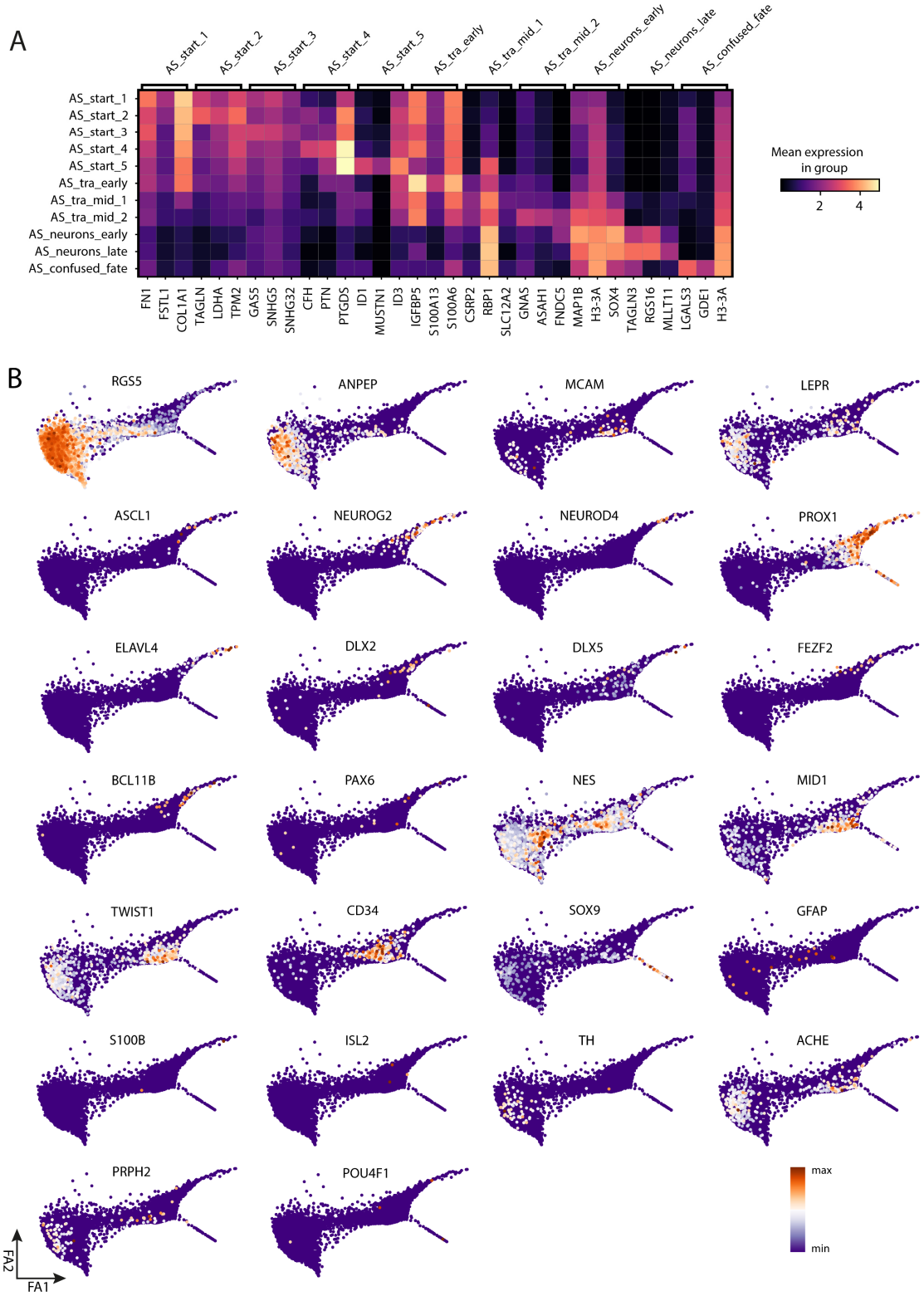

Figure 9 | Various markers characterize cellular identities along the trajectory. (**A**) Heatmap of the mean expression values of the top 3 upregulated genes in each cluster vs. all other clusters. DE was performed as a Wilcoxon rank-sum test, filtered for minimum expression in a fraction of 0.2 per group, a log fold change of 1, and p-value (adjusted using Benjamini-Hochberg correction) <0.05. (**B**) Expression of selected marker genes visualized on the embedding. Color scale is scaled between individual min/max levels.

The result that the postmitotic neuron marker *ELAVL4* was only found in cells at the end of the trajectory, indicated that even the late neurons were not fully mature yet, which would not be expected at d14. With the GABAergic neuron markers *DLX2* and *DLX5* in a fraction of cells in the neuronal clusters, it could be shown that different kinds of neurons were being generated after reprogramming. While the cortical layer V marker gene *BCL11B* (*CTIP2*) was found in neurons and the telencephalic region progenitor marker *FEZF2* was expressed between early and late neurons, the neural progenitor markers *PAX6* was only rarely found, suggesting that the intermediate state in direct reprogramming does not rely on this classical neurogenesis regulator. In contrast, the neural progenitor gene *NES* (coding for Nestin) was highly upregulated between the starting population and early trajectory. Also *MID1*, which plays an important role in CNS development (Baldini et al., 2020), could be observed on the trajectory. In the mid trajectory, we also saw the neural crest marker *TWIST1* and the progenitor marker *CD34* expressed, but not in neurons or confused fate.

Since we found the confused fate cluster marked by the TF-coding *SOX9*, which is involved in various developmental processes and also found in astrocytes, we additionally checked the expression of astrocytic markers *S100B* and *GFAP*, none of which was expressed in the confused cell population, and only in very few other cells.

To exclude that the confused fate cluster represents a different class of neurons, we investigated several potential lineages. The spinal cord marker *ISL2* was almost not expressed at all and not in the confused fate cluster. The dopaminergic neuron marker *TH*, the cholinergic neuron marker *ACHE*, the retinal neuron marker *PRPH2* and the peripheral neuron marker *POU4F1* were not specifically expressed in either neuron or confused clusters.

Thus, we concluded that while the neuronal clusters resemble existing neuronal identities, the confused fate cluster identity remained elusive and seemed to convey traits of multiple identities.

3.1.6 Lineage determination confirms terminal identity of mid trajectory

With the observation of distinct transcriptional identities along the trajectory, the question arose which ones of the cellular reprogramming outcomes were terminal and if it was possible to identify the fate an individual cell on the trajectory was most likely to assume eventually. To investigate the cellular dynamics of AS-transduced cells regarding these issues, we made use of the Cellrank package (Lange et al., 2022), which allows for single cell fate mapping by utilization of various single cell data like transcriptomics, velocity, and pseudotime, additionally taking velocity uncertainties into consideration.

Strikingly, application of CellRank revealed six terminal cellular identities in AS-transduced cells (**Figure 10A, B**): A large fraction of cells remained in the starting population or returned there from the early trajectory, as shown by velocities as well. Therefore, also the starting population itself was considered terminal for many cells. As we knew that different neuronal subtypes existed, but most neurons were rather immature at the time points of the experiment, it was not surprising that only few cells in the late neuron cluster belonged to either neurons type 1 or neurons type 2, which were different neuronal lineages identified with the CellRank algorithm. Most cells from the neuronal clusters, however, also had high absorption probabilities for this early neuron fate, meaning that cells reaching the early neurons state were unlikely to revert to an earlier state.

Interestingly, the highest absorption probabilities towards confused fate on the main trajectory were not found in the indentation of the AS_tra_mid_2 cell population but rather earlier during early AS_tra_mid_1 cells (**Figure 10B**), prompting the conclusion that the cellular decision to become confused is taken before the decision to become neurons. Still, the absorption probabilities suggest that both decisions are taken during the trajectory, not yet in the starting population.

The most intriguing finding was, however, that cells on the trajectory did not only have the possibility to return to the starting population fate, to proceed towards confused fate or different neuronal fates but instead may also have had the mid trajectory as their terminal identity. This suggested that many cells initially entering the path between the

starting population and neurons were getting stuck midway. The highest absorption probabilities for this fate were found in the AS_tra_mid_2 cluster, which might also explain the different facilitator genes marking progressing cells in this cluster.

The patterns of absorption probabilities were also reflected in each individual cell's connections (**Figure 10C**). We scored cells by the strength of their connections, indicating their similarities to neighboring cells. There we could show that while early neurons and AS_tra_mid_2 clusters were well connected to their surrounding cells, the confused fate population seemed only sparsely connected to the main trajectory, suggesting that the transition towards this terminal fate is less smooth than the transition towards the other fates. The connection scores further confirmed that fate decision towards confused fate was taken prior to the decision to become neuronal.

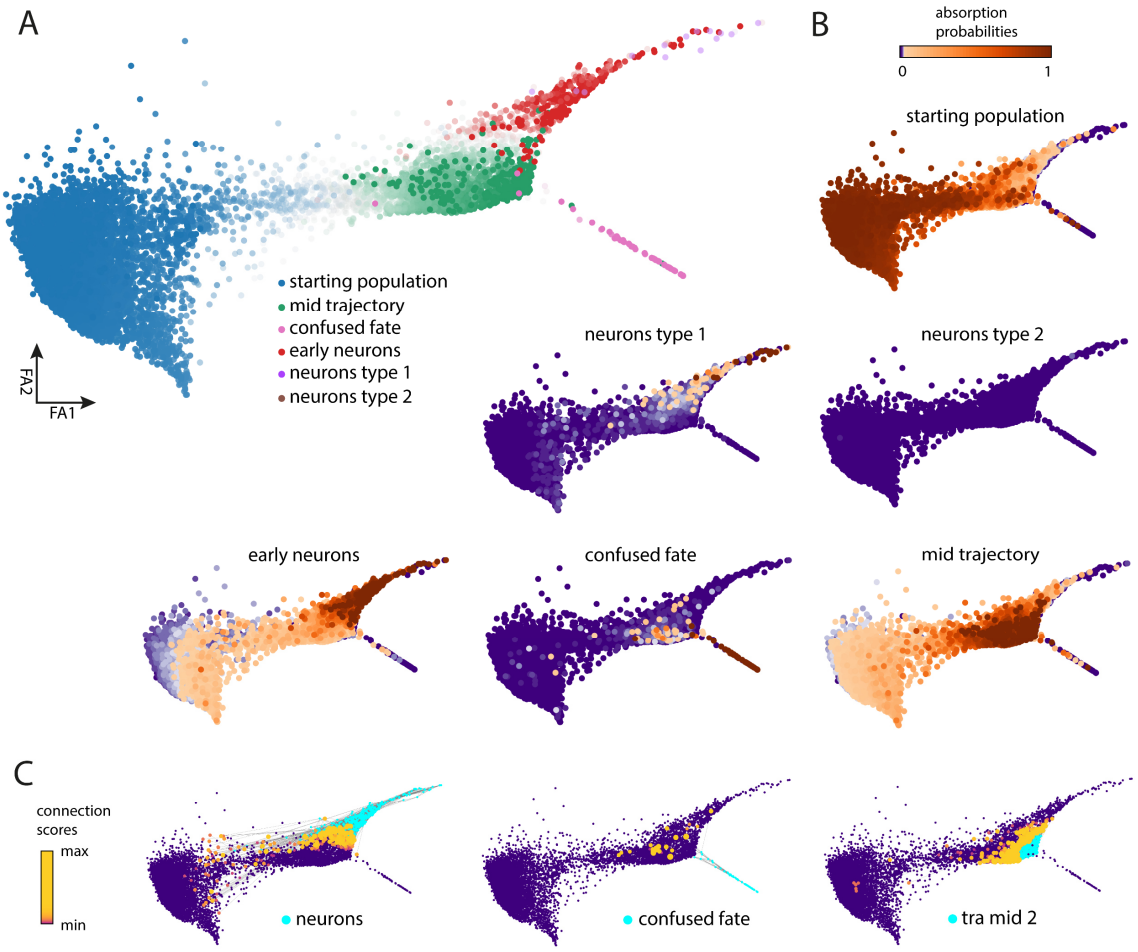

Figure 10 | Determination of different terminal states along the trajectory. (**A**) Combined CellRank (Lange et al., 2022) plot of the absorption probabilities of all identified terminal states. The color depicts the terminal state with highest absorption probability for a particular cell, the alpha value is indicative of the magnitude of the

absorption probability (pale color: low absorption probability; bold color: high absorption probability). (**B**) Individual CellRank plots of the absorption probabilities of all identified terminal states. Color scale depicts the magnitude from 0 (no absorption; blue) to 1 (highest absorption; brown). (**C**) Connection scores marking neurons, confused fate, and AS_tra_mid_2 clusters (cyan), and indicating all cells that are directly connected (and therefore similar) to them. Visualization of the connection by color scale and size ranging from blue and minimum size (no connection) to yellow and maximum size (highly connected). A non-linear color scale was used to improve perception of cells with low connection scores. Connections, if present, between cells of the respective cluster and any other cell are depicted by a grey line between these cells.

3.1.7 Increased NOTCH and TGF-β signaling during mid trajectory lineage

After discovering that many cells did not progress during mid trajectory, we went on to elucidate if this corresponded to changes in gene expression comparing the lineages recovered by CellRank. These gene trends, which were also generated using CellRank, showed a highly diverging NOTCH (**Figure 11A**) and TGF-β (**Figure 11B**) signaling between the fate maps.

In particular, comparing gene expression in mid trajectory to early neurons along the trajectory, the gene trends of several NOTCH and TGF-β signaling genes were transiently (*HEY1*, *NOTCH2*, *ID1/4*) or terminally (*SMAD2/3*, *ATF3*) significantly upregulated, while others were significantly downregulated (*HES1*, *SMAD7*, *ID2*), not upregulated (*HES4*) or insufficiently upregulated (*HES6*) or downregulated (*ID3*). All these gene expression trends aberrant in the mid trajectory lineage compared to the early neuron lineage suggested a direct or indirect involvement of NOTCH and TGF-β signaling in the reprogramming process.

Additionally, we showed that several NOTCH (*HEY2*, *HES1/6*) and TGF-β signaling targets (*ID1/2/3/4*, *VEGFA*, *CDKN1A*, *SERPINE1*) were differentially regulated in confused fate lineage compared to early neurons, which was indicative of a contribution of NOTCH and TGF-β signaling in the decision to become confused. Moreover, other NOTCH (*HES1*) and TGF-β signaling genes (*AHR*, *SERPINE1*, *TGFB1*) were upregulated in the starting population lineage while they were downregulated in all other lineages, probably representing a molecular barrier for cells to leave the starting population. The neuronal subtypes also exhibited differences regarding NOTCH (*HES1*, *HEY2*, *NOTCH2*) and TGF-β signaling (*ID1/3*, *SMAD2*, *SERPINE1*, *TGFB1*), with gene expression levels significantly

higher in neurons type 2 lineage than in neurons type 1. This suggested that also subtype specification might involve these two signaling pathways.

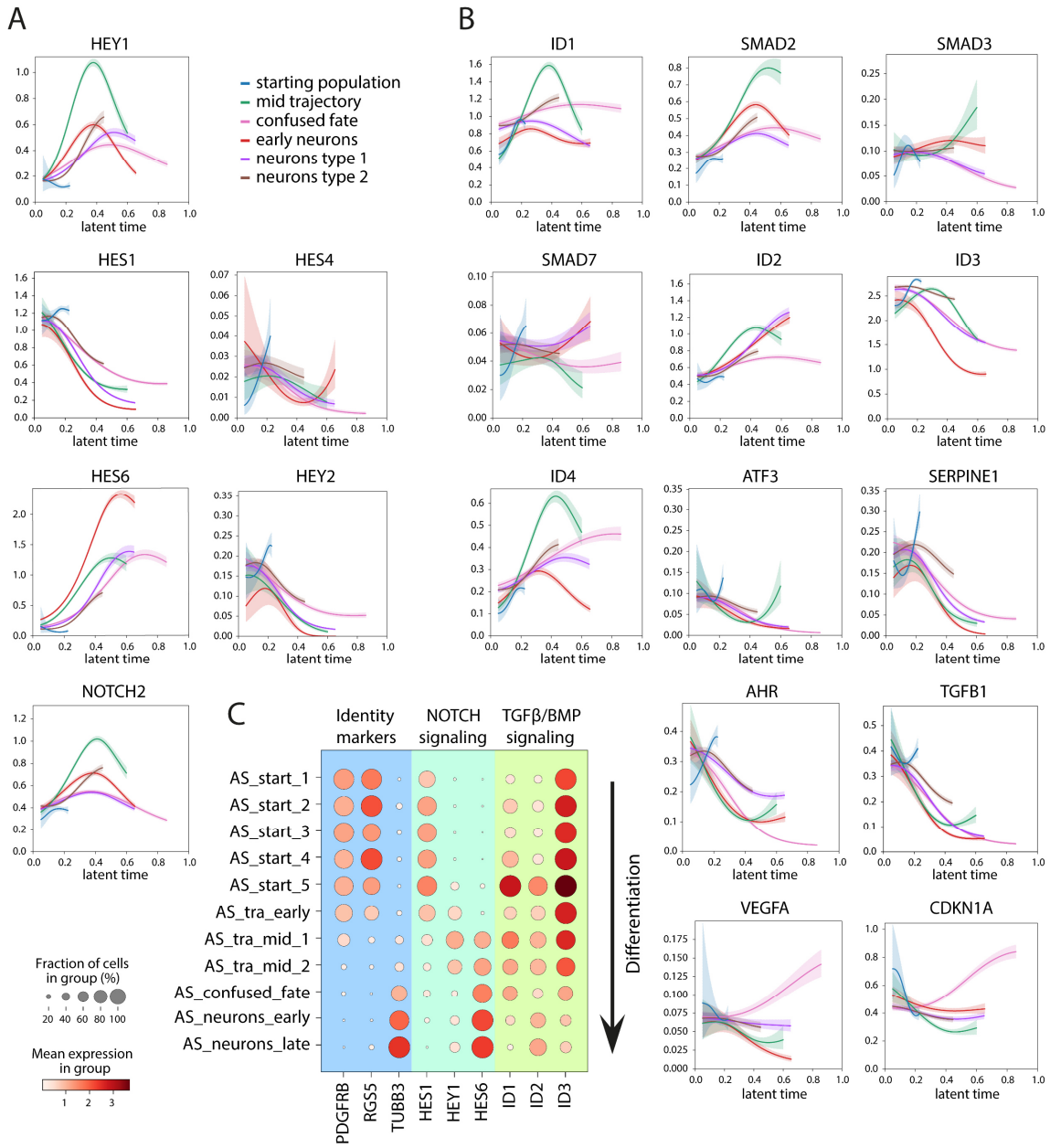

Figure 11 | High NOTCH and TGF-β signaling in cells with a terminal mid trajectory fate. (**A**) Gene trends of several NOTCH signaling genes. Gene expression is visualized for all lineages along latent time. Lineage confidence interval > 0.95. (**B**) Gene trends of several TGF-β signaling genes. Gene expression is visualized for all lineages along latent time. Lineage confidence interval > 0.95. (**C**) Dot plot showing the average gene expression per cluster for selected NOTCH targets and TGF-β signaling targets. Cellular identity change from pericytes (*PDGFRB*, *RGS5*) to neuronal identity (*TUBB3*) is depicted for scale of the general direction of the cellular differentiation (see black arrow). Color scale ranges from white (no expression) to red (high expression). The fraction of cells per cluster expressing the gene is visualized by dot size.

The distinct expression patterns of TGF-β/BMP and NOTCH targets could also be confirmed by their expression in the previously identified clusters (**Figure 11C**): While *HES1* was expressed in the starting clusters, it was expressed less distinctly along the trajectory, which seemed to be a precondition to proceed on the reprogramming path. *HEY1* showed a transient expression mainly during early and mid trajectory, which confirmed its definition as a "switch gene" by Karow et al. (2018). *HES6* seemed to be expressed in a contrasting way to *HES1*, being upregulated only after pericyte genes have declined. *ID1* and *ID3* were also downregulated in the early trajectory but while *ID1* was decreasing in neurons, *ID2* remained high and only decreased in confused fate. *ID3* was downregulated from the early trajectory on but only dropped distinctly once *TUBB3* was expressed. Overall, we saw a highly dynamical NOTCH and TGF-β pathway regulation.

3.2 Modulation of signaling pathways alleviates conquest of reprogramming barriers

3.2.1 Reprogramming trajectories are changed upon inhibition of NOTCH and TGF-β signaling

As our experiments showed the importance of NOTCH and TGF-β signaling in the process of direct AS-reprogramming from pericytes into iNs, we concluded that inhibition of these pathways might be sufficient to improve the reprogramming process, leading to more cells becoming iNs and fewer cells assuming a terminal mid trajectory or confused identity. Since DAPT (Geling et al., 2002) has been shown to efficiently inhibit Notch signaling, while SB431542 (SB) and Dorsomorphin (DM) (Kim et al., 2010) inhibits TGBF/BMP signaling via dual SMAD inhibition, we designed an experiment (**Figure 12A**), in which we applied these small molecules to AS-transduced cells on d1, d3, and d5 after transduction. We confirmed reprogramming to iNs via immunostainings for the neuronal marker TUBB3 (**Figure 12B, C**), while we could not detect TUBB3 expression in cells without AS transduction that had not been treated with small molecules (data not shown). With both DAPT and SB/DM treatments, iNs appeared to have longer axons and a more complex morphology than without small molecule treatment.

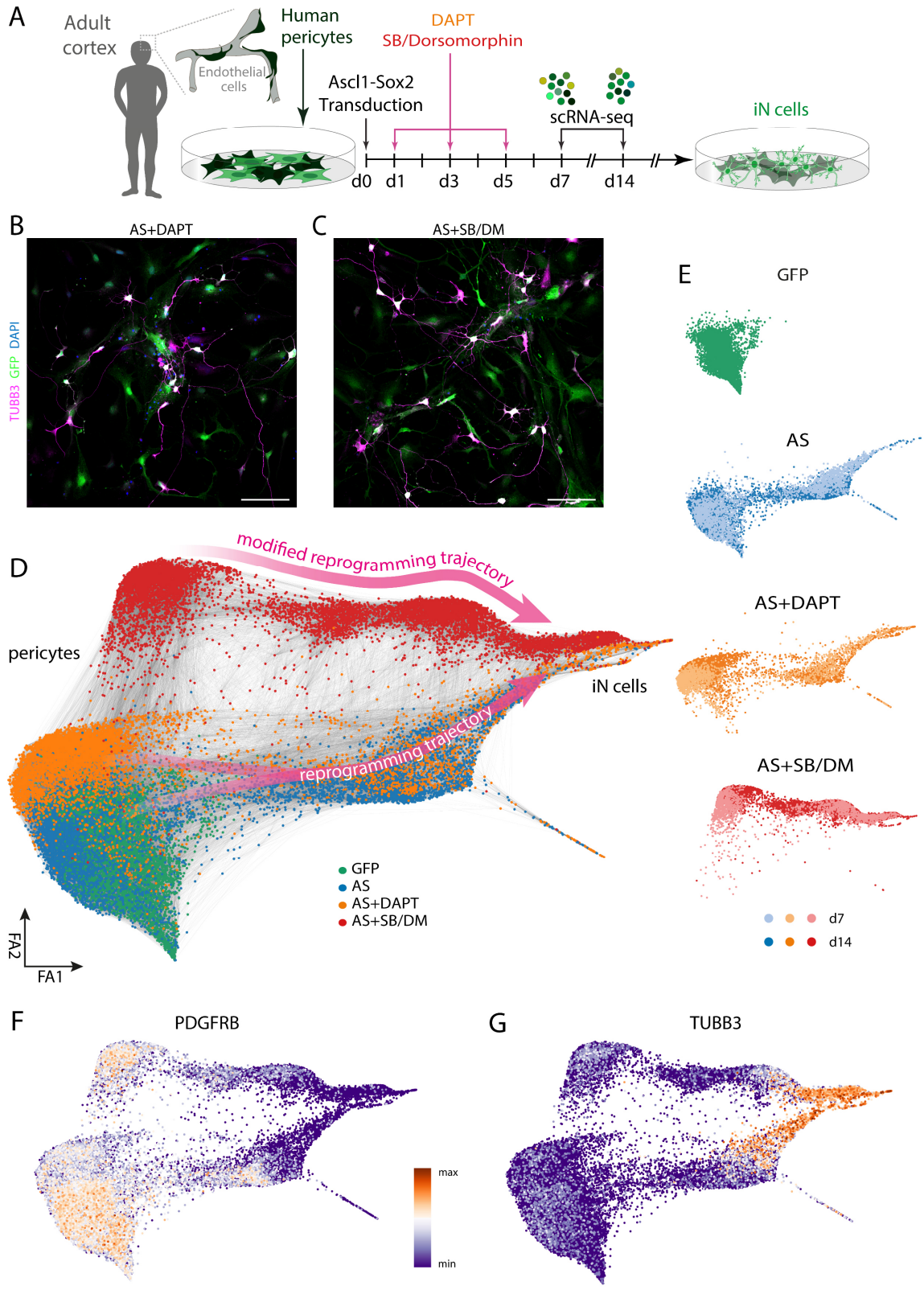

Figure 12 | Modulation of NOTCH and TGF-β signaling pathways during reprogramming affects starting populations and the trajectory. (**A**) Schematic of the experimental design: Cultured brain pericytes derived from adult human patients were retrovirally transduced to express Ascl1 and Sox2 (AS) with GFP as an expression

control. On d1, d3, and d5 after transduction, the NOTCH inhibitor DAPT (10 µM) or the SMAD signaling inhibitors SB431542 (10 µM) and Dorsomorphin (DM; 1 µM) were added to the culture medium. On d7 and d14 after transduction, cells were FAC sorted for GFP expression and GFP+ cells were used for single cell transcriptomic analysis using the 10x Genomics system. (**B,C**) Representative image of successfully reprogrammed pericytes 28 days after transduction, treated with (**B**) DAPT or (**C**) SB/DM: immunostained for neuronal cells (TUBB3, magenta), AS-transduced cells (GFP, green) and nuclei (DAPI, blue) are visible. Scale bars, 50 µm. (**D**) Transcriptome data was analyzed using Scanpy (Wolf et al., 2018). Force directed graph was used to visualize 6170 AS-transduced and DAPT treated cells (yellow) (d7: 1722 cells, d14: 4448 cells) and 7701 AS-transduced and SB/DM treated cells (red) (d7: 1751 cells, d14: 5950 cells), together with the previously analyzed 8259 AS-transduced cells (blue) and 5382 GFP-transduced control cells (green) in a 2-dimensional embedding. Each dot represents one cell and their order represents their similarity. The pericytic AS+DAPT starting population is slightly shifted, while the trajectory is mostly identical to that of untreated AS-transduced cells. AS+SB/DM starting population is completely separate from that of untreated AS-transduced cells, subsequently following a likewise separate trajectory towards an overlapping target cell population of treated and untreated AS-transduced cells. Grey lines between the cells indicate the 20 closest neighbors of each cell over all dimensions used in the embedding. (**E**) Embeddings shown separately for each experimental condition with color indicating the two experimental timepoints in AS-transduced cells. The smaller d7 cell batch is plotted on top of d14 cells to improve its visibility. (**F**) *PDGFRB* as a pericyte marker is expressed mostly in the starting populations of all treatments and its expression declines during the trajectory. (**C**) *TUBB3* as a neuronal marker is shown to be upregulated during the trajectory of all treatments towards the neuronal fate.

We analyzed the transcriptomes of a filtered total of 27512 cells, of which 6170 were AS-transduced and DAPT treated cells (AS+DAPT, experimental timepoints d7: 1722 cells, d14: 4448 cells), 7701 were AS-transduced and SB/DM treated cells (AS+SB/DM, experimental timepoints d7: 1751 cells, d14: 5950 cells), and including the previously analyzed AS-transduced cells (AS) and GFP-transduced control cells (GFP) (**Table 1**). In a force-directed graph, we could show that both treatments led to significant changes in the trajectory (**Figure 12D**), however we saw a great difference between the treatments. For AS+DAPT cells in comparison to AS cells, only the starting population seemed to be shifted in the embedding with only little overlap (and therefore similarity) to AS cells, while a large majority of the cells that had left the starting population towards iNs took the same route as AS cells. In contrast, AS+SB/DM cells were not only embedded very distant from AS cells (indicating high transcriptional differences) in the starting populations but continued to be very distant during the most part of their modified reprogramming trajectory. Most strikingly, despite them taking a completely distinct route, AS+SB/DM cells still ended up in the same location on the embedding as iNs from AS.

Visualization of the experimental timepoints of the treatments showed that for large parts of the trajectories, cells of both d7 and d14 could be found, indicating that reprogramming is a stochastic process (**Figure 12E**). In addition, in each treatment's

embedding both for the starting population and the trajectory some locations seemed to accumulate cells at d14, suggesting these cells to be non-progressing towards iNs.

Interestingly, despite the different starting populations of AS, AS+DAPT and AS+SB/DM, the cells in all starting populations were expressing *PDGFRB*, which was lost shortly after the cells entered the trajectory towards iNs (**Figure 12F**). On the neuronal end, all treatments generated similar highly *TUBB3*-expressing cells (**Figure 12G**). The formation of a second iN cell tip again suggested a heterogeneity in the resulting neurons.

3.2.2 Successful modulation of NOTCH and TGF-β signaling upon small molecule treatments

To confirm that our treatments worked, we looked at the NOTCH signaling targets *HES1* and *HES5* (**Figure 13A**) and the TGF-β signaling targets *ID1* and *SERPINE1* (**Figure 13B**). We could confirm a strong downregulation of *HES1* after in AS+DAPT compared to AS, as well as a strong decrease in *HES5*+ cells. *ID1* and *SERPINE1* were expressed at lower levels in AS+SB/DM than in the AS condition. Interestingly, *ID1* and *SERPINE1* expression was also downregulated in AS+DAPT compared to AS, indicating a crosstalk effect between both pathways.

To detect other effects of signaling modulation on global gene expression, we used DE analysis of all cells of each treatment vs. all other treatments (**Figure 13C**). We showed that both AS+DAPT and AS+SB/DM led to a downregulation of the pericyte marker *RGS5*, of several collagen family members (*COL3A1*, *COL1A1*, *COL18A1*, *COL8A1*), and the NOTCH target *ID3*. We further found that *LDHA*, which is involved in glycolysis (**Table 3**), was downregulated upon either DAPT or SB/DM treatment, as well as the stress response gene *GADD45B*.

AS+DAPT cells in turn exhibited an increase in the cytoskeleton marker *VIM* and metabolic genes *PLTP* and *AKR1C1*. AS+SB/DM cells expressed the highest levels of lipid metabolism genes *SCD*, *NPC2* and *INSIG1*. Both AS+DAPT and AS+SB/DM upregulated expression of the growth factor *MDK*. Hence, we suggest an individual and a convergent action of the modulations of the NOTCH and TGF-β pathways.

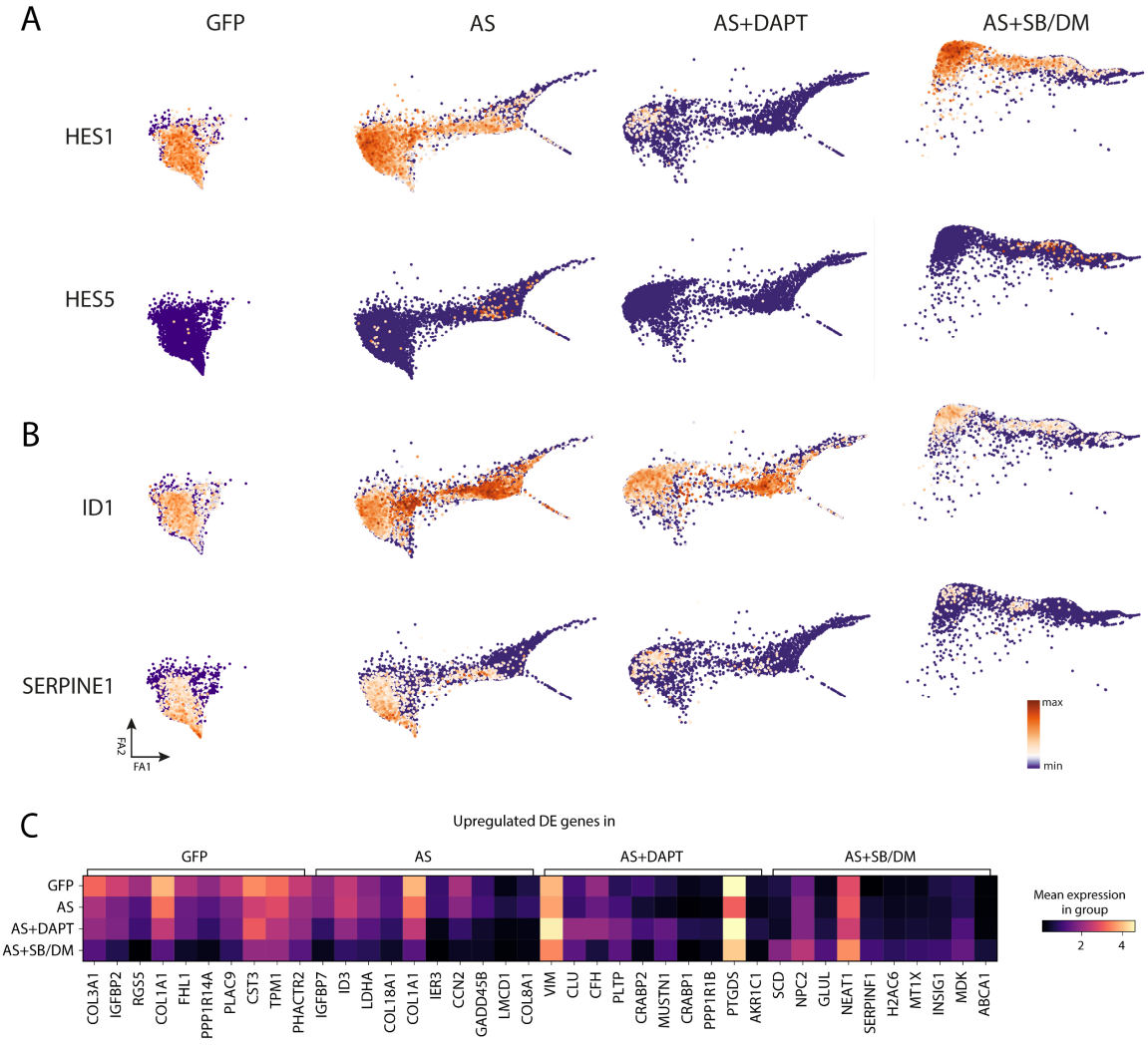

Figure 13 | Verification of NOTCH and TGF-β pathway modulation. (**A**) Embedding separated by treatment with NOTCH target genes *HES1* and *HES5* expression depicted by color scale. (**B**) Embedding separated by treatment with TGF-β/BMP target genes *ID1* and *SERPINE1* expression depicted by color scale. (**C**) Heatmap of top 10 DE average gene expression per treatment. DE results of a Wilcoxon rank-sum test, filtered for minimum expression in a fraction of 0.2 per group, a log fold change of 1, and p-value (adjusted using Benjamini-Hochberg correction) <0.05.

3.2.3 Different trajectories comprise similar segments

Since AS cells and AS+SB/DM cells followed different trajectories, we intended to match sections of both trajectories in order to investigate if they exhibited similar patterns, e.g. an NSC-like state. To achieve this, we clustered the cells of each treatment individually using the Leiden algorithm (**Figure 14A, Table 2**). Then we used asymmetric integration to match each cell of the AS+SB/DM dataset to the clusters defined on the AS dataset. We saw that among the starting population of AS+SB/DM despite their large distance on the embedding, the cells had the highest similarities with the AS start 3 cluster. Cells in the

early trajectory clusters of AS+SB/DM were also mapped to the AS_tra_early cluster. Most cells in the mid trajectory of AS+SB/DM were similar to the mid trajectory of AS; interestingly, they were more similar to AS_tra_mid_1 than AS_tra_mid_2. Among AS+SB/DM neurons, we reported a high match with AS neurons, although many neurons of type 1 seemed rather similar to AS neurons early, suggesting that these were still less mature. Notably, the neurons of type 2 generated with AS+SB/DM completely matched with AS neurons early instead of AS neurons late, indicating that these were already more differentiated from the common parent identity of early neurons. Confused fate cells of the AS+SB/DM dataset were matching confused fate cells of the AS dataset.

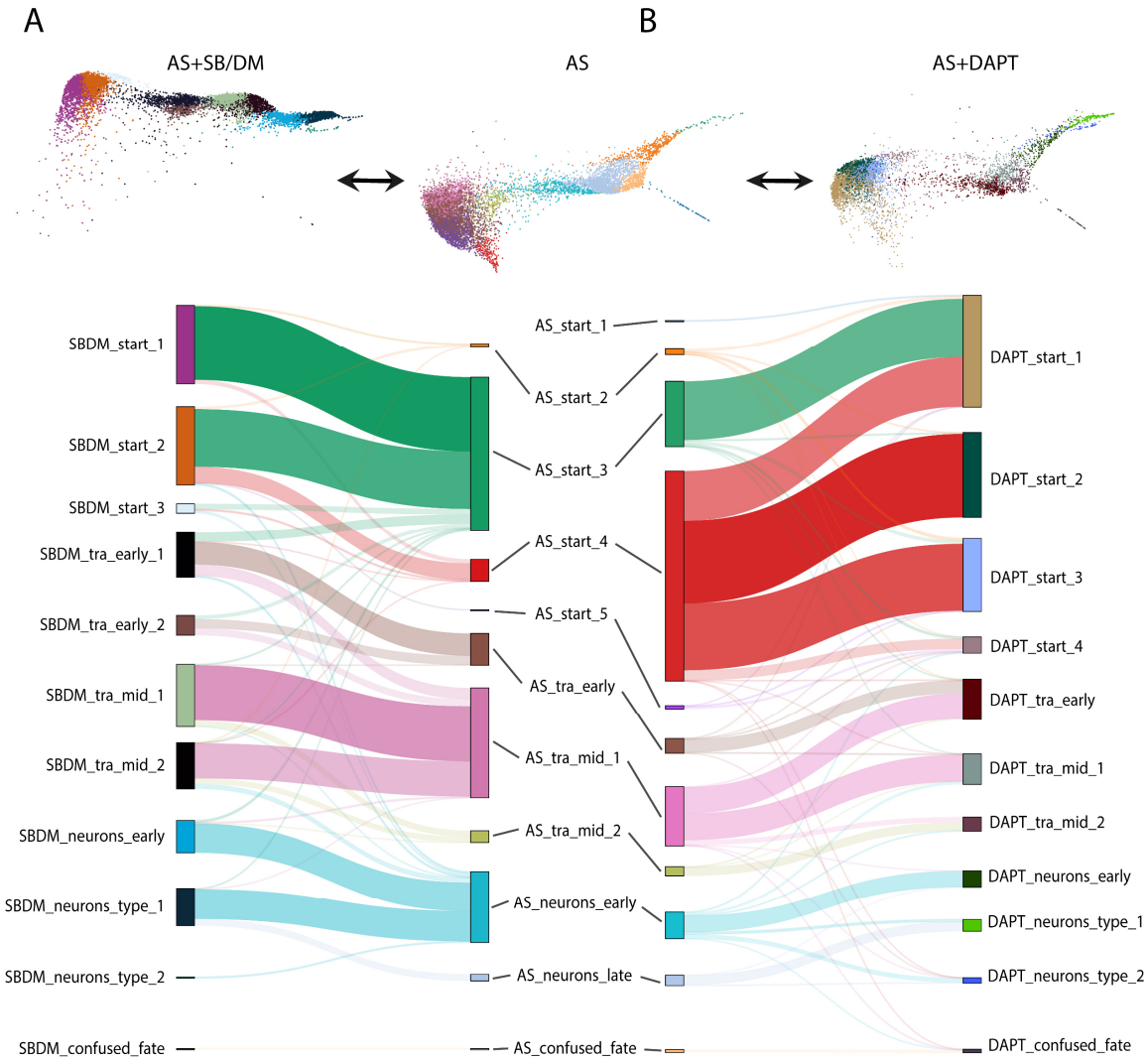

Figure 14 | Modified trajectories can be mapped onto AS trajectory. (**A**) Sankey plot of the clusters defined on the AS+SB/DM dataset compared with those defined on the AS dataset. Separated embeddings with individual cluster assignment are shown above. Nodes on the left of the Sankey plot depict cells belonging to a particular

AS+SB/DM cluster, nodes on the right depict the same cells asymmetrically mapped to AS clusters. Links indicate the classification of cells after mapping, with only links consisting of at least 3 cells shown. Differences in cellular contributions are depicted by diameter and alpha levels of the links. Node colors represent the colors of the respective clusters, link colors represent the mapped AS cluster identity. (**B**) Sankey plot of the clusters defined on the AS+DAPT dataset compared with those defined on the AS dataset. Separated embeddings with individual cluster assignment are shown above. Nodes on the right of the Sankey plot depict cells belonging to a particular AS+DAPT cluster, nodes on the left depict the same cells asymmetrically mapped to AS clusters. Other plot attributes according to (A).

Although the trajectory of AS cells and AS+DAPT cells was highly overlapping, we had found that their starting population is different. Therefore, we applied the same asymmetric integration approach to the clusters defined on the AS+DAPT dataset (**Figure 14B, Table 2**). For the starting clusters of AS+DAPT, we still saw cells matching with AS start 3, however the majority of cells in the AS+DAPT starting populations was assigned to AS_start_4, which showed that the effects of the treatments onto the starting cell identity differed. Interestingly, only a small set of cells treated with DAPT was matched with AS_tra_early, while most DAPT_tra_early cells were more closely related to AS_tra_mid_1, suggesting a faster progression following the DAPT treatment. Neurons generated with AS+DAPT were similar to neurons generated with AS. In contrast to SB/DM_neurons_type_1, most cells in DAPT_neurons_type_1 were matching with AS_neurons_late. Type 2 neurons, which were not separated yet in AS, were again more similar to AS_neurons_early, indicating a transcriptional difference between the neuronal subtypes. Most confused fate cells in AS+DAPT were also assigned to confused fate in AS. Thus, we were able to show that the reprogramming trajectories of all treatments could be segmented in transcriptionally related clusters that follow a similar order.

3.2.4 Cellular dynamics are modulated by NOTCH and TGF-β signaling interference

After investigation of transcriptomic differences and mapping the trajectories modulated by small molecules onto the *AS-only* trajectory, we were further interested how the modulation of the signaling pathways affects the dynamics that we had seen in transcription for untreated AS-transduced cells. Therefore, we used the scVelo package (Bergen et al., 2020) to uncover each individual cell's predicted identity shift (**Figure 15A, B**). Coloring of the cells according to their deviation from the known trajectories from

pericyte to neuronal identity showed that the vast majority of cells in the starting populations would not proceed to enter the trajectory. While AS+DAPT cells did not appear to have notable differences in dynamics compared to AS cells, we find that the AS+SB/DM trajectory was denoted by two phases of high progression interrupted by a phase of non-progression (or even reversion to an earlier fate). Unexpectedly, the proportion of cells that had left the starting population and were progressing was lower in consequence of the treatments than with only AS-transduced cells (**Figure 15C**).

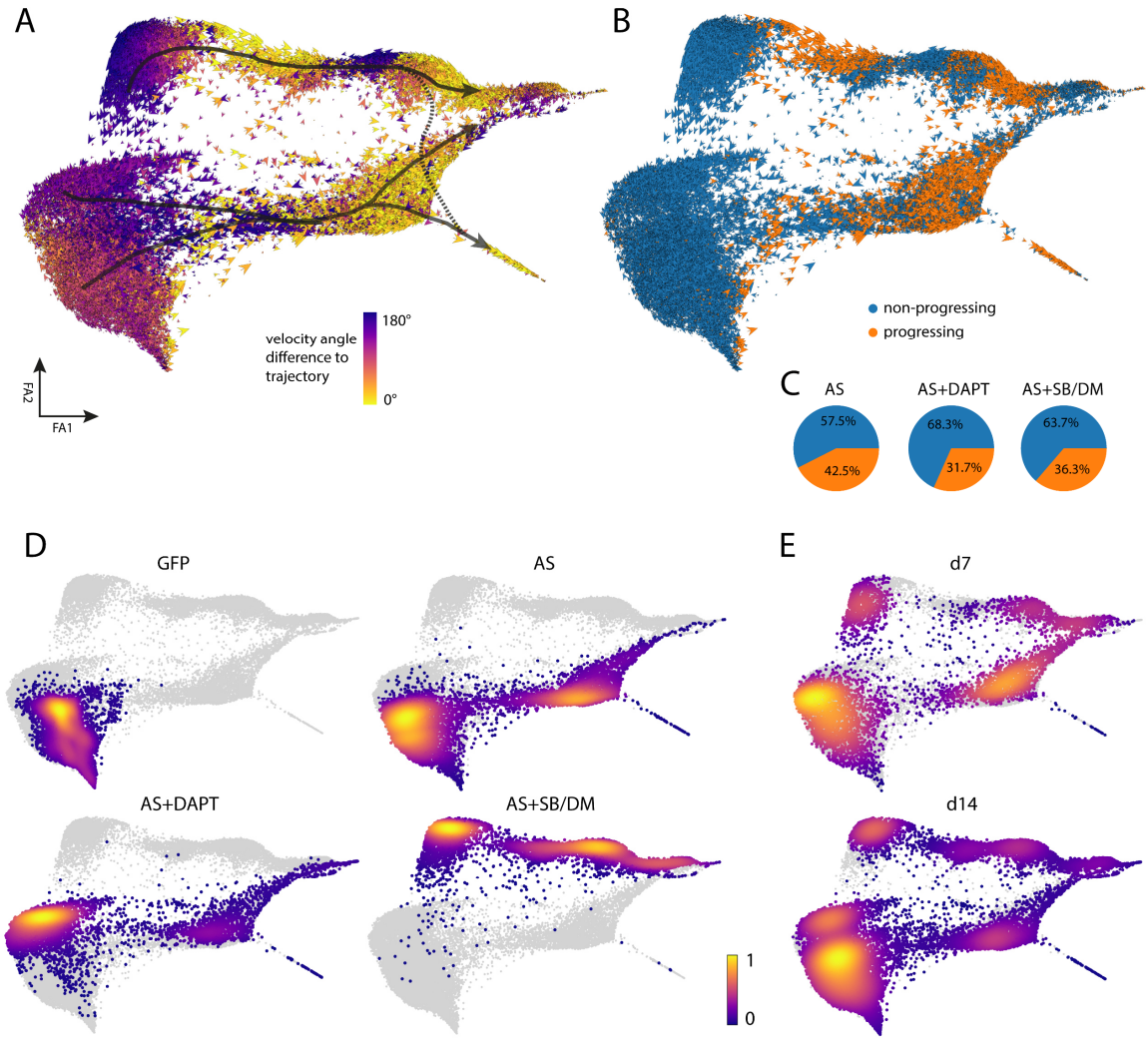

Figure 15 | Velocities and cellular densities differ between the trajectories. (**A**) The force-directed graph including all treatments with velocities calculated by scVelo (Bergen et al., 2020). Arrow directions indicate an individual cell's predicted development based on the most dynamically expressed genes. Arrow size indicates the speed of an individual cell's development. The individual cells' velocity directions are compared to the previously identified reprogramming trajectory (dark grey arrows) and indicated via color scale ranging from 0° difference (the same direction as the reprogramming trajectory) to 180° difference (the opposite direction of the

reprogramming trajectory). (**B**) The same force-directed graph showing progression categories. Individual cells' velocities are categorized based on the velocity angle difference towards the trajectory into progressing cells (orange; less than 30° deviation from the trajectory) and non-progressing cells (blue; more than 30° deviation from the trajectory). (C) Pie chart showing the abundance of cellular progression categories of cells on the trajectory (excluding the starting populations). Colors indicate progressing cells (orange) or non-progressing cells (blue). (**D**) Density plots separated by treatment shown on the embedding. Color scale from purple (sparse) to yellow (dense). (**E**) Density plots separated by experimental timepoint shown on the embedding. Color scale from purple (sparse) to yellow (dense).

This might be attributable to effects that we saw in the density distributions of cells after treatments (**Figure 15D**): While all cells showed a clear peak in the starting population, locations where cells accumulate along the trajectory were changed. We saw the accumulation of cells during mid trajectory that we had found earlier along latent time. However, this peak had almost vanished in AS+DAPT despite its trajectory similarity, indicative of a molecular reprogramming barrier lifted in these cells. In AS+SB/DM, we still found a strong peak on the trajectory, which however appeared to be much more elongated, suggesting a smoother transition of cellular identities along the trajectory instead of a stepwise "peak hopping" behavior. In both AS+DAPT and AS+SB/DM, the density in the iN population was clearly increased compared to AS, which could indicate that since more cells had already reached the target identity, the ones remaining on the trajectory were those types that were also less progressing in AS cells, explaining the lower progression rates after treatments. When looking at the density by experimental timepoints (**Figure 15E**), we found that the outermost tips of the neuronal trajectory were only reached by d14. In addition, we showed that there were not only shifts within the starting populations between d7 and d14 but also shifts of the density peaks on the trajectories. This was particularly notable for AS+SB/DM, where at d7 starting population and trajectory seemed almost disconnected, whereas at d14 we saw more cells with an intermediate identity between those populations, which had likely returned to a more stable state.

3.2.5 Induction of blocker score is part of a safeguarding mechanism for cellular identity

We had identified facilitator and blocker genes associated with progression or non-progression during the AS reprogramming trajectory, respectively. Despite the trajectory

differences, we showed that the facilitator score was expressed in a comparable manner in all treatments (**Figure 16A**). Strikingly, we found the blocker score to be expressed in lower levels along the trajectory of AS+DAPT and AS+SB/DM compared with AS (**Figure 16B**), indicating that these treatments caused reduction of the blocker score rather than increasing the facilitator score. Surprisingly, the blocker score appeared not only higher in AS than in the treatments but even higher in AS than in the GFP control. We further demonstrated that already in the starting populations, this difference was highly significant (**Figure 16C**): The blocker score was upregulated in response to AS-induced reprogramming, suggesting these genes to function as a safeguarding mechanism for the starting cell identity. Treatments help cells to overcome this hurdle and enter the trajectory to become iNs.

To investigate the score levels along the trajectories, we scaled each treatment's latent time values to make them comparable (**Figure 16D**). The comparison of the score trends (**Figure 16E**) revealed that the facilitator score showed highly similar expression dynamics along latent time until the peak. The slope of the facilitator score in AS+DAPT turned out to be steeper, indicating a reason for faster progression on the trajectory which led to the decrease in accumulation during mid trajectory. By contrast, the dynamics of the blocker score along latent time not only confirmed the initial upregulation of the blocker score in relation to the GFP control but also the significant downregulation of the blocker score in both AS+DAPT and AS+SB/DM. Still, the blocker score curves of the treated conditions displayed very similar dynamics as the AS curve. In early latent time, treatment with DAPT and even more with SB/DM reduced the blocker score even below baseline. Interestingly, both treatments shared the same local minimum in blocker score expression. However, fewer cells led to lower confidence in the results during late latent time, while we had shown the earlier effects to be highly significant. Overall, we concluded that the blocker score is a cellular safeguarding response to an attempted identity change via AS and can be effectively downregulated using NOTCH and TGF-β signaling inhibition.

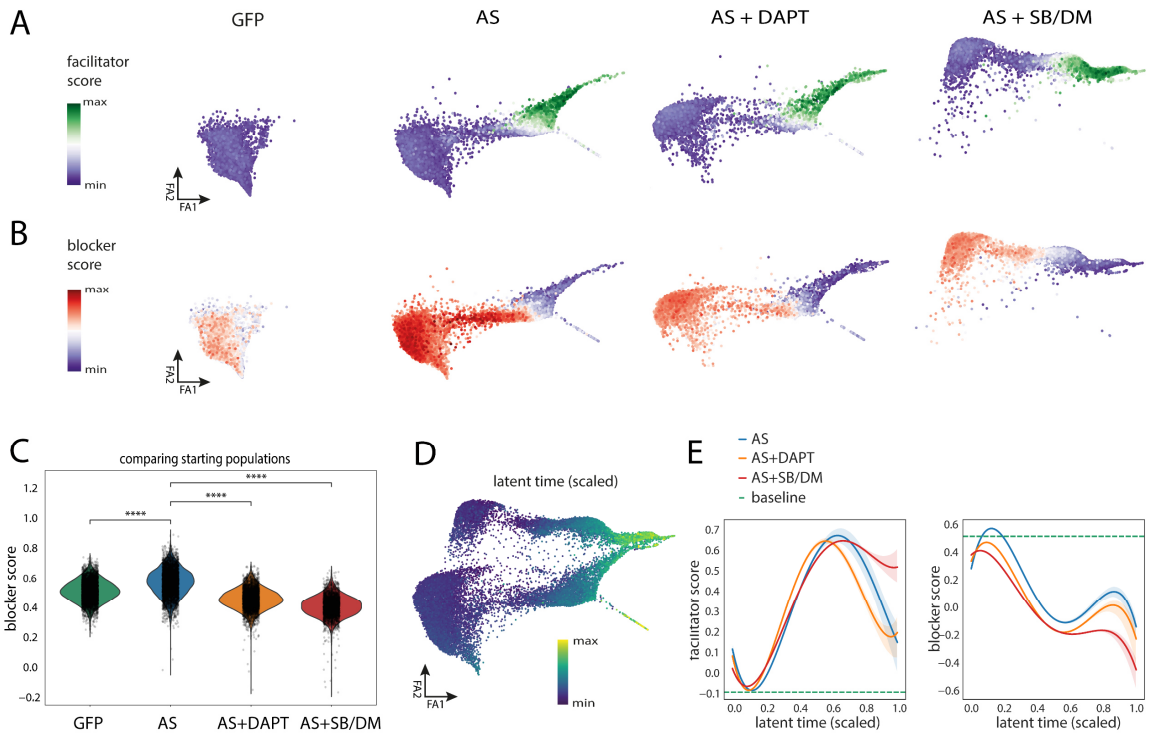

Figure 16 | Facilitator and blocker scores are affected differently by signaling modulation. (**A**) Facilitator score (comprising subsets 1 and 2 of facilitator genes) plotted on the force-directed graph separated by treatment. Color scale indicates score values from minimum (purple) to maximum (green). (**B**) Blocker score plotted in the force-directed graph separated by treatment. Color scale indicates score values from minimum (purple) to maximum (red). (**C**) Violin plot of blocker scores of all cells of the starting populations separated by treatment. Strip plots on top depict each individual cell. Two-sided Mann-Whitney-Wilcoxon test with Bonferroni correction, p-value: **** <= 0.0001. (**D**) Force-directed graph of AS, AS+DAPT and AS+SB/DM cells colored by scaled latent time (developmentally early: blue; developmentally late: green->yellow). (**E**) Average facilitator score and average blocker score shown along latent time separately for all treatments. Confidence interval > 0.95. Score in GFP-transduced control cells indicated as dotted green baseline.

3.2.6 Reprogramming outcome is directed by NOTCH and TGF-β signaling modulation

Having identified a mechanism that prevents lineage changes in AS-transduced cells, we sought to investigate how lineages are affected by the small molecule treatments in general. Therefore, we used CellRank to calculate absorption probabilities for all known terminal fates (**Figure 17A**). Interestingly, the spatial segmentation of the trajectory in starting population, mid trajectory and early neurons as the fates with the highest absorption probabilities remained highly similar for the modulated cells. The individual observation of each fate (**Figure 17B**) additionally revealed higher absorption probabilities for the late neuronal lineages type 1 and type 2, indicating that the cells

generated by the treatments were more likely to progress towards one of these targeted terminal states. Moreover, while the absorption probabilities for the confused fate lineage on the main (AS and AS+DAPT) trajectory were still the highest in the early mid trajectory, we did not observe a similar cluster of cells on the AS+SB/DM trajectory, suggesting that these cells were less likely to acquire a confused fate.

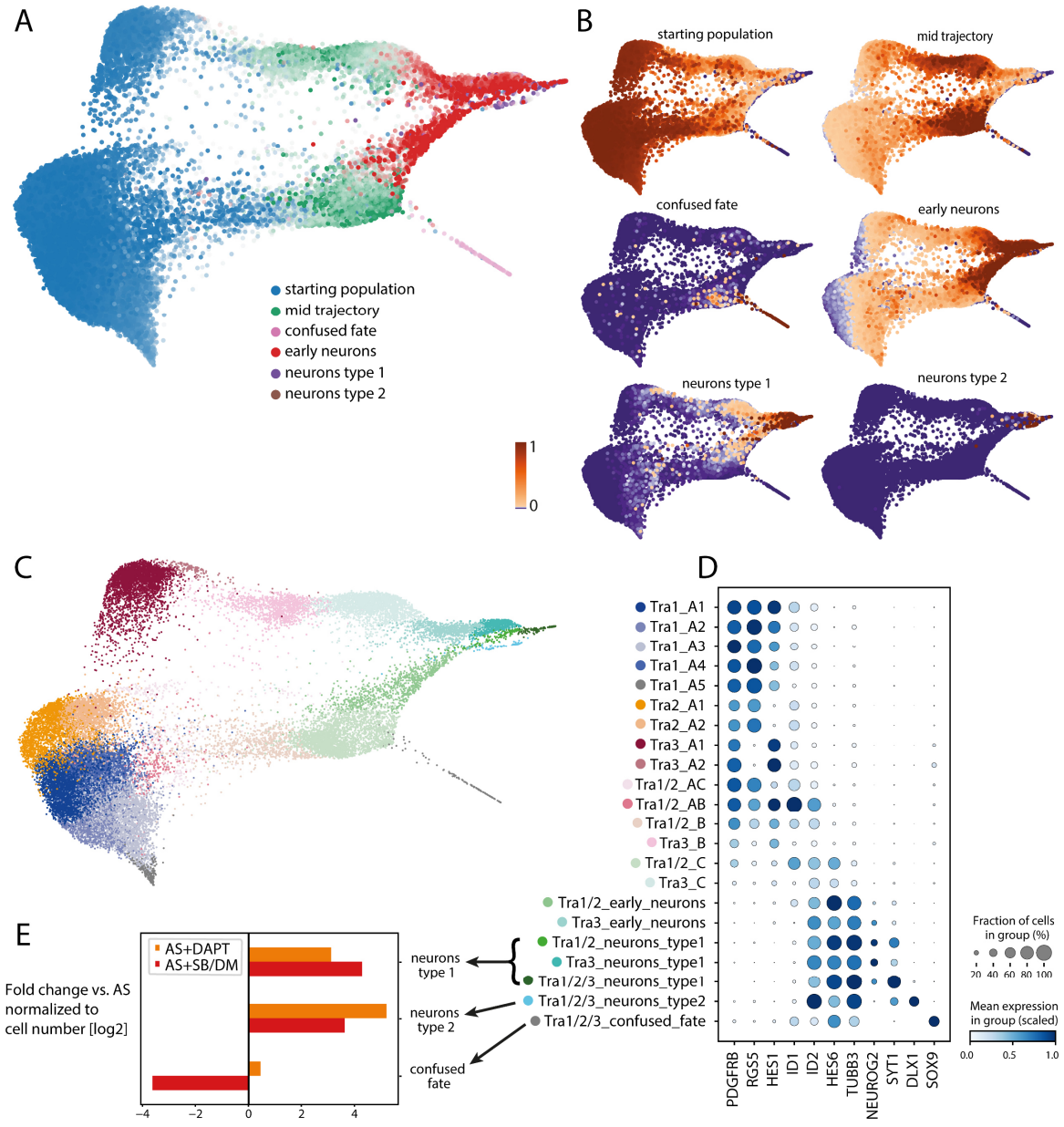

Figure 17 | NOTCH and TGF-β signaling modulation cause changes in the reprogramming outcome. (A) Combined CellRank (Lange et al., 2022) plot of the absorption probabilities of all identified terminal states. The color depicts the terminal state with highest absorption probability for a particular cell, the alpha value is indicative of

the magnitude of the absorption probability (pale color: low absorption probability; bold color: high absorption probability). (**B**) Individual CellRank plots of the absorption probabilities of all identified terminal states. Color scale depicts the magnitude from 0 (no absorption; blue) to 1 (highest absorption; brown). (**C**) Force-directed graph of the AS dataset including treatments clustered using the Leiden algorithm. Colors depict all 22 cluster identities as shown on the right. Names were assigned according to the contribution of AS (Tra1), AS+DAPT (Tra2) or AS+SB/DM (Tra3) to the respective cluster, A indicating starting population clusters, B indicating early trajectory and C indicating mid trajectory, while the outcomes are named by type. (**D**) Dot plot of the mean gene expression (scaled to maximum) of selected marker genes in clusters as indicated. Expression values are scaled per gene and color scale ranges from white (no expression) to dark blue (high expression). The fraction of cells per cluster expressing the gene is visualized by dot size. (**E**) Bar graph of the changes in reprogramming outcomes of AS+DAPT (yellow) and AS+SB/DM (red), depicted as fold change (Log2) compared to AS, normalized to the total cell number per treatment. Only trajectory endpoints are shown as outcomes: For confused fate (marked by *SOX9*) and neurons type 2 (marked by *DLX1*), these are identical to the clusters with the respective names. Neurons type 1 comprise all clusters with high expression levels of *TUBB3* and additional expression of *NEUROG2* or specific synaptic markers like *SYT1*, and which are adjacent to the neurons type 2 cluster but do not express *DLX1*.

To assess this conclusion, we clustered the complete dataset including the treated cells using the Leiden algorithm to receive clusters that contained cells of either experimental treatment (**Figure 17C, Table 2**). As the neuronal end of the trajectory appeared quite heterogeneous compared to the rest of the embedding, we also performed sub-clustering of this population and obtained a total of 22 clusters.

To define cluster identities, apart from their position on the trajectory we utilized their gene expression profiles (**Figure 17D**). We could show that starting clusters of all treatments were marked by either high *PDGFRB* and/or *RGS5* expression. AS+DAPT seemed to downregulate both genes slightly in the starting clusters, while the starting clusters of the AS+SB/DM trajectory exhibited high *PDGFRB* but almost no *RGS5* expression. The cellular progression along the cells could be displayed by the expression of different NOTCH and TGF-β signaling target genes as shown previously: *HES1* was downregulated once cells enter the trajectory (and gone from the start after NOTCH inhibition), *ID1* peaked between starting and trajectory clusters (not reported for TGF-β inhibition), while *ID1* only came up on the trajectory (later after SB/DM treatment) and from mid trajectory onwards cells upregulated *HES6* expression. Like for the embedding of AS, for the complete embedding we identified neuronal clusters by their *TUBB3* expression. The first neuronal cluster in each trajectory before coalescence of the trajectories we termed early neurons. The other four clusters were found in close vicinity to the late neuron cluster identified in AS cells without further treatment. They expressed in varying ratios synaptic markers like *SYT1* and either the glutamatergic fate marker

NEUROG2 or the GABAergic fate marker *DLX1*. Confused cells were still defined by their *SOX9* expression (**Figure 17D**).

Our target population on the neuronal end of the trajectory were the neurons type 1 clusters and the neurons type 2 cluster. Confused cells were considered an undesired off-target population. With regard to these three types of cells generated, we normalized the cell number within the clusters to the total cell number of each treatment and calculated the fold change in normalized cell numbers compared to untreated AS cells (**Figure 17E**). As expected, due to the increased density at the neuronal end, both AS+DAPT and AS+SB/DM led to a massive increase in iNs. In addition, DAPT treatment slightly favored generation of type 2 neurons, whereas SB/DM treatment slightly favored generation of type 1 neurons. Strikingly, however, while DAPT did barely change the number of confused cells generated, SB/DM treatment caused a strong decline in the generation of confused cells, confirming that we could steer the reprogramming process away from of this off-target population.

3.2.7 Treatments counteract on predicted reprogramming-induced TF activity

We had shown that both treatments lead to a substantial increase in iN numbers, in part concomitant with a reduction of confused cell fates. To get a broader understanding of the molecular processes involved in this improved target cell generation, we went on to investigate not only the expression of single genes but regulons, sets of genes, which are regulated by the same TF. We found that AS-transduction triggered upregulation of TF activity of several regulons in cells of the starting population compared to GFP-transduced cells (**Figure 18A**). Strikingly, DAPT (**Figure 18B**) and SB/DM (**Figure 18C**) treatments appeared to downregulate most of those AS-triggered regulons, indicating these to be safeguarding the cellular identity of the starting population. Interestingly, despite the different pathways inhibited by the treatments, most regulons were affected in a comparable manner by both treatments. Among these were the TGF-β signaling transducer *SMAD3*, the cellular differentiation and proliferation regulator *MYB*, and the cellular growth and survival regulator *ATF1*.

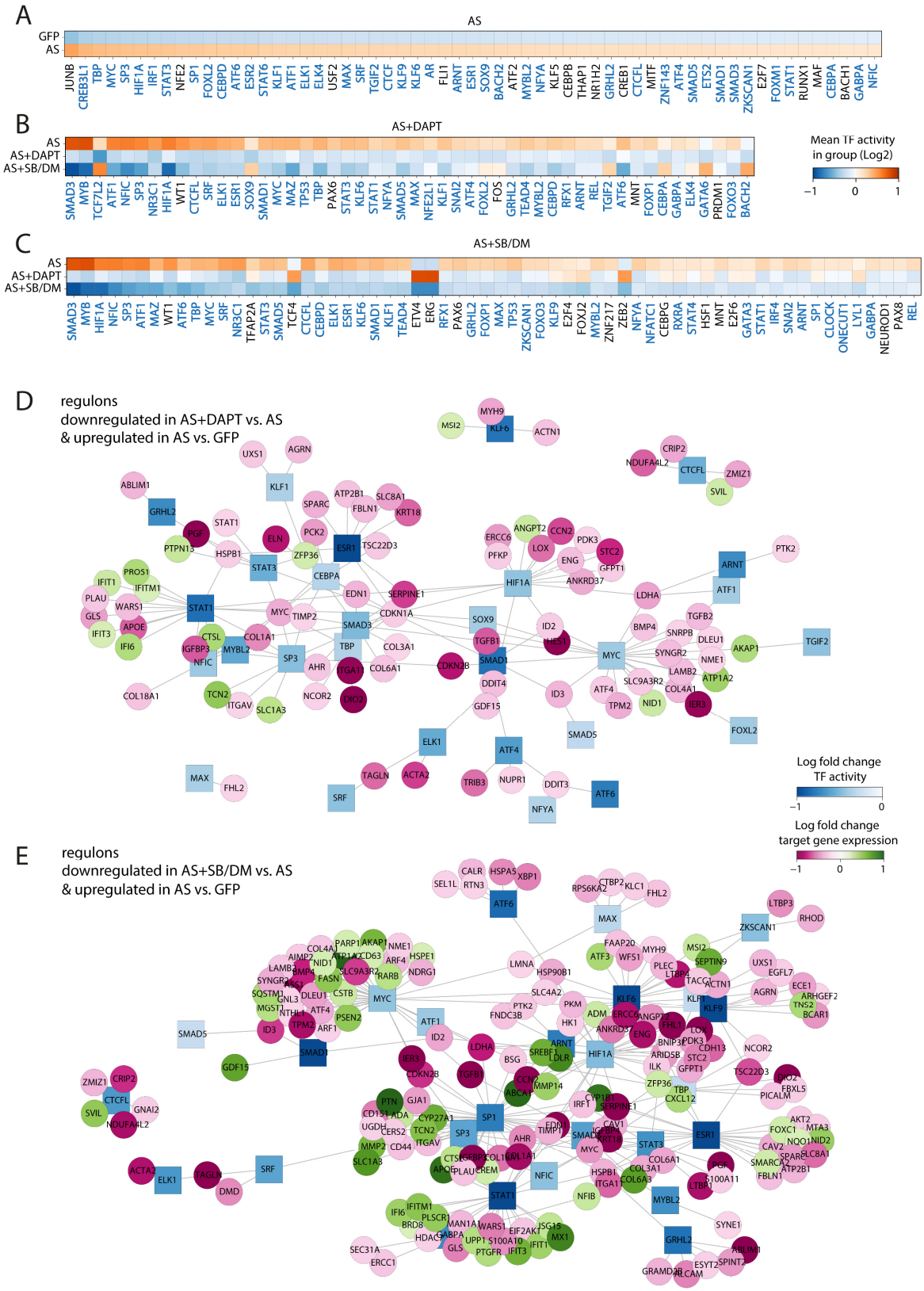

Figure 18 | Reprogramming-induced changes in TF activity are counteracted by NOTCH and TGF-β signaling modulation. (**A.B,C**) Heatmaps of mean regulon expression levels in the starting populations, predicted with DoRothEA (Garcia-Alonso et al., 2019; Holland et al., 2020). Regulons shown are found in DE analysis to be (**A**)

upregulated in AS vs. GFP, (**B**) downregulated in AS+DAPT vs. AS, (**C**) downregulated in AS+SB/DM vs. AS. Regulons were filtered for a mean change of >0.25 and adjusted p-value <0.05. All DE analyses of regulons were performed using Wilcoxon rank-sum test with Benjamini-Hochberg correction. Regulons that are both upregulated in AS vs. GFP and downregulated either in AS+DAPT vs. AS or AS+SB/DM vs. AS are marked with blue font, also if the up- or downregulation has an absolute mean change lower than 0.25. (**D,E**) Network graphs of regulons downregulated in (**D**) AS+DAPT vs. AS or (**E**) AS+SB/DM vs. AS and upregulated in AS vs. GFP. TFs are shown as rectangles, target genes are shown as circles. Color for TFs indicates the mean change in TF activity compared to AS, ranging from white (no downregulation) to blue (strong downregulation). Color for target genes indicates the log fold change compared to AS. DE is determined using a t-test with Benjamini-Hochberg correction and only significantly differentially expressed with a minimum absolute fold change of 0.75 and a minimum in group fraction of 0.2 are shown.

One of the regulons both strongest upregulated by AS and strongest downregulated by DAPT or SB/DM was *HIF1A*, which codes for the hypoxia master regulator HIF-1α. This implied that major changes in cellular metabolism are required early on for the cells to leave the starting population. To verify that our findings regarding TF activity were also reflected by gene expression, we compared the expression of the genes in the most differentially active regulons for AS+DAPT (**Figure 18D**) and AS+SB/DM (**Figure 18E**) compared to AS in the starting population. This analysis revealed that TF activity differences were supported by differential gene expression, with multiple HIF1A target genes substantially differentially expressed in AS+DAPT compared to AS, and in AS+SB/DM compared to AS, respectively.

3.2.8 Metabolic transition functions as a safeguarding mechanism for cellular identity

Interestingly, HIF-1α TF activity seemed to depend on the cellular context, as HIF1A gene expression showed only minor differences between treatments along the trajectories (**Figure 19A**), whereas HIF1A regulon activity clearly peaked in the starting population and was downregulated during the trajectory (**Figure 19B**). A similar behavior is found in the starting populations, where HIF1A gene expression appeared only slightly changed between the treatments (**Figure 19C**), while HIF1A regulon activity was upregulated in AS compared to GFP, and downregulated in treatments compared to AS (**Figure 19D**).

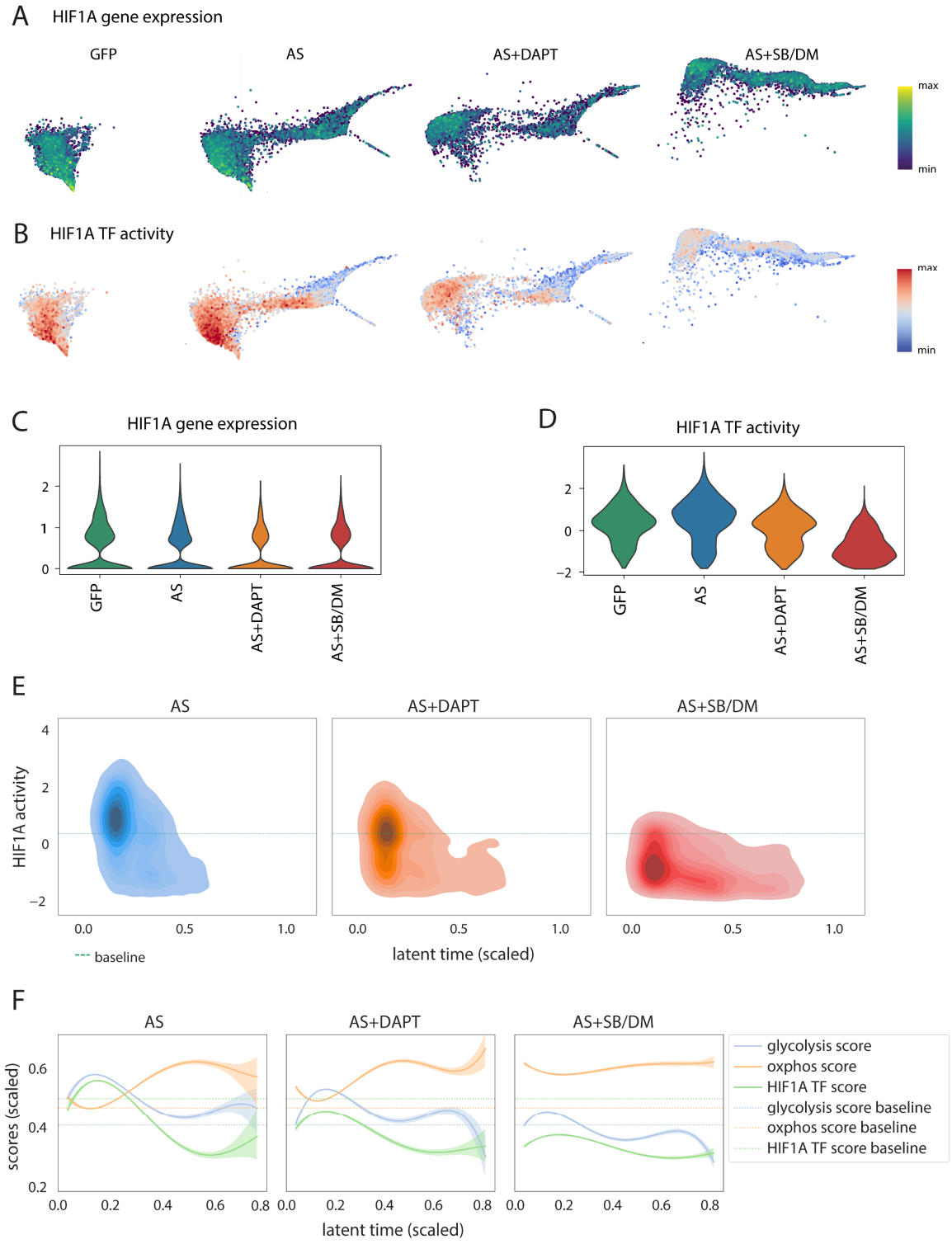

Figure 19 | Metabolic transition between glycolysis and oxidative phosphorylation works as a safeguarding mechanism for cellular identity. (**A**) HIF1A gene expression depicted on the force-directed graph separated by treatment. Color scale indicates min (blue) and max (green->yellow) values. (**B**) HIF1A TF activity as predicted using DoRothEA (Garcia-Alonso et al., 2019; Holland et al., 2020) displayed on the force-directed graph separated by treatment. Color scale indicates min (blue) and max (red) values. (**C**) Violin plot of the HIF1A gene expression in starting populations separated by treatment. (**D**) Violin plot of the predicted HIF1A TF activity in starting

populations separated by treatment. (**E**) Density plot of HIF1A TF activity along latent time (scaled) shown for AS and both treatments separately. Average HIF1A TF activity in the GFP control experiment is shown as baseline (green, dotted). (**F**) Plots depicting scores (scaled to min/max between 0 and 1) generated from the expression of glycolysis-related genes, OxPhos-related genes and the HIF1A regulon along latent time (scaled). Latent time is capped at the ends due to low cell numbers. Scores in GFP-transduced control cells are indicated as dotted baseline. Confidence interval > 0.95.

Density plotting of HIF1A TF activity (**Figure 19E**) confirmed that the starting population of AS-transduced cells exhibited higher HIF1A regulon activity than the control population, while in the AS+DAPT starting population the activity was similar to the baseline activity and in the AS+SB/DM stating population the activity was massively downregulated. In all treatments, cells exceeding a latent time of 0.5 had lower than baseline HIF1A regulon activity, indicating that downregulated is necessary to proceed towards iN fate.

Due to the implication of HIF1A in the switch from OxPhos to glycolysis (Candelario et al, 2013), we assumed that inhibition of HIF1A supports the switch from glycolysis to OxPhos, which is required to acquire a neuronal identity. We therefore used the KEGG database to generate scores for genes implicated in glycolysis and genes involved in OxPhos (**Table 3**). Interestingly, only one gene of the OxPhos score, *COX6A2*, was also identified as a facilitator, while no gene of the glycolysis score was among the blocker genes identified earlier, which was not surprising as the metabolic transition appeared to affect cell fate prior to the blockers and facilitators.

We then followed the scores' expression over latent time along with the HIF1A activity score (**Figure 19F**). It showed that both HIF1A activity and the glycolysis score were significantly upregulated upon AS-transduction in the starting population compared to baseline, while the OxPhos score was not immediately affected by AS-transduction. During latent time, as seen earlier, the glycolysis score was then downregulated, while the OxPhos score was upregulated. Large confidence intervals during late latent time were likely due to fewer cells and to the difference between iNs and confused fate cells in particular. Upon DAPT treatment, glycolysis score was significantly downregulated compared to AS in the early latent time, whereas OxPhos score was significantly elevated already in early latent time. In late latent time, neither glycolysis nor OxPhos score differed between AS+DAPT and AS. Upon SB/DM treatment, the effect on the starting population was massive, as the glycolysis score was significantly lowered and OxPhos score lifted

significantly so that it almost reached its maximum early on. Similarly, HIF1A activity levels were significantly lowered, which might also explain the downregulation of the pericyte marker *RGS5* in AS+SB/DM starting population, since it is regulated by HIF1A (Jin et al., 2009). The lowered slopes of glycolysis score and OxPhos score in SB/DM treated cells might further represent a reduced barrier for cellular identity changes, which had been reflected earlier in the density distribution.

3.2.9 Oxidative stress response gene VDR is implicated in confused cell generation

The gene regulatory changes caused by SB/DM treatment had further been shown to lead close to a complete erasure of the confused fate population. To determine which regulons were particularly involved in reducing this off-target population, we investigated differences in regulon activity between cells giving rise to confused cells and cells that were less likely to do so. We know by absorption probabilities and connection scores that cell fate decision towards confused fate was taken during mid trajectory. We further knew by asymmetric integration that the mid trajectory clusters of both the AS/AS+DAPT trajectory and the AS+SB/DM trajectory were mapped onto each other. By thresholding the absorption probability, for AS+AS/DAPT mid trajectory we generated one population with lower tendency to become confused, while we identified 'confused root cells' as the population with higher confused fate absorption probability (**Figure 20A**). Subsequently, we determined differentially active regulons between both populations (**Figure 20B**). AS+SB/DM mid trajectory cells had a low tendency to become confused from the start. Therefore, we went on to identify differentially active regulons between the AS/AS+DAPT mid trajectory and AS/AS+SB/DM mid trajectory (**Figure 20C, D**). Since SB/DM prevents confused fate, regulons driving confused fate decision should be downregulated here, and regulons preventing confused fate should be upregulated. Interestingly, almost all regulons detected as being differentially expressed in confused root cells compared to AS/AS+DAPT mid trajectory, were also regulated in an opposing manner in AS+SB/DM mid trajectory. This was also supported by differential expression of target genes of the respective TFs (**Figure 20E**).

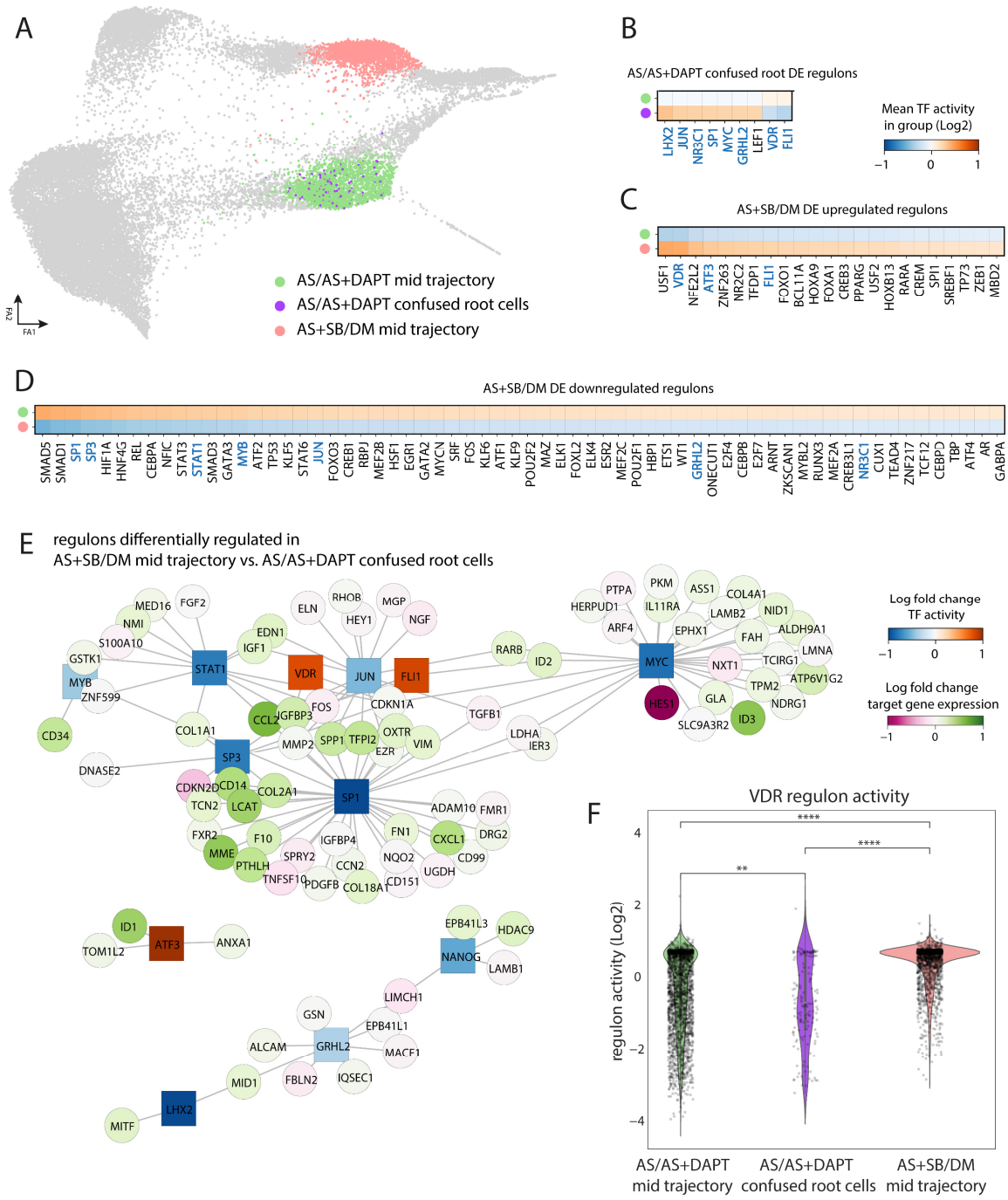

Figure 20 | Confused fate repression after TGF-β signaling modulation is accompanied by increased VDR regulon activity. (**A**) Both mid trajectories and confused root cells of AS/AS+DAPT indicated in force-directed graph. Confused root cells have been obtained by using an absorption probability threshold of 0.0075. (**B**,**C**,**D**) Heatmaps of mean regulon expression levels in the mid trajectory and confused root cell populations, predicted with DoRothEA (Garcia-Alonso et al, 2019; Holland et al, 2020). Regulons shown are found in DE analysis to be (**B**) up- or downregulated in confused root cells vs. AS/AS+DAPT mid trajectory, (**C**) upregulated in AS+SB/DM vs. AS/AS+DAPT mid trajectory, (**D**) downregulated in AS+SB/DM vs. AS/AS+DAPT mid trajectory. Regulons were filtered for a mean change of >0.25 and adjusted p-value <0.05. All DE analyses of regulons were performed using Wilcoxon rank-sum test with Benjamini-Hochberg correction. Regulons that are differentially regulated in an opposing manner in confused root cells vs. AS/AS+DAPT mid trajectory and AS+SB/DM mid trajectory vs. AS/AS+DAPT mid trajectory are marked with blue font, also if the up- or downregulation has an absolute mean

change lower than 0.25. (**E**) Network graphs of regulons differentially regulated in AS+SB/DM mid trajectory vs. AS/AS+DAPT confused root cells. TFs are shown as rectangles, target genes are shown as circles. Color for TFs indicates the mean change in TF activity compared to AS, ranging from white (no downregulation) to blue (strong downregulation). Color for target genes indicates the log fold change compared to AS. DE is determined using a t-test with Benjamini-Hochberg correction and only significantly differentially expressed with a minimum absolute fold change of 0.5 and a minimum in group fraction of 0.1 are shown. (**F**) Violin plot of VDR regulon activity in the three populations of interest. Strip plots on top depict each individual cell. Two-sided Mann-Whitney-Wilcoxon test with Bonferroni correction, p-value: ** <= 0.01, **** <= 0.0001.

One of the regulons with the strongest downregulation in confused root cells and the strongest upregulation in AS+SB/DM mid trajectory was the vitamin D receptor (VDR) regulon. It was not only significantly differentially active between confused root cells and AS/AS+DAPT mid trajectory, but also between confused root cells and AS+SB/DM mid trajectory as well as between both mid trajectory populations (**Figure 20F**). VDR has been shown to be involved in the cellular anti-oxidative stress reaction (Bao et al., 2008; Dong et al., 2012), indicating that confused fate represents a failure to deal with the metabolic transition from glycolysis to OxPhos, which can be prevented by inhibition of TGF-β signaling.

3.2.10 iNs generated by AS reprogramming resemble features of developing human brain structures

While only SB/DM treatment was able to reduce the confused cell population, we had shown that both DAPT and SB/DM treatments led to an increase in neurons. To determine the identity of the iNs generated, we embedded the previously identified neuronal clusters with UMAP to improve cluster separation. This confirmed that the early iNs were mostly separated between treatments, whereas the most differentiated clusters contained cells from both the AS/AS+DAPT and the AS+SB/DM trajectory (**Figure 21A, B**). However, the connectivities revealed that even the early neurons of both trajectories had high similarities. As expected of differentiated cells, the two trajectory tip populations, neurons type 1 and 2, did not project to each other but to developmentally earlier cells in other populations.

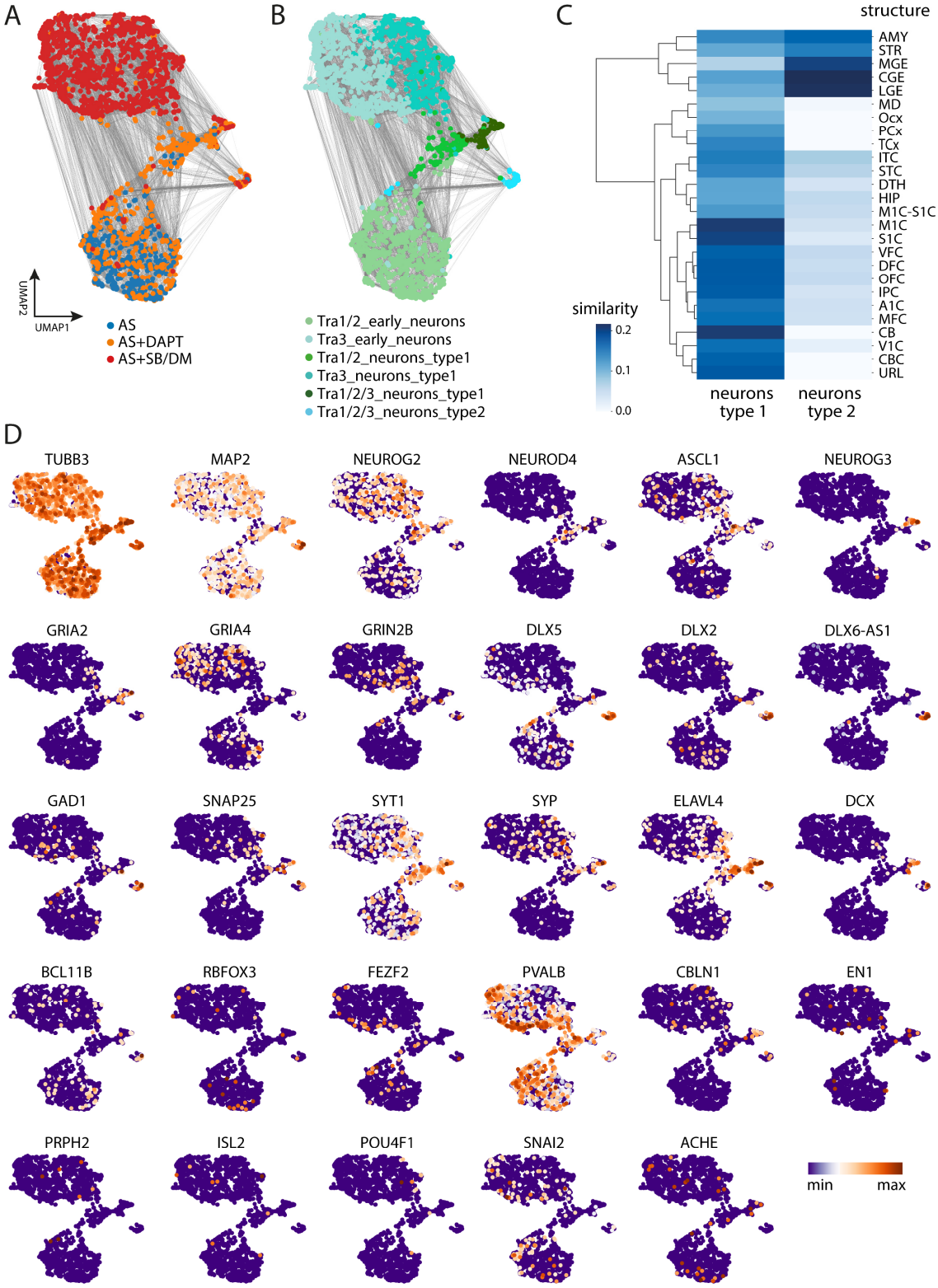

Figure 21 | iNs generated exhibit gene expression profiles similar to human brain structures. (**A**) UMAP graph of the neuronal clusters colored by treatment. Grey lines between the cells indicate the 20 closest neighbors of each cell over all dimensions used in the embedding. (**B**) UMAP graph of the neuronal clusters colored by cluster. Grey lines between the cells indicate the 20 closest neighbors of each cell over all dimensions used in the embedding. (**C**) Heatmap depicting the similarity of the most mature iN clusters (Tra1/2/3_neurons_type1,

Tra1/2/3_neurons_type2) to developing human brain structures generated via Voxhunt. A1C: primary auditory cortex (core), AMY: amygdaloid complex, CB: cerebellum, CBC: cerebellar cortex, CGE: caudal ganglionic eminence, DFC: dorsolateral prefrontal cortex, DTH: dorsal thalamus, HIP: hippocampus (hippocampal formation), IPC: posteroventral (inferior) parietal cortex, ITC: inferolateral temporal cortex (area TEv, area 20), LGE: lateral ganglionic eminence, M1C: primary motor cortex (area M1, area 4), M1C-S1C: primary motor-sensory cortex (samples), MD: mediodorsal nucleus of thalamus, MFC: anterior (rostral) cingulate (medial prefrontal) cortex, MGE: medial ganglionic eminence, Ocx: occipital neocortex, OFC: orbital frontal cortex, PCx: parietal neocortex, S1C: primary somatosensory cortex (area S1, areas 3,1,2), STC: posterior (caudal) superior temporal cortex (area 22c), STR: striatum, TCx: temporal neocortex, URL: upper (rostral) rhombic lip, V1C: primary visual cortex (striate cortex, area V1/17), VFC: ventrolateral prefrontal cortex. Color scale from low similarity (white) wo high similarity (blue). Human developing brain structures are ordered by expression similarities depicted in a hierarchically clustered dendrogram (similarity distance shown by length of branches). (**D**) UMAP graphs indicating expression of various genes. Color scale from low expression (blue) to high expression (orange).

As our neurons had been generated by forced neurogenesis, it was important to understand how close they were to developmental *bona fide* neurons. Therefore, we intended to compare the iNs generated with AS reprogramming with and without signaling manipulation to developing human neurons. Since up to now no high-resolution single-cell transcriptomic data exists for the developing human brain, we utilized the structure annotations from bulk transcriptome data of microdissected brain regions as provided by Voxhunt to map our iN populations (**Figure 21C**). We confirmed that they were in fact comparable to these developing human brain structures regarding their gene expression: Neurons of type 1 appeared more ambiguous in their identity and had their highest similarities with primary motor as well as somatosensory cortex and the cerebellum, in general more similar to dorsal brain structures. By contrast, neurons of type 2 had a clear ventral identity and appeared most similar to caudal, lateral and medial ganglionic eminence of the developing human brain.

We further characterized the iNs by their expression of several neuronal genes (**Figure 21D**). While *TUBB3* and *MAP2* were widely expressed throughout all clusters, the neurogenic factors *ASCL1* and *NEUROG2* were mostly expressed in the more mature neurons. Notably, *NEUROG2* was downregulated in Tra1/2/3_neurons_type2, while *ASCL1* was downregulated in Tra1/2/3_neurons_type1. Interestingly, the neuronal differentiation regulator *NEUROD4* was upregulated in Tra1/2_neurons_type1, before cells became more mature and started to express *NEUROG3* in Tra1/2/3_neurons_type1. *GRIA2* expression underlined a glutamatergic identity in Tra1/2/3_neurons_type1, whereas *GRIA4* and *GRIN2B* expression showed a sequential change of NMDA and AMPA receptors. More members of the *DLX* family like *DLX2* and *DLX5*, as well as *DLX6-AS1* and *GAD1*

marked the GABAergic identity of neurons type 2. Synaptic markers like *SNAP25*, *SYT1* and *SYP*, as well as the postmitotic neuron marker *ELAVL4* confirmed that the respective clusters had a mature neuronal identity. The neuronal migration marker *DCX* was also found in both Tra1/2/3_neurons_type1 and Tra1/2/3_neurons_type2. *RBFOX3* (*NEUN*), another postmitotic neurons marker, and *BCL11B* (*CTIP2*) as a cortical layer V marker, were only sparsely expressed and not restricted to late neurons. Early neurons of both trajectories exhibited expression of *FEZF2* and *PVALB*. While the postsynaptic cerebellar marker *CBLN1* was found in subfraction of neurons type 1 in accordance with the brain structure mapping, only few potentially dopaminergic (marked by *EN1*) neurons or cholinergic neurons (marked by *ACHE*) were found in neurons type 1, none in neurons type 2.

We further assessed non-CNS identity and found that some cells of the early neuron clusters expressed the neural crest marker *SNAI2*. There was, however, no meaningful expression of the retinal neuron marker *PRPH2*, the spinal cord marker *ISL2* and the peripheral neuron marker *POU4F1*. Overall, we therefore concluded that the two neuronal populations generated were a mostly glutamatergic and a GABAergic population.

3.3 Reprogramming using different neurogenic factors

3.3.1 Forced Neurog2/Sox2 expression triggers a reprogramming process towards a population distinct from Ascl1/Sox2-generated iNs

Since we had found increased *NEUROG2* expression in late neurons, even more abundant than the intrinsic *ASCL1* expression, and due to the vital role of Neurog2 in neurogenesis (Bertrand et al., 2002), we assumed that Neurog2 could function as an even more potent reprogramming factor than Ascl1. Additionally, we expected that Neurog2/Sox2 (NS) transduction might work as a shortcut to generate iNs, in particular those with a glutamatergic subtype identity. To investigate the reprogramming potential of NS compared to AS, we designed an experiment, where we transduced cultured human

brain pericytes with either of the two factor combinations and on d7 and d14 performed scRNA-seq after ensuring successful transduction via FACS (**Figure 22A**). Strikingly, also NS-transduction gave rise to TUBB3+ cells with neuronal morphology, even though cell processes appeared less branchy than AS iNs (**Figure 22B**).

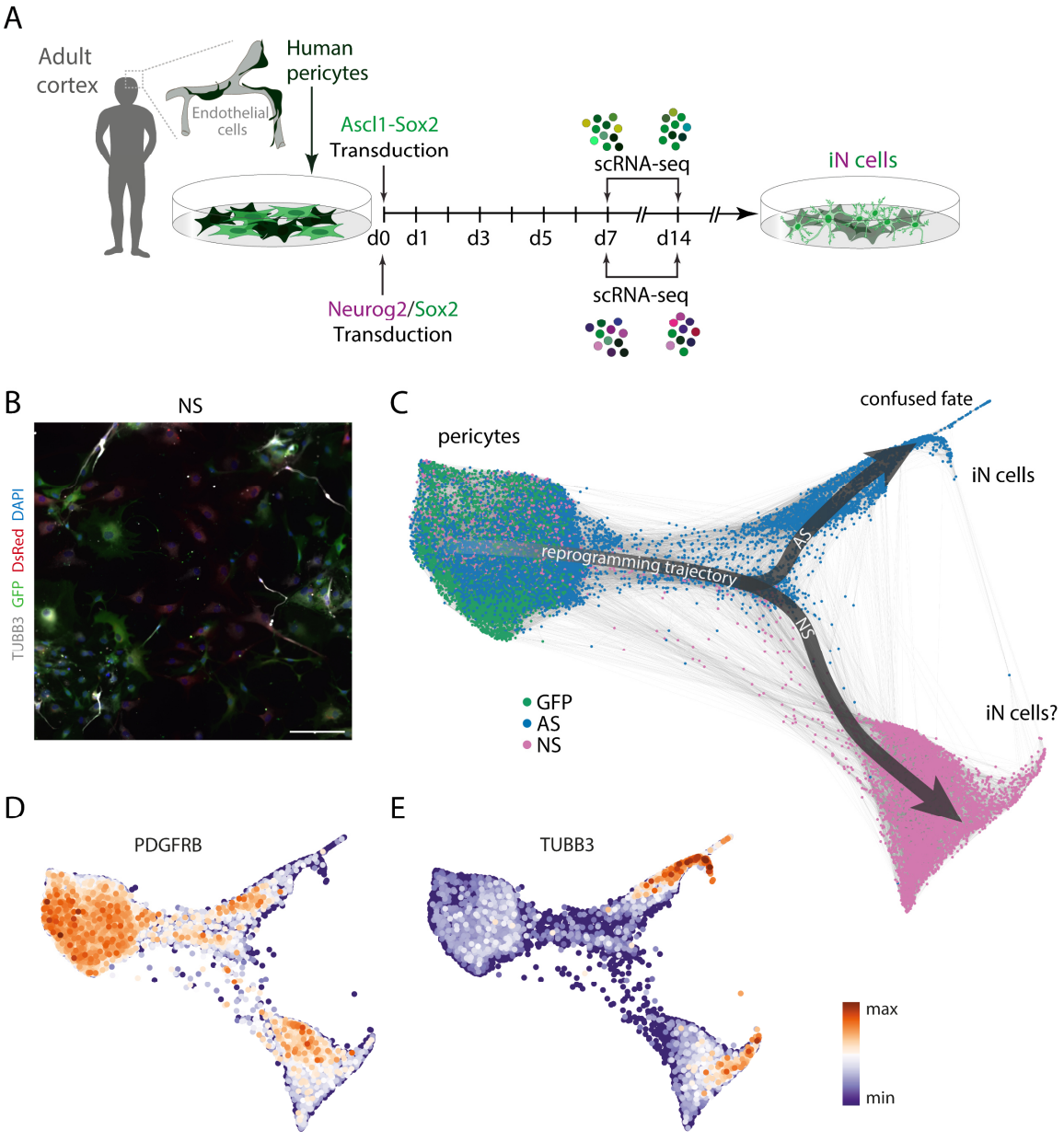

Figure 22 | Cells transduced with Neurog2/Sox2 take a distinct reprogramming route and produce TUBB3+ cells. (**A**) Schematic of the experimental design: Cultured brain pericytes derived from adult human patients were retrovirally transduced to express Ascl1 and Sox2 (AS) with GFP as an expression control or to express Neurog2 and Sox2 (NS) with DsRed and GFP as an expression control, respectively. On d7 and d14 after transduction, cells were FAC sorted for GFP and DsRed expression and GFP+ cells (AS) and GFP+/DsRed+ cells (NS) were used for single cell transcriptomic analysis using the 10x Genomics system. (**B**) Representative image of successfully NS-reprogrammed pericytes 28 days after transduction: immunostained for neuronal cells (TUBB3, white), Neurog2-

transduced cells (DsRed, red), Sox2-transduced cells (GFP, green) and nuclei (DAPI, blue) are visible. Scale bars, 50 µm. (**C**) 10x Genomics transcriptome data was analyzed using Scanpy (Wolf et al., 2018). Force directed graph was used to visualize 6116 NS-transduced cells (magenta) (d7: 2029 cells, d14: 4087 cells), 9393 AS-transduced cells (blue) (d7: 2875 cells, d14: 6518 cells), and 5686 GFP-transduced control cells (green) in a 2-dimensional embedding. Each dot represents one cell and their order represents their similarity. Starting populations overlap with GFP control cells, the trajectories of AS and NS cells bifurcate into two clearly separated trajectories. Grey lines between the cells indicate the 20 closest neighbors of each cell over all dimensions used in the embedding. (**D**) *PDGFRB* as a pericyte marker is confirmed to be expressed mostly in the starting population and to decline during the trajectories. (**E**) *TUBB3* as a neuronal marker is shown to be upregulated during the trajectory of both AS and NS-transduced cells towards the neuronal fate.

We analyzed the transcriptomes of a filtered total of 21195 cells, of which 6170 were NS-transduced cells (NS, experimental timepoints d7: 2029 cells, d14: 4087 cells), 9393 were AS-transduced cells (AS, experimental timepoints d7: 2875 cells, d14: 6518 cells), and 5686 GFP-transduced control cells (GFP) (**Table 1**). In a force-directed graph, AS and NS both overlapped with GFP, which indicated the starting population, although NS appeared to contribute much less to the starting population than AS (**Figure 22C**). There was another population of cells next to the starting population, which as well consisted of both AS and NS cells, while the large majority of NS cells cluster clearly separated from AS cells. The cellular connectivities indicated that AS and NS initially shared the same trajectory before they split up into different populations. Interestingly, the iN population of the AS trajectory was connected to the right corner of the NS main population, indicating some transcriptional similarity, which suggested that these were the iNs generated by NS. The pericyte marker *PDGFRB* was found in the starting population and was decreasing along the trajectories of both AS and NS (**Figure 22D**). Analogically to the *TUBB3* expression in late AS trajectory, *TUBB3* was also found in the right end of the NS trajectory, which also implied that these were neuronal cells (**Figure 22E**).

3.3.2 Overexpression of NS facilitates exit from starting cell identity and results in different cellular populations

We had already seen that NS cells contribute less to the starting population. This could be confirmed by looking at the density distribution (**Figure 23A**). It showed that there was only one density peak on the NS trajectory, which was located in the upper left edge of the main NS cell population before cells started to upregulate *TUBB3*. Density plotting also confirmed that the main pathway from starting population towards NS

reprogramming outcome was shared with AS cells, while a smaller group of NS cells was taking a more direct route from the starting population. No NS transduced cell was embedded in mid or late AS trajectory, almost no AS transduced cell was co-embedded in the mid or late NS trajectory, indicating an irreversible transcriptional difference of cellular identities. Upon Leiden clustering of the embedding, the last common population after the start shared between AS and NS was represented by a single cluster, Tra_AS_NS_B (**Figure 23B**). A total of 20 clusters was obtained, of which 6 were shared between AS and NS, 7 were unique to AS, and 7 were unique to NS (**Table 2**).

We identified marker genes for all clusters by DE analysis (**Figure 23C**). The genes characterizing the starting populations were mostly identical with the marker genes identified earlier for the *AS-only* starting populations. Interestingly, we found the TGF-β signaling targets *ID1* and *ID3* not only expressed in AS early trajectory, but also NS early trajectory clusters, whereas genes like the microtubule dynamics regulator *TPPP3* were not expressed in the NS early trajectory. In the early trajectory the protein metabolism gene *PGA5* peaked in expression, underlining the importance of the metabolic state also during NS reprogramming. The WNT pathway regulator *DKK3* was upregulated from Tra_NS_B1 on and was later downregulated in neurons. The common Tra_AS_NS_B cluster was characterized by the same three genes as the previous Tra_AS_early cluster, two of which, *S100A6* and *S100A13*, we had identified as blocker genes. The NS mid trajectory clusters exhibited high expression of the cytoskeleton protein-coding *ACTG2*, suggesting a cytoskeleton modulation during the trajectory.

The NS trajectory was less elongated than the AS trajectory, instead the triangle shape of the force-directed graph indicated the existence of another population of cells, which was not neuronal and therefore termed ‘alternative fate’. Apart from the collagen-coding *COL2A1* and the ER-translocation protein-coding *SSR3*, this cluster was characterized by *SCRG1* expression, which has been identified as a mesenchymal stem cells regulator gene (Aomatsu et al., 2014). The retinol transporter protein-coding *RBP1*, which was upregulated during early trajectory and stayed high in iN clusters,

was downregulated in the alternative fate, suggesting a difference in retinoid homeostasis between these clusters.

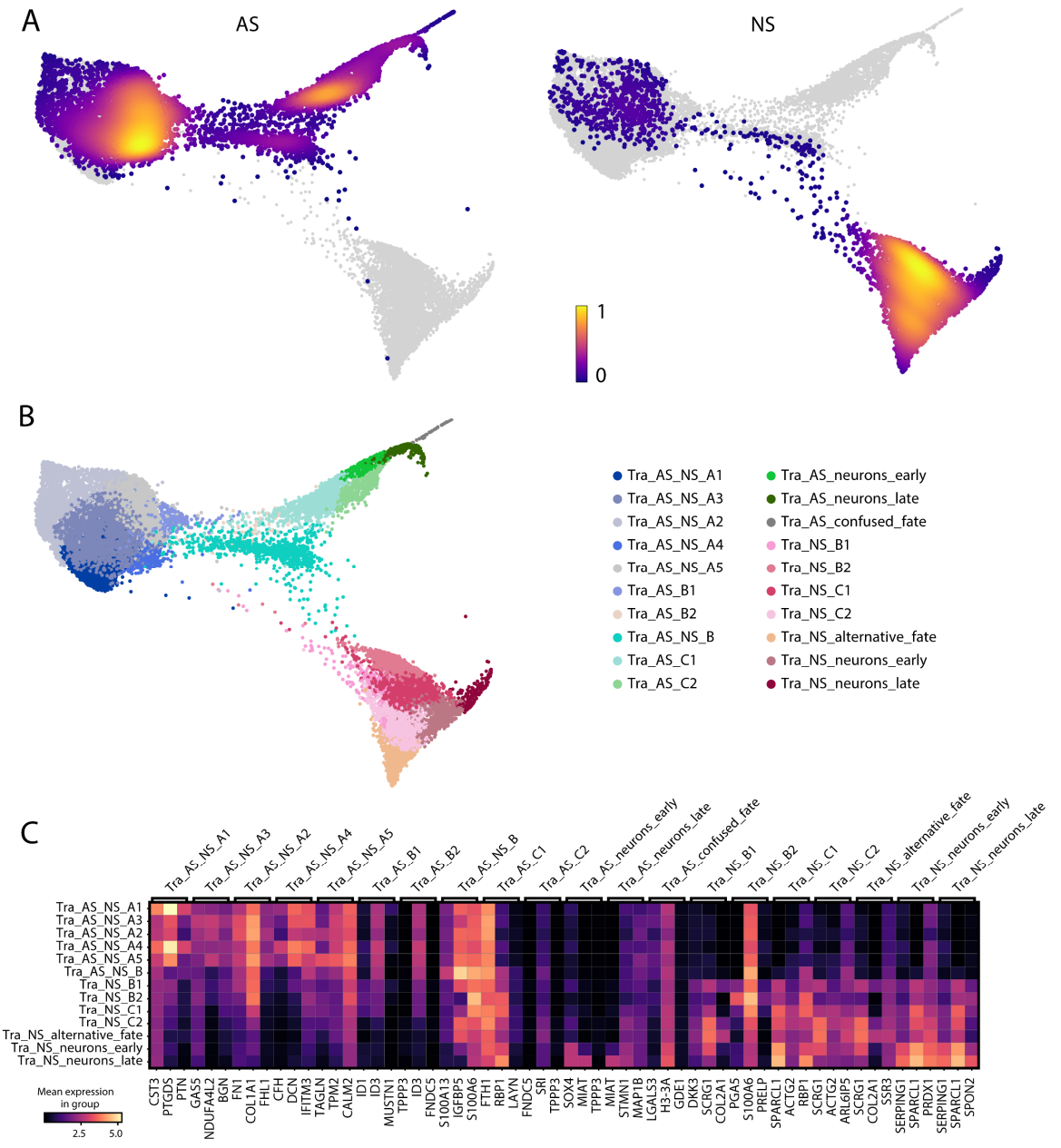

Figure 23 | Forced NS-expression generates both similar and different cell populations as AS-transduced cells. (**A**) Density plotted onto force-directed graph embedding separated by TF combination. Color scale from purple (sparse) to yellow (dense). (**B**) Force-directed graph of the *AS+NS* dataset clustered using the Leiden algorithm. Colors depict–– all 20 cluster identities as shown on the right. Names were assigned according to the contribution of AS (Tra_AS) or NS (Tra_NS) to the respective cluster, A indicating starting population clusters, B indicating early trajectory and C indicating mid trajectory, while the outcomes are named by type. (**C**) Heatmap of the mean expression values of the top 3 upregulated genes in each cluster vs. all other clusters. Only clusters with NS cells shown. DE was performed as a Wilcoxon rank-sum test, filtered for minimum expression in a fraction of 0.2 per group, a log fold change of 1, and p-value (adjusted using Benjamini-Hochberg correction) <0.05.

The two clusters that were classified as neuronal by their *TUBB3* expression, were further defined by increased *SERPING1* expression, which we had identified as a facilitator gene earlier. Other facilitator genes like *MIAT*, *STMN1* and *SOX4*, which also marked the AS neuronal clusters, were as well upregulated in NS neuronal clusters. However, at the same time *SPARCL1*, which we had found among the blocker genes in AS-transduced cells, was still expressed in both Ns iN clusters. The parallel expression of antioxidant enzyme-coding *PRDX1*, which was found to control neuronal differentiation (Yan et al., 2009), as well as *SPON2*, which promotes neural cell adhesion and neurite extension (Klar et al., 1992), additionally confirmed that cells belonging to these clusters are in fact on the trajectory towards iNs.

3.3.3 iNs generated by NS reprogramming are less mature than AS iNs

Since iNs generated with NS did not co-embed with iNs generated with AS, we further investigated the transcriptional differences between those target cell populations. UMAP embedding of the iN clusters of both trajectories confirmed that the cell types generated were different, with just one single AS-transduced cell co-embedding with NS-transduced iNs (**Figure 24A, B**). However, while early AS and NS iNs did not share connections indicating transcriptional similarities, late neurons of both clusters were more related to each other as shown by connections. We verified that cells from within all clusters were *TUBB3*+, although levels appeared lower in NS-generated iNs (**Figure 24C**). *MAP2* was found expressed in cells within all iN clusters. Further, NS-transduction also increased intrinsic *NEUROG2* expression, while *ASCL1* expression was eliminated, suggesting a change in subtype specification. *NEUROD4* and *NEUROG3* expressing cells were found in both late neuron clusters, although in few cells only. Despite the increase in *NEUROG2* expression, we did not see an increase in glutamatergic markers like *GRIA4* and while *DLX2* as a GABAergic neuron marker was almost not expressed in NS iNs, *DLX5* was still expressed in the tip of the late NS neuron cluster. Even the interneuron subtype marker *PVALB* was still present in late NS neurons, although not as abundant as in AS neurons.

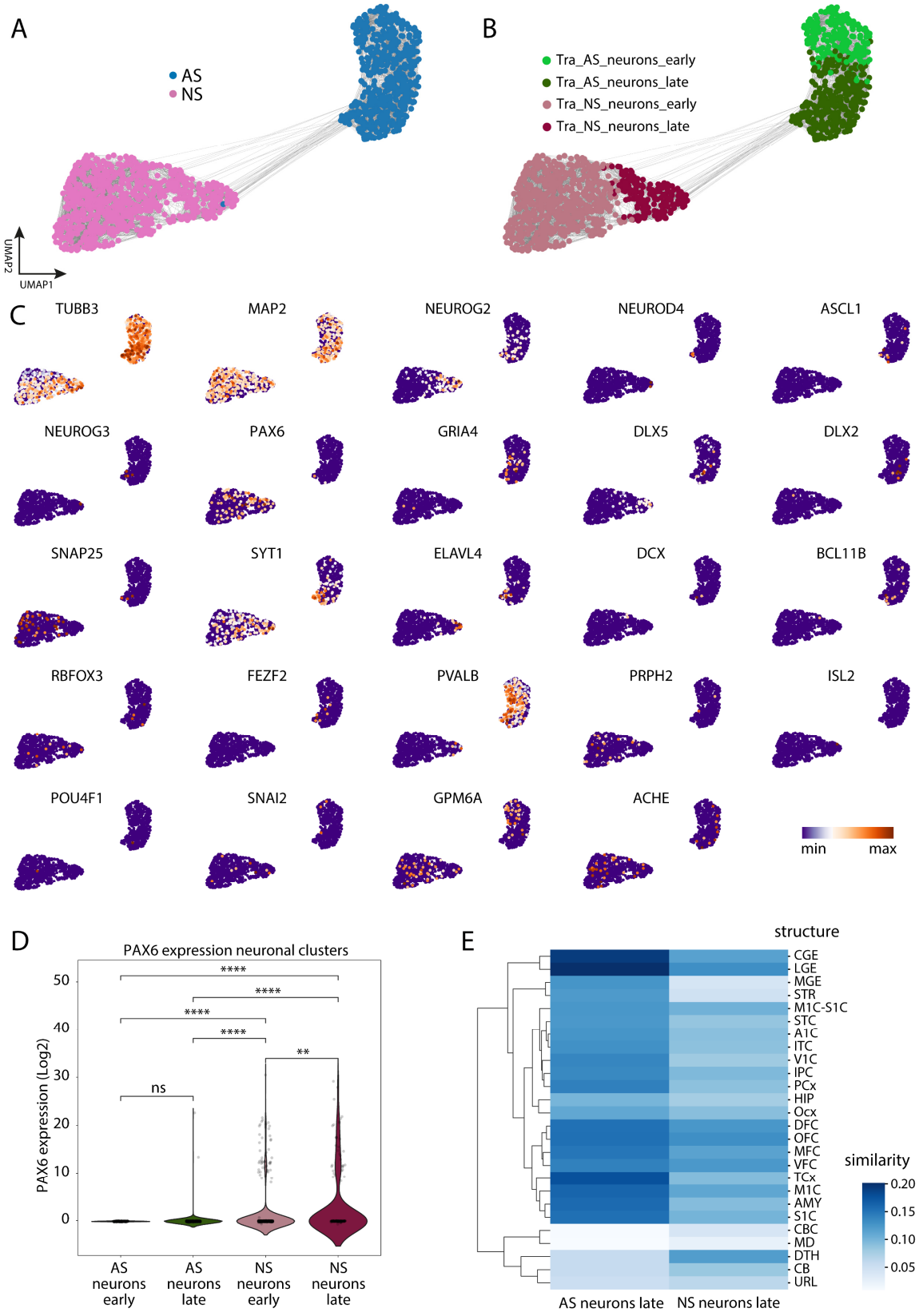

Figure 24 | *TUBB3+* NS-transduced cells exhibit neural progenitor features. (**A**) UMAP graph of the neuronal clusters colored by TF combination used. Grey lines between the cells indicate the 20 closest neighbors of each cell over all dimensions used in the embedding. (**B**) UMAP graph of the neuronal clusters colored by cluster. Grey lines

between the cells indicate the 20 closest neighbors of each cell over all dimensions used in the embedding. (**C**) UMAP graphs indicating expression of various genes. Color scale from low expression (blue) to high expression (orange). (**D**) Violin plot of PAX6 expression in *TUBB3*+ clusters of both TF combinations (Log2). Strip plots on top depict each individual cell. Two-sided Mann-Whitney-Wilcoxon test with Bonferroni correction, p-value: ** <= 0.01, **** <= 0.0001, ns = not significant. (**E**) Heatmap depicting the similarity of the *TUBB3*+ clusters to developing human brain structures generated via Voxhunt. A1C: primary auditory cortex (core), AMY: amygdaloid complex, CB: cerebellum, CBC: cerebellar cortex, CGE: caudal ganglionic eminence, DFC: dorsolateral prefrontal cortex, DTH: dorsal thalamus, HIP: hippocampus (hippocampal formation), IPC: posteroventral (inferior) parietal cortex, ITC: inferolateral temporal cortex (area TEv, area 20), LGE: lateral ganglionic eminence, M1C: primary motor cortex (area M1, area 4), M1C-S1C: primary motor-sensory cortex (samples), MD: mediodorsal nucleus of thalamus, MFC: anterior (rostral) cingulate (medial prefrontal) cortex, MGE: medial ganglionic eminence, Ocx: occipital neocortex, OFC: orbital frontal cortex, PCx: parietal neocortex, S1C: primary somatosensory cortex (area S1, areas 3,1,2), STC: posterior (caudal) superior temporal cortex (area 22c), STR: striatum, TCx: temporal neocortex, URL: upper (rostral) rhombic lip, V1C: primary visual cortex (striate cortex, area V1/17), VFC: ventrolateral prefrontal cortex. Color scale from low similarity (white) wo high similarity (blue). Human developing brain structures are ordered by expression similarities depicted in a hierarchically clustered dendrogram (similarity distance shown by length of branches).

A very remarkable difference was that the neuronal progenitor marker *PAX6*, which was almost absent in AS neurons with no significant difference between early and late neurons, was widely expressed in NS clusters, suggesting that NS iNs are generated through a progenitor-like cell type (**Figure 24D**). The presence of synaptic markers like *SYT1* and postmitotic neuronal markers like *ELAVL4* at the tip of late NS neurons still indicated that cells did not remain in a progenitor state (**Figure 24C**). Interestingly, the synaptic marker *SNAP25* was present already in early NS neurons but not early AS neurons, and downregulated from early to late NS neurons. The neuronal migration marker *DCX* was almost absent in both AS and NS neuronal clusters, and the postmitotic neurons marker *RBFOX3* (*NEUN*) was even more abundant in NS than AS cells, though still sparsely expressed.

As cortex marker *BCL11B* (*CTIP2*) and telencephalic progenitor marker *FEZF2* were not present in NS neurons, we continued our approach to specify the cellular identity further. Some cells in the early NS neuron cluster expressed the retinal neuron marker *PRPH2*. There was almost no expression of the spinal cord marker *ISL2* and only sparse expression of the neural crest marker *SNAI2*. There was no clear difference in cholinergic *ACHE* levels between AS and NS late neurons. Additionally, we checked for expression of markers found by a recent study using Neurog2 to reprogram iPSCs into different lineages (Lin et al., 2021). Of these markers, we were not able to detect *LHX9*, *PHOXB2*, *PRPH* and *CD99*, whereas we found the lineage marker and peripheral neuron marker *POU4F1* to be almost non-expressed, while many of the early NS neurons, but also early AS neurons,

expressed the lineage marker and neuronal differentiation factor *GPM6A*, which was found to be expressed during development in both CNS and spinal cord (Diez-Roux et al., 2011). Overall, the gene expression pattern supported our impression that the cellular identity of NS iNs was less defined than that of AS iNs.

This could be further confirmed by Voxhunt assessment of transcriptomic similarities between the generated iNs and developing human brain structures (**Figure 24E**). Only dorsal and mediodorsal thalamus, cerebellum and upper (rostral) rhombic lip were regions more similar to NS iNs than AS iNs. As seen by GABAergic marker expression, ventral structures like the ganglionic eminence map were mapped to NS late neurons with similar correlation as diverse cortex structures. For most structures, AS iNs were more similar to human brain regions than NS iNs. Together with the more pronounced progenitor identity in NS iNs that we had identified earlier, we therefore concluded that at the experimental timepoints assessed, NS reprogramming gives rise to less differentiated cells than AS reprogramming.

3.3.4 NS reprogramming is accompanied by lower facilitator and OxPhos score levels

To investigate the reasons for this delay in iN development during NS reprogramming despite its early advantage resembled by the major reduction in starting population accumulation, we assessed the expression of the previously identified facilitator subscores (**Figure 8F**) in NS- compared to AS-induced reprogramming (**Figure 25A**). While subscore 1 seemed to be more AS-specific and its levels were not nearly as high anywhere along the NS trajectory, subscore 2 followed a similar increase towards iN identity, however on a much lower level. Interestingly, the alternative fate was marked by high facilitator subscore 3 expression, suggesting that this fate represented a similar dead end in development as the mid trajectory fate during AS reprogramming. Therefore, we removed subscore 3 also here to generate a new combined facilitator score, which showed that the NS iN clusters exhibited score levels similar to the AS mid trajectory (**Figure 25B**). At the same time, the blocker score was expressed similarly in both AS and NS early trajectory and was gone in NS iN

clusters, while still not completely down in the alternative fate, giving an additional explanation for the absence of *TUBB3* expression here (**Figure 25C**). In general, we concluded that the developmental retardation of NS iNs was not caused due to failed blocker downregulation but rather by low facilitator gene levels.

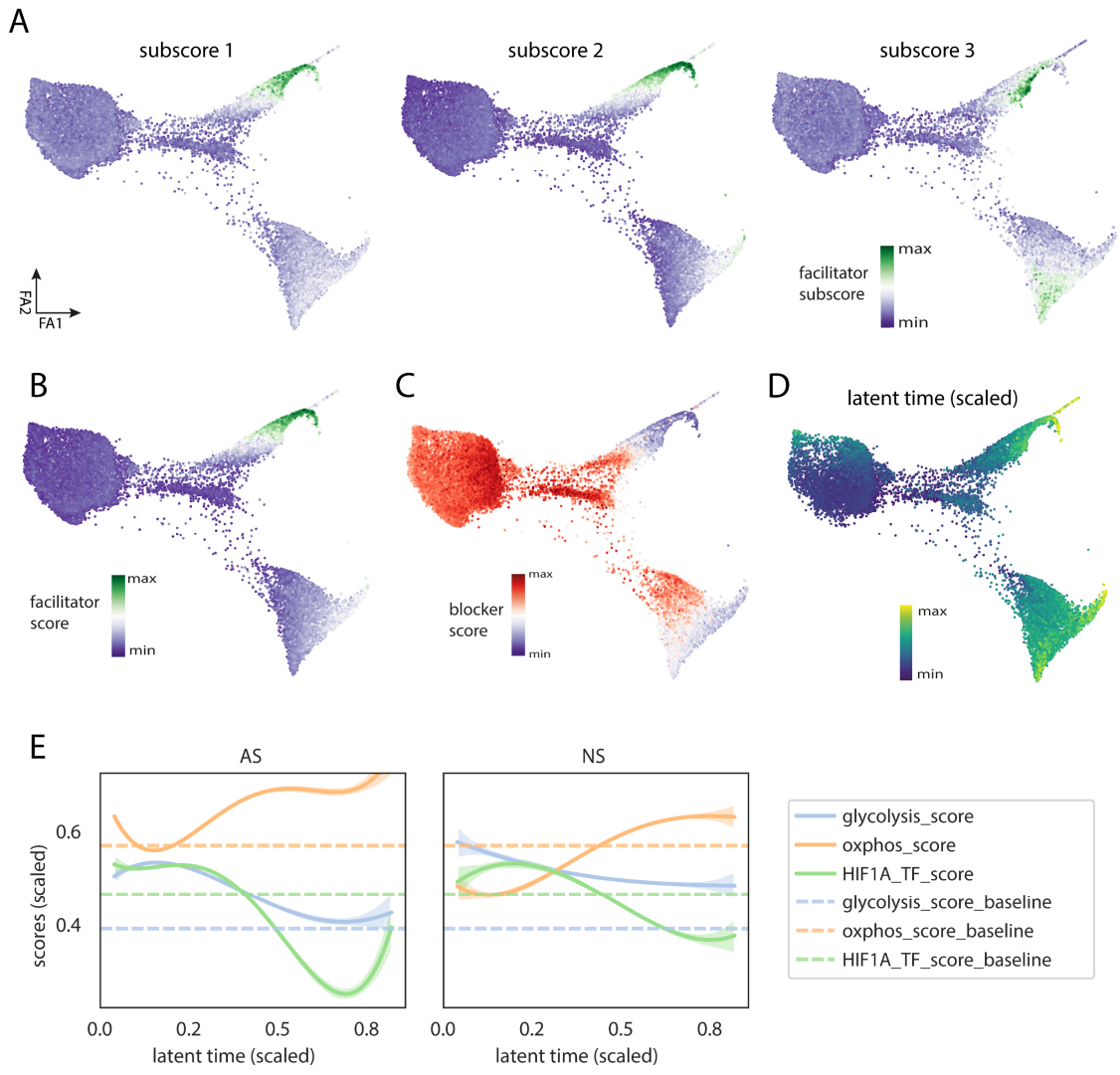

Figure 25 | Facilitators and blockers identified in AS reprogramming are also found in NS reprogramming. (**A**) Force-directed graph of the *AS+NS* dataset colored by the three facilitator subscores as identified in AS-transduced cells. (**B**) Facilitator and (**C**) blocker score as identified in AS-transduced cells, visualized on the *AS+NS* embedding. Facilitator score only contains subscores 1 and 2. (**D**) Force-directed graph of the *AS+NS* dataset without GFP colored by scaled latent time (developmentally early: blue; developmentally late: green->yellow). (**E**) Plots depicting scores generated from the expression of glycolysis-related genes, OxPhos-related genes and the HIF1A regulon along latent time (scaled) among AS and NS cells. Latent time is capped at the ends due to low cell numbers. Scores in GFP-transduced control cells are indicated as dotted baseline. Confidence interval > 0.95.

Since we identified the metabolic transition from glycolysis to OxPhos as a major barrier for successful reprogramming using AS, we intended to determine its impact also in NS reprogramming. Therefore, to compare both trajectories, we first calculated a latent time (**Figure 25D**). It showed that similar to the confused fate in AS reprogramming, the NS-induced alternative fate was also terminal given its high latent time.

Comparing scores along this scaled latent time (**Figure 25E**), it evinced that HIF1A TF activity was similar at the starting population between AS and NS, was then increasingly downregulated in both TF combinations along latent time, but with significantly different slopes. In congruency to the HIF1A regulon, the glycolysis score was also downregulated more slowly in NS than AS and at maximum latent time in NS reached levels similar to mean latent time in the AS trajectory. In the meanwhile, the OxPhos score in NS started from significantly lower levels in the starting population, then increased along latent time with a similar slope as in AS, however its peak was still significantly lower than in AS.

In conclusion, the delayed progress of NS iNs can be attributed not only to lower facilitator score levels but also to partly failed glycolysis downregulation and lower initial OxPhos acitivity in relation to AS reprogramming.

4 Discussion

It is known that the identity of differentiated cells is not set in stone. Many cell types have been shown to be reprogrammable to adopt a different fate, even across lineages, without undergoing mitosis (Vierbuchen & Wernig, 2011). Direct pericyte-to-neuron reprogramming represents promising means for future cell-replacement therapies. However, many factors involved in the reprogramming process remained elusive so far. Through this study, we did not only reveal molecular barriers but could also identity experimental approaches how to overcome them by signaling modulation to improve the reprogramming outcome and direct the cells towards an iN fate.

4.1 Molecular reprogramming barriers in pericyte-to-iN conversion

Our data obtained from single-cell transcriptome analyses show that during the process of AS-induced pericyte-to-iN reprogramming, the NSC-like intermediate state proposed by Karow et al. (2018) is part of a plastic process involving different states of transcriptional identity. The finding that more cells progress at d7 after AS-transduction than at d14 (**Figure 7B**) was in line with our concept of the reprogramming course being a stochastic process: Cells that haven't made it past the density peak by d14 are less likely to be progressing at all, while cells that have passed the decision point are more likely to progress at the later experimental timepoint. By single-cell RNA velocity and DE analysis, we identified different sets of genes associated with progression or non-progression along the reprogramming trajectory, which we therefore defined as facilitator and blocker genes, respectively (**Table 4**).

Falk et al. (2021) describe three decision points in successful direct reprogramming: metabolic changes, chromatin changes, and cytoskeletal changes. The blocker and facilitator genes we identified here comprise genes involved in all three of these processes (**Figure 8A**), confirming that they control several vital aspects of cellular identity conversion. It has been shown recently that mitochondria differ between cell types (Fecher et al., 2019) and that they play an important role in cell fate decision during neurogenesis (Iwata et al., 2020). Moreover, it has been demonstrated that the loss of

certain mitochondrial genes is required for successful conversion to neurons (Russo et al., 2021), one of which, *MGST1*, we also identified as a blocker gene in our present study.

It is important to point out that the cells we compared to identify blocker and facilitator genes were already principally amenable to reprogramming since they had already left the starting population. However, the expression of the blocker score not only on the trajectory but also in the starting population (**Figure 8B**) demonstrated the relevance of these blocker genes from the very beginning of the cellular conversion process.

Among facilitator genes, we further demonstrated the existence of several subsets of genes with different temporal expression pattern (**Figure 8F, H**). Strikingly, our data confirm the proposed sequence of events during reprogramming, as the transiently expressed facilitator gene subset 1 includes several genes coding for proteins involved in chromatin remodeling, which is the second decision point after metabolism change (Falk et al., 2021). The third decision point of cytoskeletal changes is then represented in both facilitator gene subset 1 and even more facilitator gene subset 2, which contain several genes coding for tubulins and microtubule associated proteins, that are vital factors in remodeling of the cytoskeleton. It has been shown that many changes in microtubule organization are centrally orchestrated and do not only instruct a morphological transition but are also necessary for neuronal migration during neurogenesis (Camargo Ortega et al., 2019).

As this study shows, failure to downregulate genes of the blocker score sufficiently during the trajectory results in cells being either less likely to continue their progression towards iNs (**Figure 8D**) or even cells adopting a confused fate (**Figure 8H**). Additionally, we have demonstrated that decreased blocker score in combination with predominant expression of genes of the facilitator subset 3 instead of the other facilitator genes (**Figure 8F**), is associated with cells terminating their reprogramming process prematurely during mid trajectory (**Figure 10A, B, C**).

We further uncovered that NOTCH signaling is dynamically used along the trajectory (**Figure 11A, C**). We illustrate that *HES1* expression must be downregulated to become a neuron, a function that other studies have demonstrated to be exerted by Myt1l

(Mall et al., 2017). Other members of NOTCH signaling were only temporarily upregulated during the conversion process, while *HES6* upregulation correlated with *TUBB3* expression. Hes6 has been shown to inhibit Hes1, increase Ascl1 activity and promote neuronal differentiation (Bae et al., 2000). TGF-β signaling also exhibited a very dynamic expression pattern during the conversion process (**Figure 11B, C**). We demonstrated that several ID family members and other TGF-β signaling targets need to be downregulated for cells to acquire a neuronal fate. In particular, Id1 and Id3 have been indicated to inhibit neural differentiation in earlier studies (Bai et al., 2007; Lyden et al., 1999). We also identified downregulation of TGFB1 itself as a requirement to enter the trajectory, which is supported by earlier findings that high TGFβ1 levels lead to inhibition of neural stem and progenitor cell proliferation and to reduced neurogenesis (Wachs et al., 2006).

Hence, we provided evidence that any deviation from the 'correct' signaling cascade of the neuronal fate, be it in expression trend or magnitude, leads to a different cellular terminal fate (**Figure 11A,B**): Cells ended up in the starting population with only minor transcriptomic changes compared to the control, mid-way on the trajectory, while unable to progress further towards iNs since molecular requirements had not been met, or cells assumed a confused fate, which is a dead-end on the reprogramming trajectory.

4.2 Signaling modulation reduces cellular identity safeguarding mechanisms induced by AS-transduction

Since we identified NOTCH and TGF-β/BMP signaling to play vital roles in direct pericyte-to-neuron reprogramming, we manipulated each pathway by application of specific inhibitors during the conversion process. Strikingly, each treatment led to a massive increase in more mature iNs (**Figure 17E**). Although each treatment seemed to slightly favor generation of one of the two neuronal subtypes, there was no major difference in subtype contribution as an effect of the treatments. Surprisingly, while NOTCH signaling inhibition with DAPT seemed to affect the starting population but not so much the cells' route on the trajectory itself, TGF-β signaling inhibition using SB/DM led to an extensive difference in the starting population's transcriptome and also triggered a

completely different trajectory, which, however, gave rise to highly transcriptionally similar neurons as AS (**Figure 12D**). Despite the differences between the trajectories, we demonstrated that they all consisted of comparable segments (**Figure 14**). These findings prove that the underlying molecular mechanisms allow for more than a single way to generate a certain cell type. Another example for this plasticity has been provided by pericytes themselves, that have been shown to be derived from multiple developmental origins even if residing within the same tissue (Dias Moura Prazeres et al., 2017).

Remarkably, our investigations of the transcriptional mechanisms underlying the increase in mature neurons by both DAPT and SB/DM treatments revealed that these did not trigger an increase in facilitator score (**Figure 16A, E**). Instead, we uncovered that the blocker score was decreased significantly by each treatment (**Figure 16B, C, E**). Moreover, the blocker score turned out to be a response to AS expression since we demonstrated that it was significantly upregulated in AS compared to the control. We therefore propose that the genes of the blocker score represent a cellular identity safeguarding mechanism, similar to what has been described earlier for the REST complex that has been shown to suppress differentiation and reprogramming (Drouin-Ouellet et al., 2017; Laugesen & Helin, 2014; Masserdotti et al., 2015).

However, as we illustrated in this study, the effect of NOTCH and TGF-β signaling modulation to increase the iN fraction cannot only be attributed to a reduction in blocker scores. Instead, we demonstrated that HIF1A regulon activity was increased in the starting population upon AS-transduction (**Figure 18A, Figure 19B, D, E, F**). The HIF-1α protein encoded by HIF1A has been shown to be a master regulator of oxygen homeostasis (Semenza, 2012) and to be continuously expressed in neural stem and progenitor cells (Roitbak et al., 2011). STAT3, which is known to interact with HIF-1α to activate HIF1A target genes (Pawlus et al., 2014; Pawlus et al., 2013), is upregulated as well upon AS-expression. While HIF1A supports glycolysis, in particular under hypoxic conditions, differentiation into neurons requires a metabolic change to OxPhos (Maffezzini et al., 2020; Zheng et al., 2016). In line with this mechanism, it is not surprising that usage of an HIF1α inhibitor has been shown to improve fibroblast-to-iN conversion by facilitating OxPhos (Herdy et al., 2019). Therefore, the increase in HIF1A levels upon AS-transduction might constitute an early cellular identity safeguarding mechanism in these cells and can be seen

as a metabolic 'fingerprint' of pericytes (Nwadozi et al., 2020): If energy needs of another identity are not met, an identity transition is rendered less likely or even completely averted.

Strikingly, we revealed that NOTCH and TGF-β signaling inhibition each counteracted this gatekeeping mechanism and both lowered HIF1A activity significantly (**Figure 18A, Figure 19B, D, E, F**). This was accompanied by a significant general downregulation of glycolysis-related genes as well as an upregulation of OxPhos-related genes, with the strongest effects in the starting population and the early trajectory (**Figure 19F**). Hence, we conclude that the improved iN generation at least partly depends on a modulated cellular metabolism that is primed to become neuronal.

It is interesting that, although the extent of the effect varies, both treatments trigger a similar metabolic change. We suggest that this is due to a cross-talk between both pathways that have been proven to be far from independent: They have been shown to interact in both synergistic and antagonistic ways (Klüppel & Wrana, 2005), in particular regulating neurogenesis via cooperation of Notch and Id factors (Boareto et al., 2017).

We showed that in general, TGF-β signaling modulation via dual SMAD inhibition exerted a stronger effect on metabolism than NOTCH signaling modulation via DAPT. This was not only reflected by the flatter HIF1A activity, glycolysis, and OxPhos score trends along the trajectory (**Figure 19F**), but might further explain the differences in densities distribution along the trajectory between the treatments (**Figure 15D, E**). Our results suggest that the removal of metabolic reprogramming barriers by SB/DM treatment leads to a smoother transition between different states of cellular identity during the reprogramming process.

4.3 Reprogramming process is rendered more target-oriented by dual SMAD inhibition

We propose that the observed longer overlap of OxPhos and glycolysis transcriptional signatures upon SB/DM treatment gives AS-transduced cells more time to change their identity. Therefore, a confused cell fate in cells that do not meet the metabolic

requirements for conversion into iNs might be circumvented by not enforcing fate decision through the cells' metabolic state. Strikingly, we demonstrated that TGF-β signaling modulation almost extinguished the confused fate population (**Figure 17E**). Confused cells were generated during normal AS-induced reprogramming and were marked by *SOX9* expression but had a mixed transcriptional identity with features of different cell types (**Figure 9A, B**). Confused fate cells furthermore downregulated the blocker score insufficiently (**Figure 8B, H**), indicating that molecular safeguarding mechanisms were still in place, which were more sustainably downregulated by dual SMAD inhibition from the starting population on (**Figure 16B, C, E**).

We revealed that the closest transcriptional neighbors of cells in the confused fate were cells located in mid trajectory before cells progress further towards a neuronal identity (**Figure 10B, C**). Therefore, we concluded that this is where the identity decision towards confused fate is taken. Several regulons were contrastingly regulated between cells in this part of the trajectory compared with the corresponding cells after SB/DM treatment (**Figure 20B, C, D**). As VDR was strikingly increased in dual SMAD inhibited cells (**Figure 20F**) and due to its role as an anti-oxidant (Bao et al., 2008; Dong et al., 2012), it was indicated as a potential mechanistic explanation for the reduction in confused fate cells by TGF-β signaling modulation, by lowering the oxidative stress in the cells. Co-transfection of reprogramming factors with Vdr has been shown to improve neuronal reprogramming in MEFs (mouse embryonic fibroblasts) (Gascón et al., 2016). Therefore, it would be worthwhile to see in further studies if VDR expression does also facilitate reprogramming of human brain pericytes and if co-transduction of AS with VDR and without further SB/DM treatment alone would enable cells to better deal with the metabolic transition and if that would be sufficient to reduce the confused fate population.

We demonstrate in this study that confused fate lineage adoption is accompanied by significant differences in NOTCH and TGF-β signaling compared to the iN lineage (**Figure 11A, B**). This was particularly obvious in TGF-β signaling targets like *VEGFA* (Pertovaara et al., 1994), which has been shown to be expressed dependent on HIF-1α under hypoxic conditions (Sutter et al., 2000), further underlining that the confused fate resulted from a cellular inability to handle the metabolic shifting towards OxPhos. Another highly differentially expressed gene was *CDKN1A*, which codes for the Cyclin-dependent

kinase (CDK) inhibitor p21, an important regulator of cell cycle progression (Barr et al., 2017). Interestingly, the p53-p21 pathway has been described as a safeguarding mechanism of somatic cells in cellular reprogramming (Hong et al., 2009). Therefore, we suggest that confused fate cells have not escaped these safeguarding barriers. However, we show that manipulating the starting population by dual SMAD inhibition enables cells to overcome these barriers and thereby sets the course for the cells to become iNs rather than remaining in a confused state.

4.4 The proneural factors Neurog2 and Ascl1 differ in their reprogramming capacity

Despite the effect of the SB/DM and the DAPT treatment on reprogramming pericytes, a large fraction of cells did not leave the starting population, likely due to remaining reprogramming barriers. Interestingly, when we combined Sox2 overexpression with Neurog2, we did not only demonstrate that NS-transduced cells also give rise to *TUBB3*+ cells (**Figure 22B**) but also that this TF combination allowed most cells to leave the starting population (**Figure 22C, Figure 23A**). This difference could be largely attributed to the diverging functions of the proneural TFs Ascl1 and Neurog2 that have been shown to be caused by their different genomic binding sites even in a similar cellular context (Aydin et al., 2019). Aydin et al. (2019) have demonstrated that the individual effects of Ascl1 and Neurog2 in neuronal reprogramming are not defined by the initial chromatin state but by enrichment of particular E-box sequences preferentially bound by one or the other TF, thereby changing chromatin accessibility and enhancer activity, eventually affecting binding of downstream TFs and neuronal subtype specification.

For both transcription factors, their interaction with reprogramming barriers has been studied. Ascl1 is a pioneer TF that can bind to closed chromatin (Wapinski et al., 2013) and stabilize neuronal identity (Aydin et al., 2019), but Ascl1 expression was demonstrated to be suppressed by REST (Ballas et al., 2005). Neurog2 has been shown to compete with REST to induce expression of Sox4 and Sox11, which control neural identity (Bergsland et al., 2006). REST blocks reprogramming by preventing Neurog2 from binding to the NeuroD4 promoter, which is needed for postmitotic neuronal differentiation

(Masserdotti et al., 2015). Moreover, Masserdotti et al. (2015) further demonstrated that time is a critical factor in overcoming reprogramming barriers since REST accumulates in older cell cultures.

However, the importance of the second TF in both reprogramming gene sets, Sox2, which renders chromatin more accessible (Malik et al., 2019), should not be underestimated. Karow et al. (2012) have shown that Ascl1 alone is unable to convert pericytes into neurons. Interestingly, it was discovered that SOX2, which was known earlier mainly as a pluripotency and neural progenitor regulator gene (Favaro et al., 2009; Miyagi et al., 2008), changes its interaction partners during the differentiation process, binding first to pluripotency enhancers, later to neuronal promoters (Bunina et al., 2020). Although both Ascl1 and Neurog2 were combined with Sox2 in our study, the effect of Sox2 on chromatin accessibility might differ depending on the co-expressed proneural TF. Recently, the role of Neurog2 in neuronal differentiation was highlighted again by the finding that it is sufficient to induce local chromatin accessibility (Noack et al., 2022). Moreover, while Ascl1 and Sox2 were used on a single retroviral construct, Neurog2 and Sox2 were expressed via two separated viral constructs. Since FAC-sorted NS-transduced cells were sorted for each TF individually, cells with a lower expression of one of the constructs may not have been included in the analysis. Future studies are necessary to reveal if, and if yes, how the stoichiometry between the involved TFs affects the identity of the cellular outcome and which changes of cellular identity occur due to Neurog2 alone. Additionally, since it has been shown that Ascl1 and Neurog2 are oscillatorily expressed in NSCs, controlling proliferation and differentiation (Imayoshi et al., 2013; Shimojo et al., 2008), it will be of interest to specifically look at temporal expression patterns of proneural TFs during direct reprogramming e.g. by live imaging with a fluorescent reporter.

Since we had used murine TFs for transduction, we were able to distinguish intrinsic *ASCL1* and *NEUROG2* expression in reprogramming cells. Previously, these TFs were thought to appear mutually exclusively in neurons, defining the neuronal subtype (Osório et al., 2010). Remarkably, our AS-transduced cells give rise to cells expressing either *ASCL1*, *NEUROG2*, both or none (**Figure 21D**). This matches with the results of a recent study in mice and human cerebral organoids, revealing the existence of four lineage-biased NSC pools based on the expression or non-expression of *Ascl1* and *Neurog2* (Han et

al., 2021). During the later reprogramming process, the *ASCL1*+/*NEUROG2*+ population started to express *NEUROD4*, then splits up into cells we identified as more GABAergic and cells we identified as more glutamatergic. Han et al. (2021) also described that double+ NSCs are least lineage restricted. In the most mature cells *NEUROG2* and *ASCL1* expression appeared mostly mutually exclusive (**Figure 21D**), as well as *ASCL1* and *NEUROG3*, which plays a vital role in subtype specification (Carcagno et al., 2014).

For a long time, ASCL1 was implicated in GABAergic neuron generation, while NEUROG2 was implicated in glutamatergic neuron generation (Osório et al., 2010). However, this view has been overturned by several studies showing that NEUROG2 can generate GABAergic neurons (Chouchane et al., 2017; Florio et al., 2012) as well as ASCL1 being able to produce glutamatergic neurons (Chanda et al., 2014; Vierbuchen et al., 2010), suggesting the subtype specificity of TFs to be rather context-dependent, although this might also be a consequence of the artificial approach of cellular reprogramming. Very recently, it has been highlighted that single embryonic human cortical progenitors produce both excitatory neurons and GABAergic interneurons (Delgado et al., 2022). Interestingly, through AS reprogramming we got both glutamatergic and GABAergic cellular identities (**Figure 17D, Figure 21C, D**), while NS reprogramming did not reveal a bifurcation of identities (**Figure 24C**). In general, we showed that NS-transduced *TUBB3*+ populations were less defined compared to AS-transduced iNs and were less comparable to the transcriptional makeup of distinct human brain structures (**Figure 24C, E**). We attributed this to a lower *TUBB3* and higher *PAX6* expression in NS generated iNs (**Figure 24C, D**), suggesting cells remain in a more progenitor-like state. This requires to be further investigated and compared to e.g. human progenitor populations from human brain organoids or fetal tissue.

While the differences in iN maturity could be fully ascribed to the different binding capacities of Ascl1 and Neurog2 (Aydin et al., 2019), interactions with the starting population or other generated cell types might also play a role. In addition to reduction of off-target identities for the sole purpose of increasing the fraction of iNs being generated, these off-target populations might affect development of the iN population by non-cell autonomous effects caused by secretion of different proteins. We demonstrate here (**Figure *23*C**) that cells on the NS-induced alternative fate path are characterized by

expression of *SCRG1*, which is involved in mesenchymal stem cell regulation (Aomatsu et al., 2014). Moreover, *SCRG1* codes for a secreted protein and has been shown to be associated with neurodegenerative changes observed in transmissible spongiform encephalopathies (Dandoy-Dron et al., 2003), suggesting that it could potentially affect differentiation of NS-generated iNs.

Despite our study illustrating NS being less efficient in producing differentiated neurons than AS, Lin et al. (2021) found that in principle NEUROG2 is capable of generating diverse neuronal subtypes, depending on NEUROG2 expression level and duration. While we could not find expression of several markers of NEUROG2-generated lineages described by (Lin et al., 2021), we already found different neuronal subtype markers in combination with a progenitor-like identity. However, Lin et al. (2021) used human iPSCs as a starting population, which might also indicate that the chromatin landscape of pericytes allows for a better reprogramming using Ascl1 instead of Neurog2. Karow et al. (2018) have further demonstrated that a combination of all three TFs, Ascl1, Neurog2, and Sox2 was able to induce higher *TUBB3* expression and VGLUT1 immunoreactivity in iNs, while generating mostly glutamatergic neurons.

In conclusion, it seems reasonable that reprogramming using a different dosage of single TFs in a combination of Ascl1/Sox2, Neurog2/Sox2 or all three TFs, is a promising approach to not only generate more mature neurons than Neurog2/Sox2 but also to be able to significantly affect their subtype.

4.5 Implications from pericyte-to-iN conversion for cellular identity

While the identity of differentiated cells has been viewed as terminal for a long time (Waddington, 1957), many discoveries have changed this impression since then. Recently, it was demonstrated that also in the CNS of vertebrates, neuronal identity is plastic and one subtype can turn into another, and that this process is mediated by Notch-signaling (Engerer et al., 2021). This natural occurrence of neuronal re-specification further supports the approach of modulating signaling pathways in order to change the reprogramming outcome, as we have shown in this study. We modulated NOTCH and

TGF-β signaling but also Wnt signaling modulation via small molecules has been proven to be effective to reduce variability in the neurons produced from iPSCs (Strano et al., 2020). The effects on the starting population of the signaling modulation alone, without the TFs that are the main drivers for reprogramming, remain to be investigated. While we did not find neurons being generated after only small molecule treatment, other studies have demonstrated that in fibroblasts, a complex combination of four or more small molecules was sufficient to convert them into iNs in the absence of exogenous TFs (Hu et al., 2015; Li et al., 2015).

Cellular identity can be changed; however, cells still seem to be affected by their original identity. Even when differentiating from pluripotency, intrinsic signaling differences lead to high gene expression variability in the resulting neurons (Strano et al., 2020). Strikingly, it has been demonstrated recently in astrocytes that regional specificity is conserved throughout the reprogramming process into iNs. (Herrero-Navarro et al., 2021). Therefore, it would be highly interesting to compare iNs generated from different brain regions of the same human patient to examine the regional influence on reprogramming efficiency and subtype specification.

It will further be interesting to investigate the potential of several of the identified facilitator genes to improve the reprogramming process, as it was shown that a safeguarding factor like Myt1l alone induced direct reprogramming of pericytes into cholinergic neurons (Liang et al., 2018). Once metabolic checkpoints are passed successfully, new cellular identity safeguarding mechanisms come into effect. One example for this is the induction of *MIAT* in all neuronal clusters, which has been demonstrated to reduce neuron apoptosis upon overexpression (Li et al., 2019). Since Karow et al. (2012) revealed that apoptosis occurs in a significant number of AS-transduced cells, future investigations might focus particularly on the prevention of apoptosis to further increase the neuronal outcome. Methods like cell tracking during live imaging will hereby be more informative than scRNA-seq to dissect the cellular changes along reprogramming.

This will further allow for investigations of the 'direct' nature of the reprogramming process, i.e. that the cellular conversion occurs without mitosis. Karow et al. (2012) have shown that this is the case for normal AS-reprogramming despite cells expressing NSC-like genes. Here, we confirmed the existence of this NSC-like state and even illustrate that it

indeed expresses the NSC marker *NES*, which was originally not detected by Karow et al. (2012). This might be attributable to the different methodology, pericyte culture, and, most importantly, the substantially higher cell number used in this study. Furthermore, we did not find evidence for proliferation in consequence of the small molecule treatments. However, especially the progenitor-like identity of NS-generated iNs needs to be further examined for proliferating populations. If these exist for only a limited time during the reprogramming process before further differentiation, this could allow for an expansion of the cell pool used in potential therapeutic approaches, as long as the risk of tumor formation by proliferating cells could be contained.

Although our approach to generate iNs from human brain pericytes is artificial, there is recent evidence that pericytes in mice acquire stem cell activity under hypoxic conditions, generating both vascular and neural cells (Nakagomi et al., 2015). While Karow et al. (2012) did not find TUBB3+ cells among cultured pericytes even in low oxygen conditions, the results of Nakagomi et al. (2015) show that brain pericytes with their mostly neural crest origin (Simon et al., 2012; Trost et al., 2013) represent a versatile starting cell population for reprogramming into neurons. As shown in another publication (Yamamoto et al., 2017) however, brain pericytes are quite heterogeneous in their origin. This might result in subpopulations with different reprogramming capability, as described by Karow et al. (2018). Also in this study, we observe a high heterogeneity with regard to cells being amenable to reprogramming while others do not even leave the starting population despite AS or NS transduction. In this context, it will be very instructive to look at the chromatin accessibility of different pericyte subpopulations with methods like scATAC-seq (single cell Assay for Transposase Accessible Chromatin with high-throughput sequencing) (Chen et al., 2018).

Many studies on pericytes and on direct reprogramming have been performed in different animal models. While many genes involved in human brain development are highly evolutionarily conserved in their sequence, the human brain has undergone an increase of its size and complexity compared to other lineages, which is likely attributable to changes in regulatory networks (Brawand et al., 2011; Necsulea & Kaessmann, 2014). Since in contrary to many studies in the field of reprogramming, our experiments were performed directly on human cells, we are not only able to make more precise statements

about *in situ* human brain pericyte reprogramming capabilities, but our detected blockers and facilitators might also include genes that are species-specifically involved in neurogenesis. While human brain pericytes are the perfect *in vitro* model for reprogramming due to their human transcriptome, potential human-specific mechanisms of direct reprogramming would not be targetable in future *in vivo* animal experiments. Nevertheless, valuable insights on the cellular conversion process could also be gained through direct lineage reprogramming of mouse brain pericytes *in vivo*.

New approaches to model cell fate decisions and developmental landscapes promise an even better insight into the molecular processes of cellular differentiation (Sáez et al., 2021), chromatin accessibility dynamics (Trevino et al., 2020), and might also help to better understand the nature of the reprogramming process and to identify additional leverage points for improvements, increasing the efficiency of the conversion process (Jung et al., 2021).

4.6 Hurdles towards clinical application of direct pericyte-to-neuron reprogramming

The ultimate goal of pericyte-to-iN conversion is to harness it for the development of neuronal replacement therapies for patients with diseases or brain injuries involving the loss of neurons. There is still a long way to go until application in humans and several factors might impact on the applicability.

One of these is if the reprogramming capability of human brain pericytes varies not only between cellular subpopulations but between individual patients. Interestingly, REST complex has been shown to be more abundant in cells from older patients (Drouin-Ouellet et al., 2017), indicating a decreasing reprogrammability with age. In addition, iNs from older donors have been observed to reduce expression of OxPhos-related genes and exhibit other age-related changes in energy metabolism (Kim et al., 2018). Considering that the experiments described in this study were performed on cells obtained from a 26-year-old female, it will be worthwhile to investigate age-related differences in susceptibility to direct cell conversion. This is particularly important as many diseases, where patients

might benefit from future cell replacement therapies, primarily manifest in patients of a higher age (Hou et al., 2019).

While the preservation of regional specificity would be a positive side effect of cells keeping traces of their original identity, this could be less beneficial when it concerns cellular defects present in the starting cell. For example, it has been demonstrated that age-associated nucleocytoplasmic deficiencies are preserved after reprogramming of human fibroblasts into iNs but not after reprogramming via an iPSC state (Mertens et al., 2015) and that also AD-related molecular changes are maintained upon direct reprogramming, affecting the newly generated iNs (Mertens et al., 2021). Hence, while these findings should not affect the potential treatment of brain injuries, it is important to investigate if, and which disease-related cellular features are conserved in direct pericyte-to-iN reprogramming, to allow for a targeted removal strategy of these molecular marks. A rejuvenation of cells as performed by Mertens et al. (2015) has proven to effectively revert those age-related changes. However, as this requires reprogramming to iPSCs, it would increase the risk for uncontrolled proliferation of these stem cells and thereby tumor formation.

This will also be of interest with respect to the TFs used in reprogramming. Both our TF cocktails used in this study contain Sox2, which is a potentially cancerogenic gene (Novak et al., 2020). While proliferation has not been observed in AS reprogramming (Karow et al., 2012), it will need to be further examined in NS reprogramming. Moreover, in the *in vitro* culture used so far, we were not able to follow up on effects the used TFs might have on non-pericyte cell types. This underlines the need for a precise delivery system for our TFs in a therapeutic setting. It will be necessary to develop a vector that ideally is cell type specific. Not all retroviral vectors have the ability to infect non-dividing cells (Yamashita & Emerman, 2006) and retroviruses pose a risk for mutagenesis by disruption of genes through genomic integration (De Ravin et al., 2014). Therefore, adeno-associated virus (AAV) might constitute a more promising vector for application in patients (Hamilton et al., 2004); in particular since it has been shown that AAV capsid variants enable targeting of specific cell types (Goertsen et al., 2022). However, this will require a deeper understanding of *in vivo* heterogeneity of human brain pericytes.

Additionally, although reprogrammed cells seem to autonomously downregulate the transgenes, since they could not proceed to become postmitotic neurons otherwise, it would be a great advantage to use an inducible system (Heinz et al., 2011) for only temporary expression of our reprogramming factors. If NOTCH or TGF-β signaling modulation are also to be used in a therapeutic context, is will be an additional question how to deliver these small molecules only into the target cells.

Besides, even within pericytes, it will not be useful to target all cells. With their involvement in BBB stabilization (Armulik et al., 2010; Bell et al., 2010; Daneman et al., 2010), regional blood flow (Fernández-Klett et al., 2010; Peppiatt et al., 2006) and their role in local regulation of the immune system (Jansson et al., 2014; Rustenhoven et al., 2017), they fulfil vital functions within the brain and pericyte loss might even cause neurodegeneration (Bell et al., 2010). In this regard, the fact that AS reprogramming rates are still far from 100% could be a benefit in therapeutic approaches and the mentioned heterogeneity of pericytes (Göritz et al., 2011) could allow for targeting of a pericyte subpopulation that has a lower impact on brain function when lost.

Finally, the iNs resulting from direct reprogramming need to be analyzed concerning their ability to migrate to their target position within the brain and to integrate into existing neuronal networks. In astrocyte-derived iNs, integration into local circuits has been demonstrated by evoked synaptic responses (Guo et al., 2014) and by mapping of connections of host striatal projection neurons with iNs (Torper et al., 2015). Therefore, it would certainly be meaningful to examine the integration abilities of transplanted reprogramming human pericyte-derived cells in animal models, although this again would raise issues with transferability of the results to human patients, given the regulatory differences in transcriptomics between humans and other species. Thus, another option would be the transplantation or co-culture of reprogramming human cells into a purely human model system like human cerebral organoids (Lancaster et al., 2013). The generation of dorso-ventrally patterned human cerebral organoids (Bagley et al., 2017) would further allow for the investigation of migration of iNs towards their target region. Any evidence that the cells generated by pericyte-to-iN conversion migrate and integrate into existing networks, would significantly advance the use of direct reprogramming in future neuronal replacement therapies.

4.7 Conclusions

In this study, we show that direct pericyte-to-iN reprogramming is accompanied by different hurdles that cells need to take to successfully change their identity. We demonstrate that the forced expression of Ascl and Sox2 in the cells triggers cellular identity safeguarding mechanisms which can be suppressed by additional inhibition of NOTCH or TGF-β/BMP signaling, both strongly increasing the number of iNs generated. Our results do not only reveal a set of blocker genes but also different sets of facilitator genes impacting on reprogramming. We illustrate the key role of metabolic shifting from glycolysis to oxidative phosphorylation in shifting from pericyte to neuronal identity. Our findings suggest that any failure to meet metabolic requirements results in cells being either unable to change their identity or adopting a confused fate. We further show that TGF-β signaling inhibition is more potent in lowering these metabolic barriers than NOTCH signaling inhibition and that it allows for a strong reduction in the number of confused cells, likely due to antioxidant regulon activity. Eventually, we point out that neuronal cells can also be generated with Neurog2/Sox2. However, these cells have a different transcriptomic identity, exhibiting more progenitor-like properties, illustrating the different reprogramming capacities of proneural TFs.

Altogether, these results underline that cellular identity is not as static as previously anticipated and that it can be effectively manipulated in the absence of mitosis. Moreover, this thesis sheds light on several previously unknown features of direct pericyte-to-iN reprogramming and potential ways to improve its efficiency, exemplifying general conditions for cross-lineage cellular identity change. Although it is still a long way to go, it thereby adds one more step towards potential direct cellular reprogramming-based human neuronal replacement therapies for millions of patients.

REFERENCES

Altman, J. (1962). Are New Neurons Formed in the Brains of Adult Mammals? *Science*, *135*(3509), 1127-1128. https://doi.org/10.1126/science.135.3509.1127

Aomatsu, E., Takahashi, N., Sawada, S., Okubo, N., Hasegawa, T., Taira, M., Miura, H., Ishisaki, A., & Chosa, N. (2014). Novel SCRG1/BST1 axis regulates self-renewal, migration and osteogenic differentiation potential in mesenchymal stem cells. *Scientific Reports*, *4*(1), 3652. https://doi.org/10.1038/srep03652

Armulik, A., Genové, G., & Betsholtz, C. (2011). Pericytes: Developmental, Physiological, and Pathological Perspectives, Problems, and Promises. *Developmental Cell*, *21*, 193-215. https://doi.org/https://doi.org/10.1016/j.devcel.2011.07.001

Armulik, A., Genové, G., Mäe, M., Nisancioglu, M. H., Wallgard, E., Niaudet, C., He, L., Norlin, J., Lindblom, P., & Strittmatter, K. (2010). Pericytes regulate the blood–brain barrier. *Nature*, *468*(7323), 557-561.

Artavanis-Tsakonas, S., Rand Matthew, D., & Lake Robert, J. (1999). Notch Signaling: Cell Fate Control and Signal Integration in Development. *Science*, *284*(5415), 770-776. https://doi.org/10.1126/science.284.5415.770

Arvidsson, A., Collin, T., Kirik, D., Kokaia, Z., & Lindvall, O. (2002). Neuronal replacement from endogenous precursors in the adult brain after stroke. *Nat Med*, *8*(9), 963-970. https://doi.org/10.1038/nm747

Attwell, D., Buchan, A. M., Charpak, S., Lauritzen, M., MacVicar, B. A., & Newman, E. A. (2010). Glial and neuronal control of brain blood flow. *Nature*, *468*(7321), 232-243. https://doi.org/10.1038/nature09613

Aydin, B., Kakumanu, A., Rossillo, M., Moreno-Estellés, M., Garipler, G., Ringstad, N., Flames, N., Mahony, S., & Mazzoni, E. O. (2019). Proneural factors Ascl1 and Neurog2 contribute to neuronal subtype identities by establishing distinct chromatin landscapes. *Nat Neurosci*. https://doi.org/10.1038/s41593-019-0399-y

Bae, S., Bessho, Y., Hojo, M., & Kageyama, R. (2000). The bHLH gene Hes6, an inhibitor of Hes1, promotes neuronal differentiation. *Development*, *127*(13), 2933-2943.

Bagley, J. A., Reumann, D., Bian, S., Lévi-Strauss, J., & Knoblich, J. A. (2017). Fused cerebral organoids model interactions between brain regions. *Nature methods*, *14*, 743-751. https://doi.org/10.1038/nmeth.4304

Bai, G., Sheng, N., Xie, Z., Bian, W., Yokota, Y., Benezra, R., Kageyama, R., Guillemot, F., & Jing, N. (2007). Id sustains Hes1 expression to inhibit precocious neurogenesis by releasing negative autoregulation of Hes1. *Dev Cell*, *13*(2), 283-297. https://doi.org/10.1016/j.devcel.2007.05.014

Baldini, R., Mascaro, M., & Meroni, G. (2020). The MID1 gene product in physiology and disease. *Gene*, *747*, 144655-144655. https://doi.org/10.1016/j.gene.2020.144655

Ballas, N., Grunseich, C., Lu, D. D., Speh, J. C., & Mandel, G. (2005). REST and Its Corepressors Mediate Plasticity of Neuronal Gene Chromatin throughout Neurogenesis. *Cell*, *121*(4), 645-657. https://doi.org/10.1016/j.cell.2005.03.013

Bang, O. Y., Lee, J. S., Lee, P. H., & Lee, G. (2005). Autologous mesenchymal stem cell transplantation in stroke patients. *Ann Neurol*, *57*(6), 874-882. https://doi.org/10.1002/ana.20501

Bao, B.-Y., Ting, H.-J., Hsu, J.-W., & Lee, Y.-F. (2008). Protective role of 1α, 25-dihydroxyvitamin D3 against oxidative stress in nonmalignant human prostate epithelial cells [https://doi.org/10.1002/ijc.23460]. *Int J Cancer*, *122*(12), 2699-2706. https://doi.org/https://doi.org/10.1002/ijc.23460

Barker, R. A., Barrett, J., Mason, S. L., & Björklund, A. (2013). Fetal dopaminergic transplantation trials and the future of neural grafting in Parkinson's disease. *The Lancet. Neurology*, *12*(1), 84-91. https://doi.org/10.1016/s1474-4422(12)70295-8

Barker, R. A., Drouin-Ouellet, J., & Parmar, M. (2015). Cell-based therapies for Parkinson disease—past insights and future potential. *Nature reviews. Neurology*, *11*(9), 492-503. https://doi.org/10.1038/nrneurol.2015.123

Barker, R. A., Götz, M., & Parmar, M. (2018). New approaches for brain repair—from rescue to reprogramming. *Nature*, *557*, 329-334. https://doi.org/10.1038/s41586-018-0087-1

Barr, A. R., Cooper, S., Heldt, F. S., Butera, F., Stoy, H., Mansfeld, J., Novák, B., & Bakal, C. (2017). DNA damage during S-phase mediates the proliferation-quiescence decision in the subsequent G1 via p21 expression. *Nat Commun*, *8*, 14728-14728. https://doi.org/10.1038/ncomms14728

Bartus, R. T., & Johnson, E. M., Jr. (2017a). Clinical tests of neurotrophic factors for human neurodegenerative diseases, part 1: Where have we been and what have we learned? *Neurobiol Dis*, *97*(Pt B), 156-168. https://doi.org/10.1016/j.nbd.2016.03.027

Bartus, R. T., & Johnson, E. M., Jr. (2017b). Clinical tests of neurotrophic factors for human neurodegenerative diseases, part 2: Where do we stand and where must we go next? *Neurobiol Dis*, *97*(Pt B), 169-178. https://doi.org/10.1016/j.nbd.2016.03.026

Bell, R. D., Winkler, E. A., Sagare, A. P., Singh, I., LaRue, B., Deane, R., & Zlokovic, B. V. (2010). Pericytes control key neurovascular functions and neuronal phenotype in the adult brain and during brain aging. *Neuron*, *68*(3), 409-427. https://doi.org/10.1016/j.neuron.2010.09.043

Bergen, V., Lange, M., Peidli, S., Wolf, F. A., & Theis, F. J. (2020). Generalizing RNA velocity to transient cell states through dynamical modeling. *Nat Biotechnol*, *38*(12), 1408-1414. https://doi.org/10.1038/s41587-020-0591-3

Bergsland, M., Werme, M., Malewicz, M., Perlmann, T., & Muhr, J. (2006). The establishment of neuronal properties is controlled by Sox4 and Sox11. *Genes Dev*, *20*(24), 3475-3486. https://doi.org/10.1101/gad.403406

Berninger, B., Costa, M. R., Koch, U., Schroeder, T., Sutor, B., Grothe, B., & Götz, M. (2007). Functional properties of neurons derived from in vitro reprogrammed postnatal astroglia. *J Neurosci*, *27*(32), 8654-8664. https://doi.org/10.1523/jneurosci.1615-07.2007

Bertrand, N., Castro, D. S., & Guillemot, F. (2002). Proneural genes and the specification of neural cell types. *Nature Reviews Neuroscience*, *3*(7), 517-530. https://doi.org/10.1038/nrn874

Bessho, Y., Sakata, R., Komatsu, S., Shiota, K., Yamada, S., & Kageyama, R. (2001). Dynamic expression and essential functions of Hes7 in somite segmentation. *Genes Dev*, *15 20*, 2642-2647.

Biddy, B. A., Kong, W., Kamimoto, K., Guo, C., Waye, S. E., Sun, T., & Morris, S. A. (2018). Single-cell mapping of lineage and identity in direct reprogramming. *Nature*, *564*(7735), 219-224. https://doi.org/10.1038/s41586-018-0744-4

Björklund Lars, M., Sánchez-Pernaute, R., Chung, S., Andersson, T., Chen Iris Yin, C., McNaught Kevin St, P., Brownell, A.-L., Jenkins Bruce, G., Wahlestedt, C., Kim, K.-S., & Isacson, O. (2002). Embryonic stem cells develop into functional dopaminergic neurons after transplantation in a Parkinson rat model. *Proceedings of the National Academy of Sciences*, *99*(4), 2344-2349. https://doi.org/10.1073/pnas.022438099

Blondel, V. D., Guillaume, J.-L., Lambiotte, R., & Lefebvre, E. (2008). Fast unfolding of communities in large networks. *Journal of Statistical Mechanics: Theory and Experiment*, *2008*(10), P10008. https://doi.org/10.1088/1742-5468/2008/10/p10008

Boareto, M., Iber, D., & Taylor, V. (2017). Differential interactions between Notch and ID factors control neurogenesis by modulating Hes factor autoregulation. *Development (Cambridge, England)*, *144*(19), 3465-3474. https://doi.org/10.1242/dev.152520

Bonev, B., Mendelson Cohen, N., Szabo, Q., Fritsch, L., Papadopoulos, G. L., Lubling, Y., Xu, X., Lv, X., Hugnot, J.-P., Tanay, A., & Cavalli, G. (2017). Multiscale 3D Genome Rewiring during Mouse Neural Development. *Cell*, *171*(3), 557-572.e524. https://doi.org/10.1016/j.cell.2017.09.043

Brawand, D., Soumillon, M., Necsulea, A., Julien, P., Csardi, G., Harrigan, P., Weier, M., Liechti, A., Aximu-Petri, A., Kircher, M., Albert, F. W., Zeller, U., Khaitovich, P., Grutzner, F., Bergmann, S., Nielsen, R., Paabo, S., & Kaessmann, H. (2011). The evolution of gene expression levels in mammalian organs [10.1038/nature10532]. *Nature*, *478*(7369), 343-348. https://doi.org/http://www.nature.com/nature/journal/v478/n7369/abs/nature10532.html#supplementary-information

Briggs, R., & King, T. J. (1952). Transplantation of Living Nuclei From Blastula Cells into Enucleated Frogs' Eggs. *Proc Natl Acad Sci U S A*, *38*(5), 455-463. https://doi.org/10.1073/pnas.38.5.455

Britz, O., Mattar, P., Nguyen, L., Langevin, L.-M., Zimmer, C., Alam, S., Guillemot, F., & Schuurmans, C. (2006). A Role for Proneural Genes in the Maturation of Cortical Progenitor Cells. *Cerebral Cortex*, *16*(suppl_1), i138-i151. https://doi.org/10.1093/cercor/bhj168

Bunina, D., Abazova, N., Diaz, N., Noh, K.-M., Krijgsveld, J., & Zaugg, J. B. (2020). Genomic Rewiring of SOX2 Chromatin Interaction Network during Differentiation of ESCs to Postmitotic Neurons. *Cell Systems*, *10*(6), 480-494.e488. https://doi.org/https://doi.org/10.1016/j.cels.2020.05.003

Butler, A., Hoffman, P., Smibert, P., Papalexi, E., & Satija, R. (2018). Integrating single-cell transcriptomic data across different conditions, technologies, and species. *Nat Biotechnol*, *36*(5), 411-420. https://doi.org/10.1038/nbt.4096

Caiazzo, M., Dell'Anno, M. T., Dvoretskova, E., Lazarevic, D., Taverna, S., Leo, D., Sotnikova, T. D., Menegon, A., Roncaglia, P., Colciago, G., Russo, G., Carninci, P., Pezzoli, G., Gainetdinov, R. R., Gustincich, S., Dityatev, A., & Broccoli, V. (2011). Direct generation of functional dopaminergic neurons from mouse and human fibroblasts. *Nature*, *476*(7359), 224-227. https://doi.org/10.1038/nature10284

Camargo Ortega, G., Falk, S., Johansson, P. A., Peyre, E., Broix, L., Sahu, S. K., Hirst, W., Schlichthaerle, T., De Juan Romero, C., Draganova, K., Vinopal, S., Chinnappa, K., Gavranovic, A., Karakaya, T., Steininger, T., Merl-Pham, J., Feederle, R., Shao, W., Shi, S. H., Hauck, S. M., Jungmann, R., Bradke, F., Borrell, V., Geerlof, A., Reber, S., Tiwari, V. K., Huttner, W. B., Wilsch-Bräuninger, M., Nguyen, L., & Götz, M. (2019). The centrosome protein AKNA regulates neurogenesis via microtubule organization. *Nature*, *567*(7746), 113-117. https://doi.org/10.1038/s41586-019-0962-4

Candelario, K. M., Shuttleworth, C. W., & Cunningham, L. A. (2013). Neural stem/progenitor cells display a low requirement for oxidative metabolism independent of hypoxia inducible factor-1alpha expression. *J Neurochem*, *125*(3), 420-429. https://doi.org/https://doi.org/10.1111/jnc.12204

Carcagno, A. L., Di Bella, D. J., Goulding, M., Guillemot, F., & Lanuza, G. M. (2014). Neurogenin3 restricts serotonergic neuron differentiation to the hindbrain. *J Neurosci*, *34*(46), 15223-15233. https://doi.org/10.1523/JNEUROSCI.3403-14.2014

Casarosa, S., Fode, C., & Guillemot, F. (1999). Mash1 regulates neurogenesis in the ventral telencephalon. *Development*, *126*(3), 525-534.

Castro, D. S., Skowronska-Krawczyk, D., Armant, O., Donaldson, I. J., Parras, C., Hunt, C., Critchley, J. A., Nguyen, L., Gossler, A., Göttgens, B., Matter, J. M., & Guillemot, F. (2006). Proneural bHLH and Brn proteins coregulate a neurogenic program through cooperative binding to a conserved DNA motif. *Dev Cell*, *11*(6), 831-844. https://doi.org/10.1016/j.devcel.2006.10.006

Cau, E., Casarosa, S., & Guillemot, F. (2002). Mash1 and Ngn1 control distinct steps of determination and differentiation in the olfactory sensory neuron lineage. *Development*, *129*(8), 1871-1880.

Chambers, S. M., Fasano, C. A., Papapetrou, E. P., Tomishima, M., Sadelain, M., & Studer, L. (2009). Highly efficient neural conversion of human ES and iPS cells by dual inhibition of SMAD signaling. *Nat Biotechnol*, *27*(3), 275-280. https://doi.org/10.1038/nbt.1529

Chanda, S., Ang, C. E., Davila, J., Pak, C., Mall, M., Lee, Q. Y., Ahlenius, H., Jung, S. W., Südhof, T. C., & Wernig, M. (2014). Generation of induced neuronal cells by the single reprogramming factor ASCL1. *Stem cell reports*, *3*(2), 282-296. https://doi.org/10.1016/j.stemcr.2014.05.020

Chen, X., Miragaia, R. J., Natarajan, K. N., & Teichmann, S. A. (2018). A rapid and robust method for single cell chromatin accessibility profiling. *Nat Commun*, *9*(1), 5345. https://doi.org/10.1038/s41467-018-07771-0

Chippada, B. (2018). *ForceAtlas2 for Python and NetworkX*. In https://github.com/bhargavchippada/forceatlas2

Cho, H., Kozasa, T., Bondjers, C., Betsholtz, C., & Kehrl, J. H. (2003). Pericyte-specific expression of Rgs5: implications for PDGF and EDG receptor signaling during vascular maturation. *Faseb j*, *17*(3), 440-442. https://doi.org/10.1096/fj.02-0340fje

Chouchane, M., Melo de Farias, A. R., Moura, D. M. S., Hilscher, M. M., Schroeder, T., Leão, R. N., & Costa, M. R. (2017). Lineage Reprogramming of Astroglial Cells from Different Origins into Distinct Neuronal Subtypes. *Stem cell reports*, *9*(1), 162-176. https://doi.org/10.1016/j.stemcr.2017.05.009

Chuang, W., Sharma, A., Shukla, P., Li, G., Mall, M., Rajarajan, K., Abilez, O. J., Hamaguchi, R., Wu, J. C., Wernig, M., & Wu, S. M. (2017). Partial Reprogramming of Pluripotent Stem Cell-Derived Cardiomyocytes into Neurons. *Sci Rep*, *7*, 44840. https://doi.org/10.1038/srep44840

Colasante, G., Lignani, G., Rubio, A., Medrihan, L., Yekhlef, L., Sessa, A., Massimino, L., Giannelli, S. G., Sacchetti, S., Caiazzo, M., Leo, D., Alexopoulou, D., Dell'Anno, M. T., Ciabatti, E., Orlando, M., Studer, M., Dahl, A., Gainetdinov, R. R., Taverna, S., Benfenati, F., & Broccoli, V. (2015). Rapid Conversion of Fibroblasts into Functional Forebrain GABAergic Interneurons by Direct Genetic Reprogramming. *Cell Stem Cell*, *17*(6), 719-734. https://doi.org/10.1016/j.stem.2015.09.002

Corti, S., Nizzardo, M., Simone, C., Falcone, M., Donadoni, C., Salani, S., Rizzo, F., Nardini, M., Riboldi, G., Magri, F., Zanetta, C., Faravelli, I., Bresolin, N., & Comi, G. P. (2012). Direct reprogramming of human astrocytes into neural stem cells and neurons. *Experimental cell research*, *318*(13), 1528-1541. https://doi.org/10.1016/j.yexcr.2012.02.040

Curtis, M. A., Kam, M., Nannmark, U., Anderson, M. F., Axell, M. Z., Wikkelso, C., Holtås, S., van Roon-Mom, W. M., Björk-Eriksson, T., Nordborg, C., Frisén, J., Dragunow, M., Faull, R. L., & Eriksson, P. S. (2007). Human neuroblasts migrate to the olfactory bulb via a lateral ventricular extension. *Science*, *315*(5816), 1243-1249. https://doi.org/10.1126/science.1136281

Dandoy-Dron, F., Griffond, B., Mishal, Z., Tovey, M. G., & Dron, M. (2003). Scrg1, a novel protein of the CNS is targeted to the large dense-core vesicles in neuronal cells. *Eur J Neurosci*, *18*(9), 2449-2459. https://doi.org/10.1046/j.1460-9568.2003.03009.x

Daneman, R., Zhou, L., Kebede, A. A., & Barres, B. A. (2010). Pericytes are required for blood-brain barrier integrity during embryogenesis. *Nature*, *468*(7323), 562-566. https://doi.org/10.1038/nature09513

De Ravin, S. S., Su, L., Theobald, N., Choi, U., Macpherson, J. L., Poidinger, M., Symonds, G., Pond, S. M., Ferris, A. L., Hughes, S. H., Malech, H. L., & Wu, X. (2014). Enhancers are major targets for murine leukemia virus vector integration. *J Virol*, *88*(8), 4504-4513. https://doi.org/10.1128/jvi.00011-14

De Strooper, B., Annaert, W., Cupers, P., Saftig, P., Craessaerts, K., Mumm, J. S., Schroeter, E. H., Schrijvers, V., Wolfe, M. S., Ray, W. J., Goate, A., & Kopan, R. (1999). A presenilin-1-dependent gamma-secretase-like protease

mediates release of Notch intracellular domain. *Nature*, *398*(6727), 518-522. https://doi.org/10.1038/19083

Delgado, R. N., Allen, D. E., Keefe, M. G., Mancia Leon, W. R., Ziffra, R. S., Crouch, E. E., Alvarez-Buylla, A., & Nowakowski, T. J. (2022). Individual human cortical progenitors can produce excitatory and inhibitory neurons. *Nature*, *601*(7893), 397-403. https://doi.org/10.1038/s41586-021-04230-7

Dermietzel, R., & Krause, D. (1991). Molecular anatomy of the blood-brain barrier as defined by immunocytochemistry. *Int Rev Cytol*, *127*, 57-109. https://doi.org/10.1016/s0074-7696(08)60692-0

Dias Moura Prazeres, P. H., Sena, I. F. G., Borges, I. D. T., de Azevedo, P. O., Andreotti, J. P., de Paiva, A. E., de Almeida, V. M., de Paula Guerra, D. A., Pinheiro Dos Santos, G. S., Mintz, A., Delbono, O., & Birbrair, A. (2017). Pericytes are heterogeneous in their origin within the same tissue. *Dev Biol*, *427*(1), 6-11. https://doi.org/10.1016/j.ydbio.2017.05.001

Diez-Roux, G., Banfi, S., Sultan, M., Geffers, L., Anand, S., Rozado, D., Magen, A., Canidio, E., Pagani, M., Peluso, I., Lin-Marq, N., Koch, M., Bilio, M., Cantiello, I., Verde, R., De Masi, C., Bianchi, S. A., Cicchini, J., Perroud, E., Mehmeti, S., Dagand, E., Schrinner, S., Nürnberger, A., Schmidt, K., Metz, K., Zwingmann, C., Brieske, N., Springer, C., Hernandez, A. M., Herzog, S., Grabbe, F., Sieverding, C., Fischer, B., Schrader, K., Brockmeyer, M., Dettmer, S., Helbig, C., Alunni, V., Battaini, M.-A., Mura, C., Henrichsen, C. N., Garcia-Lopez, R., Echevarria, D., Puelles, E., Garcia-Calero, E., Kruse, S., Uhr, M., Kauck, C., Feng, G., Milyaev, N., Ong, C. K., Kumar, L., Lam, M., Semple, C. A., Gyenesei, A., Mundlos, S., Radelof, U., Lehrach, H., Sarmientos, P., Reymond, A., Davidson, D. R., Dollé, P., Antonarakis, S. E., Yaspo, M.-L., Martinez, S., Baldock, R. A., Eichele, G., & Ballabio, A. (2011). A High-Resolution Anatomical Atlas of the Transcriptome in the Mouse Embryo. *PLOS Biology*, *9*(1), e1000582. https://doi.org/10.1371/journal.pbio.1000582

Dong, J., Wong, S. L., Lau, C. W., Lee, H. K., Ng, C. F., Zhang, L., Yao, X., Chen, Z. Y., Vanhoutte, P. M., & Huang, Y. (2012). Calcitriol protects renovascular function in hypertension by down-regulating angiotensin II type 1 receptors and reducing oxidative stress. *European Heart Journal*, *33*(23), 2980-2990. https://doi.org/10.1093/eurheartj/ehr459

Dore-Duffy, P., Katychev, A., Wang, X., & Van Buren, E. (2006). CNS microvascular pericytes exhibit multipotential stem cell activity. *J Cereb Blood Flow Metab*, *26*(5), 613-624. https://doi.org/10.1038/sj.jcbfm.9600272

Drouin-Ouellet, J., Lau, S., Brattås, P. L., Rylander Ottosson, D., Pircs, K., Grassi, D. A., Collins, L. M., Vuono, R., Andersson Sjöland, A., Westergren-Thorsson, G., Graff, C., Minthon, L., Toresson, H., Barker, R. A., Jakobsson, J., & Parmar, M. (2017). REST suppression mediates neural conversion of adult human fibroblasts via microRNA-dependent and -independent pathways. *EMBO Mol Med*, *9*(8), 1117-1131. https://doi.org/https://doi.org/10.15252/emmm.201607471

Eberth, C. (1871). Handbuch der Lehre von der Gewegen des Menschen und der Tiere. *Leipzig: W. Engelman*.

Engerer, P., Petridou, E., Williams, P. R., Suzuki, S. C., Yoshimatsu, T., Portugues, R., Misgeld, T., & Godinho, L. (2021). Notch-mediated re-specification of neuronal identity during central nervous system development. *Current Biology*, *31*(21), 4870-4878.e4875. https://doi.org/https://doi.org/10.1016/j.cub.2021.08.049

Eriksson, P. S., Perfilieva, E., Björk-Eriksson, T., Alborn, A.-M., Nordborg, C., Peterson, D. A., & Gage, F. H. (1998). Neurogenesis in the adult human hippocampus. *Nat Med*, *4*(11), 1313-1317. https://doi.org/10.1038/3305

Ernst, A., Alkass, K., Bernard, S., Salehpour, M., Perl, S., Tisdale, J., Possnert, G., Druid, H., & Frisén, J. (2014). Neurogenesis in the striatum of the adult human brain. *Cell*, *156*(5), 1072-1083. https://doi.org/10.1016/j.cell.2014.01.044

Falk, S., Han, D., & Karow, M. (2021). Cellular identity through the lens of direct lineage reprogramming. *Curr Opin Genet Dev*, *70*, 97-103. https://doi.org/10.1016/j.gde.2021.06.015

Favaro, R., Valotta, M., Ferri, A. L., Latorre, E., Mariani, J., Giachino, C., Lancini, C., Tosetti, V., Ottolenghi, S., & Taylor, V. (2009). Hippocampal development and neural stem cell maintenance require Sox2-dependent regulation of Shh. *Nat Neurosci*, *12*(10), 1248-1256.

Fecher, C., Trovò, L., Müller, S. A., Snaidero, N., Wettmarshausen, J., Heink, S., Ortiz, O., Wagner, I., Kühn, R., Hartmann, J., Karl, R. M., Konnerth, A., Korn, T., Wurst, W., Merkler, D., Lichtenthaler, S. F., Perocchi, F., & Misgeld, T. (2019). Cell-type-specific profiling of brain mitochondria reveals functional and molecular diversity. *Nat Neurosci*, *22*(10), 1731-1742. https://doi.org/10.1038/s41593-019-0479-z

Fernández-Klett, F., Offenhauser, N., Dirnagl, U., Priller, J., & Lindauer, U. (2010). Pericytes in capillaries are contractile in vivo, but arterioles mediate functional hyperemia in the mouse brain. *Proc Natl Acad Sci U S A*, *107*(51), 22290-22295. https://doi.org/10.1073/pnas.1011321108

Fleck, J. S. (2020). *VoxHunt Expression Maps* Version V2) [3D expression maps of the developing mouse brain of different ages derived from in situ hybridization experiments. This data was obtained from the Allen Brain Atlas and is a dependency of the VoxHunt R package.]. Mendeley Data. https://doi.org/10.17632/g4xg38mwcn.2

Fleck, J. S., Sanchís-Calleja, F., He, Z., Santel, M., Boyle, M. J., Camp, J. G., & Treutlein, B. (2021). Resolving organoid brain region identities by mapping single-cell genomic data to reference atlases. *Cell Stem Cell*, *28*(6), 1148-1159.e1148. https://doi.org/10.1016/j.stem.2021.02.015

Florio, M., Leto, K., Muzio, L., Tinterri, A., Badaloni, A., Croci, L., Zordan, P., Barili, V., Albieri, I., Guillemot, F., Rossi, F., & Consalez, G. G. (2012). Neurogenin 2 regulates progenitor cell-cycle progression and Purkinje cell dendritogenesis in cerebellar development. *Development*, *139*(13), 2308-2320. https://doi.org/10.1242/dev.075861

Fode, C., Gradwohl, G., Morin, X., Dierich, A., LeMeur, M., Goridis, C., & Guillemot, F. (1998). The bHLH protein NEUROGENIN 2 is a determination factor for epibranchial placode-derived sensory neurons. *Neuron*, *20*(3), 483-494. https://doi.org/10.1016/s0896-6273(00)80989-7

Frisén, J. (2016). Neurogenesis and Gliogenesis in Nervous System Plasticity and Repair. *Annu Rev Cell Dev Biol*, *32*, 127-141. https://doi.org/10.1146/annurev-cellbio-111315-124953

Fryer, C. J., Lamar, E., Turbachova, I., Kintner, C., & Jones, K. A. (2002). Mastermind mediates chromatin-specific transcription and turnover of the Notch enhancer complex. *Genes Dev*, *16*(11), 1397-1411. https://doi.org/10.1101/gad.991602

G. B. D. Neurological Disorders Collaborator Group. (2017). Global, regional, and national burden of neurological disorders during 1990-2015: a systematic analysis for the Global Burden of Disease Study 2015. *The Lancet. Neurology*, *16*(11), 877-897. https://doi.org/10.1016/S1474-4422(17)30299-5

G. B. D. Neurology Collaborators. (2019). Global, regional, and national burden of neurological disorders, 1990-2016: a systematic analysis for the Global Burden of Disease Study 2016. *The Lancet. Neurology*, *18*(5), 459-480. https://doi.org/10.1016/S1474-4422(18)30499-X

Garcia-Alonso, L., Holland, C. H., Ibrahim, M. M., Turei, D., & Saez-Rodriguez, J. (2019). Benchmark and integration of resources for the estimation of human transcription factor activities. *Genome Res*, *29*(8), 1363-1375. https://doi.org/10.1101/gr.240663.118

Gascón, S., Murenu, E., Masserdotti, G., Ortega, F., Russo, Gianluca L., Petrik, D., Deshpande, A., Heinrich, C., Karow, M., Robertson, Stephen P., Schroeder, T., Beckers, J., Irmler, M., Berndt, C., Angeli, José P. F., Conrad, M., Berninger, B., & Götz, M. (2016). Identification and Successful Negotiation of a Metabolic Checkpoint in Direct Neuronal Reprogramming. *Cell Stem Cell*, *18*, 396-409. https://doi.org/10.1016/j.stem.2015.12.003

Geling, A., Steiner, H., Willem, M., Bally-Cuif, L., & Haass, C. (2002). A gamma-secretase inhibitor blocks Notch signaling in vivo and causes a severe neurogenic phenotype in zebrafish. *EMBO reports*, *3*(7), 688-694. https://doi.org/10.1093/embo-reports/kvf124

Goertsen, D., Flytzanis, N. C., Goeden, N., Chuapoco, M. R., Cummins, A., Chen, Y., Fan, Y., Zhang, Q., Sharma, J., Duan, Y., Wang, L., Feng, G., Chen, Y., Ip, N. Y., Pickel, J., & Gradinaru, V. (2022). AAV capsid variants with brain-wide transgene expression and decreased liver targeting after intravenous delivery in mouse and marmoset. *Nat Neurosci*, *25*(1), 106-115. https://doi.org/10.1038/s41593-021-00969-4

Göritz, C., Dias, D. O., Tomilin, N., Barbacid, M., Shupliakov, O., & Frisén, J. (2011). A pericyte origin of spinal cord scar tissue. *Science*, *333*(6039), 238-242. https://doi.org/10.1126/science.1203165

Guillemot, F. (1999). Vertebrate bHLH genes and the determination of neuronal fates. *Exp Cell Res*, *253*(2), 357-364. https://doi.org/10.1006/excr.1999.4717

Guillemot, F., Lo, L. C., Johnson, J. E., Auerbach, A., Anderson, D. J., & Joyner, A. L. (1993). Mammalian achaete-scute homolog 1 is required for the early development of olfactory and autonomic neurons. *Cell*, *75*(3), 463-476. https://doi.org/10.1016/0092-8674(93)90381-y

Guo, Z., Zhang, L., Wu, Z., Chen, Y., Wang, F., & Chen, G. (2014). In vivo direct reprogramming of reactive glial cells into functional neurons after brain injury and in an Alzheimer's disease model. *Cell Stem Cell*, *14*(2), 188-202. https://doi.org/10.1016/j.stem.2013.12.001

Hamilton, H., Gomos, J., Berns, K. I., & Falck-Pedersen, E. (2004). Adeno-associated virus site-specific integration and AAVS1 disruption. *J Virol*, *78*(15), 7874-7882. https://doi.org/10.1128/jvi.78.15.7874-7882.2004

Han, S., Okawa, S., Wilkinson, G. A., Ghazale, H., Adnani, L., Dixit, R., Tavares, L., Faisal, I., Brooks, M. J., Cortay, V., Zinyk, D., Sivitilli, A., Li, S., Malik, F., Ilnytskyy, Y., Angarica, V. E., Gao, J., Chinchalongporn, V., Oproescu, A.-M., Vasan, L., Touahri, Y., David, L. A., Raharjo, E., Kim, J.-W., Wu, W., Rahmani, W., Chan, J. A.-w., Kovalchuk, I., Attisano, L., Kurrasch, D., Dehay, C., Swaroop, A., Castro, D. S., Biernaskie, J., del Sol, A., & Schuurmans, C. (2021). Proneural genes define ground-state rules to regulate neurogenic patterning and cortical folding. *Neuron*. https://doi.org/10.1016/j.neuron.2021.07.007

Hao, Y., Hao, S., Andersen-Nissen, E., Mauck, W. M., Zheng, S., Butler, A., Lee, M. J., Wilk, A. J., Darby, C., Zager, M., Hoffman, P., Stoeckius, M., Papalexi, E., Mimitou, E. P., Jain, J., Srivastava, A., Stuart, T., Fleming, L. M., Yeung, B., Rogers, A. J., McElrath, J. M., Blish, C. A., Gottardo, R., Smibert, P., & Satija, R. (2021). Integrated analysis of multimodal single-cell data. *Cell*, *184*(13), 3573-3587.e3529. https://doi.org/https://doi.org/10.1016/j.cell.2021.04.048

Heinrich, C., Blum, R., Gascón, S., Masserdotti, G., Tripathi, P., Sánchez, R., Tiedt, S., Schroeder, T., Götz, M., & Berninger, B. (2010). Directing Astroglia from the Cerebral Cortex into Subtype Specific Functional Neurons. *PLOS Biology*, *8*(5), e1000373. https://doi.org/10.1371/journal.pbio.1000373

Heinrich, C., Gascón, S., Masserdotti, G., Lepier, A., Sanchez, R., Simon-Ebert, T., Schroeder, T., Götz, M., & Berninger, B. (2011). Generation of subtype-specific neurons from postnatal astroglia of the mouse cerebral cortex. *Nat Protoc*, *6*(2), 214-228. https://doi.org/10.1038/nprot.2010.188

Heins, N., Malatesta, P., Cecconi, F., Nakafuku, M., Tucker, K. L., Hack, M. A., Chapouton, P., Barde, Y. A., & Götz, M. (2002). Glial cells generate neurons: the role of the transcription factor Pax6. *Nat Neurosci*, *5*(4), 308-315. https://doi.org/10.1038/nn828

Heinz, N., Schambach, A., Galla, M., Maetzig, T., Baum, C., Loew, R., & Schiedlmeier, B. (2011). Retroviral and transposon-based tet-regulated all-in-one vectors with reduced background expression and improved dynamic range. *Hum Gene Ther*, *22*(2), 166-176. https://doi.org/10.1089/hum.2010.099

Henke, R. M., Meredith, D. M., Borromeo, M. D., Savage, T. K., & Johnson, J. E. (2009). Ascl1 and Neurog2 form novel complexes and regulate Delta-like3 (Dll3) expression in the neural tube. *Dev Biol*, *328*(2), 529-540. https://doi.org/10.1016/j.ydbio.2009.01.007

Herdy, J., Schafer, S., Kim, Y., Ansari, Z., Zangwill, D., Ku, M., Paquola, A., Lee, H., Mertens, J., & Gage, F. H. (2019). Chemical modulation of transcriptionally enriched signaling pathways to optimize the conversion of fibroblasts into neurons. *Elife*, *8*, e41356. https://doi.org/10.7554/eLife.41356

Herrero-Navarro, Á., Puche-Aroca, L., Moreno-Juan, V., Sempere-Ferràndez, A., Espinosa, A., Susín, R., Torres-Masjoan, L., Leyva-Díaz, E., Karow, M., & Figueres-Oñate, M. (2021). Astrocytes and neurons share region-specific transcriptional signatures that confer regional identity to neuronal reprogramming. *Sci Adv*, *7*(15), eabe8978.

Holland, C. H., Tanevski, J., Perales-Patón, J., Gleixner, J., Kumar, M. P., Mereu, E., Joughin, B. A., Stegle, O., Lauffenburger, D. A., Heyn, H., Szalai, B., & Saez-Rodriguez, J. (2020). Robustness and applicability of transcription factor and pathway analysis tools on single-cell RNA-seq data. *Genome Biology*, *21*(1), 36. https://doi.org/10.1186/s13059-020-1949-z

Hong, H., Takahashi, K., Ichisaka, T., Aoi, T., Kanagawa, O., Nakagawa, M., Okita, K., & Yamanaka, S. (2009). Suppression of induced pluripotent stem cell generation by the p53-p21 pathway. *Nature*, *460*(7259), 1132-1135. https://doi.org/10.1038/nature08235

Honmou, O., Houkin, K., Matsunaga, T., Niitsu, Y., Ishiai, S., Onodera, R., Waxman, S. G., & Kocsis, J. D. (2011). Intravenous administration of auto serum-expanded autologous mesenchymal stem cells in stroke. *Brain*, *134*(Pt 6), 1790-1807. https://doi.org/10.1093/brain/awr063

Horton, S., Meredith, A., Richardson, J. A., & Johnson, J. E. (1999). Correct coordination of neuronal differentiation events in ventral forebrain requires the bHLH factor MASH1. *Mol Cell Neurosci*, *14*(4-5), 355-369. https://doi.org/10.1006/mcne.1999.0791

Hou, Y., Dan, X., Babbar, M., Wei, Y., Hasselbalch, S. G., Croteau, D. L., & Bohr, V. A. (2019). Ageing as a risk factor for neurodegenerative disease. *Nature reviews. Neurology*, *15*(10), 565-581. https://doi.org/10.1038/s41582-019-0244-7

Hu, W., Qiu, B., Guan, W., Wang, Q., Wang, M., Li, W., Gao, L., Shen, L., Huang, Y., Xie, G., Zhao, H., Jin, Y., Tang, B., Yu, Y., Zhao, J., & Pei, G. (2015). Direct Conversion of Normal and Alzheimer's Disease Human Fibroblasts into Neuronal Cells by Small Molecules. *Cell Stem Cell*, *17*(2), 204-212. https://doi.org/10.1016/j.stem.2015.07.006

Huang, F. J., You, W. K., Bonaldo, P., Seyfried, T. N., Pasquale, E. B., & Stallcup, W. B. (2010). Pericyte deficiencies lead to aberrant tumor vascularizaton in the brain of the NG2 null mouse. *Dev Biol*, *344*(2), 1035-1046. https://doi.org/10.1016/j.ydbio.2010.06.023

Huminiecki, L., Goldovsky, L., Freilich, S., Moustakas, A., Ouzounis, C., & Heldin, C.-H. (2009). Emergence, development and diversification of the TGF-β signalling pathway within the animal kingdom. *BMC Evolutionary Biology*, *9*(1), 28. https://doi.org/10.1186/1471-2148-9-28

Hungerford, J. E., & Little, C. D. (1999). Developmental biology of the vascular smooth muscle cell: building a multilayered vessel wall. *J Vasc Res*, *36*(1), 2-27. https://doi.org/10.1159/000025622

Imayoshi, I., Isomura, A., Harima, Y., Kawaguchi, K., Kori, H., Miyachi, H., Fujiwara, T., Ishidate, F., & Kageyama, R. (2013). Oscillatory control of factors determining multipotency and fate in mouse neural progenitors. *Science*, *342*(6163), 1203-1208. https://doi.org/10.1126/science.1242366

Inman, G. J., Nicolás, F. J., Callahan, J. F., Harling, J. D., Gaster, L. M., Reith, A. D., Laping, N. J., & Hill, C. S. (2002). SB-431542 is a potent and specific inhibitor of transforming growth factor-beta superfamily type I activin receptor-like kinase (ALK) receptors ALK4, ALK5, and ALK7. *Mol Pharmacol*, *62*(1), 65-74. https://doi.org/10.1124/mol.62.1.65

Islam, S., Kjällquist, U., Moliner, A., Zajac, P., Fan, J.-B., Lönnerberg, P., & Linnarsson, S. (2011). Characterization of the single-cell transcriptional landscape by highly multiplex RNA-seq. *Genome Res*, *21*(7), 1160-1167. http://genome.cshlp.org/content/21/7/1160.abstract

Iwata, R., Casimir, P., & Vanderhaeghen, P. (2020). Mitochondrial dynamics in postmitotic cells regulate neurogenesis. *Science*, *369*(6505), 858-862. https://doi.org/10.1126/science.aba9760

Jacomy, M., Venturini, T., Heymann, S., & Bastian, M. (2014). ForceAtlas2, a Continuous Graph Layout Algorithm for Handy Network Visualization Designed for the Gephi Software. *PLoS One*, *9*(6), e98679. https://doi.org/10.1371/journal.pone.0098679

Jan, Y. N., & Jan, L. Y. (1994). Genetic control of cell fate specification in Drosophila peripheral nervous system. *Annu Rev Genet*, *28*(1), 373-393.

Jansson, D., Rustenhoven, J., Feng, S., Hurley, D., Oldfield, R. L., Bergin, P. S., Mee, E. W., Faull, R. L. M., & Dragunow, M. (2014). A role for human brain pericytes in neuroinflammation. *Journal of neuroinflammation*, *11*, 104-104. https://doi.org/10.1186/1742-2094-11-104

Jiménez, F., & Modolell, J. (1993). Neural fate specification in Drosophila. *Curr Opin Genet Dev*, *3*(4), 626-632. https://doi.org/10.1016/0959-437x(93)90099-b

Jin, Y., An, X., Ye, Z., Cully, B., Wu, J., & Li, J. (2009). RGS5, a hypoxia-inducible apoptotic stimulator in endothelial cells. *J Biol Chem*, *284*(35), 23436-23443. https://doi.org/10.1074/jbc.M109.032664

Jouve, C., Palmeirim, I., Henrique, D., Beckers, J., Gossler, A., Ish-Horowicz, D., & Pourquié, O. (2000). Notch signalling is required for cyclic expression of the hairy-like gene HES1 in the presomitic mesoderm. *Development (Cambridge, England)*, *127*, 1421-1429.

Jung, S., Appleton, E., Ali, M., Church, G. M., & del Sol, A. (2021). A computer-guided design tool to increase the efficiency of cellular conversions. *Nat Commun*, *12*(1), 1659. https://doi.org/10.1038/s41467-021-21801-4

Kageyama, R., Ochi, S., Sueda, R., & Shimojo, H. (2020). The significance of gene expression dynamics in neural stem cell regulation. *Proc Jpn Acad Ser B Phys Biol Sci*, *96*(8), 351-363. https://doi.org/10.2183/pjab.96.026

Kageyama, R., Ohtsuka, T., & Kobayashi, T. (2007). The Hes gene family: repressors and oscillators that orchestrate embryogenesis. *Development*, *134*(7), 1243-1251. https://doi.org/10.1242/dev.000786

Kageyama, R., Ohtsuka, T., Shimojo, H., & Imayoshi, I. (2008). Dynamic Notch signaling in neural progenitor cells and a revised view of lateral inhibition. *Nat Neurosci*, *11*(11), 1247-1251. https://doi.org/10.1038/nn.2208

Kageyama, R., Ohtsuka, T., Shimojo, H., & Imayoshi, I. (2009). Dynamic regulation of Notch signaling in neural progenitor cells. *Curr. Opin. Cell Biol.*, *21*. https://doi.org/10.1016/j.ceb.2009.08.009

Kalia, L. V., & Lang, A. E. (2015). Parkinson's disease. *The Lancet*, *386*(9996), 896-912. https://doi.org/10.1016/S0140-6736(14)61393-3

Kaltezioti, V., Kouroupi, G., Oikonomaki, M., Mantouvalou, E., Stergiopoulos, A., Charonis, A., Rohrer, H., Matsas, R., & Politis, P. K. (2010). Prox1 regulates the notch1-mediated inhibition of neurogenesis. *PLOS Biology*, *8*(12), e1000565-e1000565. https://doi.org/10.1371/journal.pbio.1000565

Kanehisa, M. (2019). Toward understanding the origin and evolution of cellular organisms. *Protein Sci*, *28*(11), 1947-1951. https://doi.org/10.1002/pro.3715

Kanehisa, M., Furumichi, M., Sato, Y., Ishiguro-Watanabe, M., & Tanabe, M. (2021). KEGG: integrating viruses and cellular organisms. *Nucleic Acids Res*, *49*(D1), D545-d551. https://doi.org/10.1093/nar/gkaa970

Kanehisa, M., & Goto, S. (2000). KEGG: kyoto encyclopedia of genes and genomes. *Nucleic Acids Res*, *28*(1), 27-30. https://doi.org/10.1093/nar/28.1.27

Karow, M., Camp, J. G., Falk, S., Gerber, T., Pataskar, A., Gac-Santel, M., Kageyama, J., Brazovskaja, A., Garding, A., Fan, W., Riedemann, T., Casamassa, A., Smiyakin, A., Schichor, C., Götz, M., Tiwari, V. K., Treutlein, B., & Berninger, B. (2018). Direct pericyte-to-neuron reprogramming via unfolding of a neural stem cell-like program. *Nat Neurosci*. https://doi.org/10.1038/s41593-018-0168-3

Karow, M., Sánchez, R., Schichor, C., Masserdotti, G., Ortega, F., Heinrich, C., Gascón, S., Khan, Muhammad A., Lie, D. C., Dellavalle, A., Cossu, G., Goldbrunner, R., Götz, M., & Berninger, B. (2012). Reprogramming of Pericyte-Derived Cells of the Adult Human Brain into Induced Neuronal Cells. *Cell Stem Cell*, *11*, 471-476. https://doi.org/10.1016/j.stem.2012.07.007

Karow, M., Schichor, C., Beckervordersandforth, R., & Berninger, B. (2014). Lineage-reprogramming of Pericyte-derived Cells of the Adult Human Brain into Induced Neurons. *Journal of Visualized Experiments*. https://doi.org/10.3791/51433

Kikuchi, T., Morizane, A., Doi, D., Magotani, H., Onoe, H., Hayashi, T., Mizuma, H., Takara, S., Takahashi, R., Inoue, H., Morita, S., Yamamoto, M., Okita, K., Nakagawa, M., Parmar, M., & Takahashi, J. (2017). Human iPS cell-derived dopaminergic neurons function in a primate Parkinson's disease model. *Nature*, *548*(7669), 592-596. https://doi.org/10.1038/nature23664

Kim, D. S., Lee, J. S., Leem, J. W., Huh, Y. J., Kim, J. Y., Kim, H. S., Park, I. H., Daley, G. Q., Hwang, D. Y., & Kim, D. W. (2010). Robust enhancement of neural differentiation from human ES and iPS cells regardless of their innate difference in differentiation propensity. *Stem Cell Rev Rep*, *6*(2), 270-281. https://doi.org/10.1007/s12015-010-9138-1

Kim, Y., Zheng, X., Ansari, Z., Bunnell, M. C., Herdy, J. R., Traxler, L., Lee, H., Paquola, A. C. M., Blithikioti, C., Ku, M., Schlachetzki, J. C. M., Winkler, J., Edenhofer, F., Glass, C. K., Paucar, A. A., Jaeger, B. N., Pham, S., Boyer, L., Campbell, B. C., Hunter, T., Mertens, J., & Gage, F. H. (2018). Mitochondrial Aging Defects Emerge in Directly Reprogrammed Human Neurons due to Their Metabolic Profile. *Cell Reports*, *23*(9), 2550-2558. https://doi.org/https://doi.org/10.1016/j.celrep.2018.04.105

Kirkeby, A., Grealish, S., Wolf, D. A., Nelander, J., Wood, J., Lundblad, M., Lindvall, O., & Parmar, M. (2012). Generation of regionally specified neural progenitors and functional neurons from human embryonic stem cells under defined conditions. *Cell Rep*, *1*(6), 703-714. https://doi.org/10.1016/j.celrep.2012.04.009

Klar, A., Baldassare, M., & Jessell, T. M. (1992). F-spondin: a gene expressed at high levels in the floor plate encodes a secreted protein that promotes neural cell adhesion and neurite extension. *Cell*, *69*(1), 95-110. https://doi.org/10.1016/0092-8674(92)90121-r

Klüppel, M., & Wrana, J. L. (2005). Turning it up a Notch: cross-talk between TGF beta and Notch signaling. *Bioessays*, *27*(2), 115-118. https://doi.org/10.1002/bies.20187

Kunz, J., Krause, D., Kremer, M., & Dermietzel, R. (1994). The 140-kDa protein of blood-brain barrier-associated pericytes is identical to aminopeptidase N. *J Neurochem*, *62*(6), 2375-2386. https://doi.org/10.1046/j.1471-4159.1994.62062375.x

Kurowska, Z., Englund, E., Widner, H., Lindvall, O., Li, J. Y., & Brundin, P. (2011). Signs of degeneration in 12-22-year old grafts of mesencephalic dopamine neurons in patients with Parkinson's disease. *J Parkinsons Dis*, *1*(1), 83-92. https://doi.org/10.3233/jpd-2011-11004

La Manno, G., Soldatov, R., Zeisel, A., Braun, E., Hochgerner, H., Petukhov, V., Lidschreiber, K., Kastriti, M. E., Lönnerberg, P., Furlan, A., Fan, J., Borm, L. E., Liu, Z., van Bruggen, D., Guo, J., He, X., Barker, R., Sundström, E., Castelo-Branco, G., Cramer, P., Adameyko, I., Linnarsson, S., & Kharchenko, P. V. (2018). RNA velocity of single cells. *Nature*, *560*(7719), 494-498. https://doi.org/10.1038/s41586-018-0414-6

Lancaster, M. A., Renner, M., Martin, C.-A., Wenzel, D., Bicknell, L. S., Hurles, M. E., Homfray, T., Penninger, J. M., Jackson, A. P., & Knoblich, J. A. (2013). Cerebral organoids model human brain development and microcephaly. *Nature*, *501*(7467), 373-379. https://doi.org/10.1038/nature12517

Lange, M., Bergen, V., Klein, M., Setty, M., Reuter, B., Bakhti, M., Lickert, H., Ansari, M., Schniering, J., Schiller, H. B., Pe'er, D., & Theis, F. J. (2022). CellRank for directed single-cell fate mapping. *Nature methods*. https://doi.org/10.1038/s41592-021-01346-6

Laping, N. J., Grygielko, E., Mathur, A., Butter, S., Bomberger, J., Tweed, C., Martin, W., Fornwald, J., Lehr, R., Harling, J., Gaster, L., Callahan, J. F., & Olson, B. A. (2002). Inhibition of transforming growth factor (TGF)-beta1-induced extracellular matrix with a novel inhibitor of the TGF-beta type I receptor kinase activity: SB-431542. *Mol Pharmacol*, *62*(1), 58-64. https://doi.org/10.1124/mol.62.1.58

Laugesen, A., & Helin, K. (2014). Chromatin repressive complexes in stem cells, development, and cancer. *Cell Stem Cell*, *14*(6), 735-751. https://doi.org/10.1016/j.stem.2014.05.006

Lee, A. S., Tang, C., Rao, M. S., Weissman, I. L., & Wu, J. C. (2013). Tumorigenicity as a clinical hurdle for pluripotent stem cell therapies. *Nat Med*, *19*(8), 998-1004. https://doi.org/10.1038/nm.3267

Lee, J. E. (1997). Basic helix-loop-helix genes in neural development. *Curr Opin Neurobiol*, *7*(1), 13-20. https://doi.org/10.1016/s0959-4388(97)80115-8

Leimeister, C., Externbrink, A., Klamt, B., & Gessler, M. (1999). Hey genes: a novel subfamily of hairy- and Enhancer of split related genes specifically expressed during mouse embryogenesis. *Mech Dev*, *85*(1-2), 173-177. https://doi.org/10.1016/s0925-4773(99)00080-5

Li, E. Y., Zhao, P. J., Jian, J., Yin, B. Q., Sun, Z. Y., Xu, C. X., Tang, Y. C., & Wu, H. (2019). LncRNA MIAT overexpression reduced neuron apoptosis in a neonatal rat model of hypoxic-ischemic injury through miR-211/GDNF. *Cell Cycle*, *18*(2), 156-166. https://doi.org/10.1080/15384101.2018.1560202

Li, J. Y., Englund, E., Holton, J. L., Soulet, D., Hagell, P., Lees, A. J., Lashley, T., Quinn, N. P., Rehncrona, S., Björklund, A., Widner, H., Revesz, T., Lindvall, O., & Brundin, P. (2008). Lewy bodies in grafted neurons in subjects with Parkinson's disease suggest host-to-graft disease propagation. *Nat Med*, *14*(5), 501-503. https://doi.org/10.1038/nm1746

Li, Q., Yu, Y., Bischoff, J., Mulliken, J. B., & Olsen, B. R. (2003). Differential expression of CD146 in tissues and endothelial cells derived from infantile haemangioma and normal human skin. *The Journal of Pathology: A Journal of the Pathological Society of Great Britain and Ireland*, *201*(2), 296-302.

Li, X., Zuo, X., Jing, J., Ma, Y., Wang, J., Liu, D., Zhu, J., Du, X., Xiong, L., Du, Y., Xu, J., Xiao, X., Wang, J., Chai, Z., Zhao, Y., & Deng, H. (2015). Small-Molecule-Driven Direct Reprogramming of Mouse Fibroblasts into Functional Neurons. *Cell Stem Cell*, *17*(2), 195-203. https://doi.org/10.1016/j.stem.2015.06.003

Liang, X. G., Tan, C., Wang, C. K., Tao, R. R., Huang, Y. J., Ma, K. F., Fukunaga, K., Huang, M. Z., & Han, F. (2018). Myt1l induced direct reprogramming of pericytes into cholinergic neurons. *CNS Neurosci Ther*, *24*(9), 801-809. https://doi.org/10.1111/cns.12821

Lie, D. C., Song, H., Colamarino, S. A., Ming, G. L., & Gage, F. H. (2004). Neurogenesis in the adult brain: new strategies for central nervous system diseases. *Annu Rev Pharmacol Toxicol*, *44*, 399-421. https://doi.org/10.1146/annurev.pharmtox.44.101802.121631

Lin, H.-C., He, Z., Ebert, S., Schörnig, M., Santel, M., Nikolova, M. T., Weigert, A., Hevers, W., Kasri, N. N., Taverna, E., Camp, J. G., & Treutlein, B. (2021). NGN2 induces diverse neuron types from human pluripotency. *Stem cell reports*, *16*(9), 2118-2127. https://doi.org/10.1016/j.stemcr.2021.07.006

Lindahl, P., Johansson, B. R., Levéen, P., & Betsholtz, C. (1997). Pericyte loss and microaneurysm formation in PDGF-B-deficient mice. *Science*, *277*(5323), 242-245. https://doi.org/10.1126/science.277.5323.242

Lindsell, C. E., Shawber, C. J., Boulter, J., & Weinmaster, G. (1995). Jagged: a mammalian ligand that activates Notch1. *Cell*, *80*(6), 909-917. https://doi.org/10.1016/0092-8674(95)90294-5

Liu, M. L., Zang, T., Zou, Y., Chang, J. C., Gibson, J. R., Huber, K. M., & Zhang, C. L. (2013). Small molecules enable neurogenin 2 to efficiently convert human fibroblasts into cholinergic neurons. *Nat Commun*, *4*, 2183. https://doi.org/10.1038/ncomms3183

Liu, Y., & Halloran, M. C. (2005). Central and peripheral axon branches from one neuron are guided differentially by Semaphorin3D and transient axonal glycoprotein-1. *J Neurosci*, *25*(45), 10556-10563. https://doi.org/10.1523/jneurosci.2710-05.2005

Luecken, M. D., Büttner, M., Chaichoompu, K., Danese, A., Interlandi, M., Mueller, M. F., Strobl, D. C., Zappia, L., Dugas, M., Colomé-Tatché, M., & Theis, F. J. (2020). Benchmarking atlas-level data integration in single-cell genomics. *bioRxiv*, 2020.2005.2022.111161. https://doi.org/10.1101/2020.05.22.111161

Lyden, D., Young, A. Z., Zagzag, D., Yan, W., Gerald, W., O'Reilly, R., Bader, B. L., Hynes, R. O., Zhuang, Y., Manova, K., & Benezra, R. (1999). Id1 and Id3 are required for neurogenesis, angiogenesis and vascularization of tumour xenografts. *Nature*, *401*(6754), 670-677. https://doi.org/10.1038/44334

Ma, S., Zhang, B., LaFave, L. M., Earl, A. S., Chiang, Z., Hu, Y., Ding, J., Brack, A., Kartha, V. K., Tay, T., Law, T., Lareau, C., Hsu, Y.-C., Regev, A., & Buenrostro, J. D. (2020). Chromatin Potential Identified by Shared Single-Cell Profiling of RNA and Chromatin. *Cell*, *183*(4), 1103-1116.e1120. https://doi.org/https://doi.org/10.1016/j.cell.2020.09.056

Maffezzini, C., Calvo-Garrido, J., Wredenberg, A., & Freyer, C. (2020). Metabolic regulation of neurodifferentiation in the adult brain. *Cellular and Molecular Life Sciences*, *77*(13), 2483-2496. https://doi.org/10.1007/s00018-019-03430-9

Malik, V., Glaser, L. V., Zimmer, D., Velychko, S., Weng, M., Holzner, M., Arend, M., Chen, Y., Srivastava, Y., Veerapandian, V., Shah, Z., Esteban, M. A., Wang, H., Chen, J., Schöler, H. R., Hutchins, A. P., Meijsing, S. H., Pott, S., & Jauch, R. (2019). Pluripotency reprogramming by competent and incompetent POU factors uncovers temporal dependency for Oct4 and Sox2. *Nat Commun*, *10*(1), 3477. https://doi.org/10.1038/s41467-019-11054-7

Mall, M., Kareta, M. S., Chanda, S., Ahlenius, H., Perotti, N., Zhou, B., Grieder, S. D., Ge, X., Drake, S., Euong Ang, C., Walker, B. M., Vierbuchen, T., Fuentes, D. R., Brennecke, P., Nitta, K. R., Jolma, A., Steinmetz, L. M., Taipale, J., Südhof, T. C., & Wernig, M. (2017). Myt1l safeguards neuronal identity by actively repressing many non-neuronal fates. *Nature*, *544*(7649), 245-249. https://doi.org/10.1038/nature21722

Marro, S., Pang, Z. P., Yang, N., Tsai, M. C., Qu, K., Chang, H. Y., Südhof, T. C., & Wernig, M. (2011). Direct lineage conversion of terminally differentiated hepatocytes to functional neurons. *Cell Stem Cell*, *9*(4), 374-382. https://doi.org/10.1016/j.stem.2011.09.002

Massagué, J. (2012). TGFβ signalling in context. *Nature Reviews Molecular Cell Biology*, *13*(10), 616-630. https://doi.org/10.1038/nrm3434

Masserdotti, G., Gillotin, S., Sutor, B., Drechsel, D., Irmler, M., Jørgensen, Helle F., Sass, S., Theis, Fabian J., Beckers, J., Berninger, B., Guillemot, F., & Götz, M. (2015). Transcriptional Mechanisms of Proneural Factors and REST in Regulating Neuronal Reprogramming of Astrocytes. *Cell Stem Cell*, *17*(1), 74-88. https://doi.org/https://doi.org/10.1016/j.stem.2015.05.014

Mattugini, N., Bocchi, R., Scheuss, V., Russo, G. L., Torper, O., Lao, C. L., & Gotz, M. (2019). Inducing Different Neuronal Subtypes from Astrocytes in the Injured Mouse Cerebral Cortex. *Neuron*. https://doi.org/10.1016/j.neuron.2019.08.009

McInnes, L., Healy, J., & Melville, J. (2018). Umap: Uniform manifold approximation and projection for dimension reduction. *arXiv preprint arXiv:1802.03426*.

McKay, N. D., Robinson, B., Brodie, R., & Rooke-Allen, N. (1983). Glucose transport and metabolism in cultured human skin fibroblasts. *Biochimica et Biophysica Acta (BBA) - Molecular Cell Research*, *762*(2), 198-204. https://doi.org/https://doi.org/10.1016/0167-4889(83)90071-X

Mertens, J., Herdy, J. R., Traxler, L., Schafer, S. T., Schlachetzki, J. C. M., Böhnke, L., Reid, D. A., Lee, H., Zangwill, D., Fernandes, D. P., Agarwal, R. K., Lucciola, R., Zhou-Yang, L., Karbacher, L., Edenhofer, F., Stern, S., Horvath, S., Paquola, A. C. M., Glass, C. K., Yuan, S. H., Ku, M., Szücs, A., Goldstein, L. S. B., Galasko, D., & Gage, F. H. (2021). Age-dependent instability of mature neuronal fate in induced neurons from Alzheimer's patients. *Cell Stem Cell*, *28*(9), 1533-1548.e1536. https://doi.org/10.1016/j.stem.2021.04.004

Mertens, J., Paquola, A. C. M., Ku, M., Hatch, E., Böhnke, L., Ladjevardi, S., McGrath, S., Campbell, B., Lee, H., Herdy, J. R., Gonçalves, J. T., Toda, T., Kim, Y., Winkler, J., Yao, J., Hetzer, M. W., & Gage, F. H. (2015). Directly Reprogrammed Human Neurons Retain Aging-Associated Transcriptomic Signatures and Reveal Age-Related Nucleocytoplasmic Defects. *Cell Stem Cell*, *17*(6), 705-718. https://doi.org/10.1016/j.stem.2015.09.001

Middleton, J., Americh, L., Gayon, R., Julien, D., Mansat, M., Mansat, P., Anract, P., Cantagrel, A., Cattan, P., Reimund, J.-M., Aguilar, L., Amalric, F., & Girard, J.-P. (2005). A comparative study of endothelial cell markers expressed in chronically inflamed human tissues: MECA-79, Duffy antigen receptor for chemokines, von Willebrand factor, CD31, CD34, CD105 and CD146. *The Journal of Pathology*, *206*(3), 260-268. https://doi.org/https://doi.org/10.1002/path.1788

Mitchell, T. S., Bradley, J., Robinson, G. S., Shima, D. T., & Ng, Y. S. (2008). RGS5 expression is a quantitative measure of pericyte coverage of blood vessels. *Angiogenesis*, *11*(2), 141-151. https://doi.org/10.1007/s10456-007-9085-x

Miyagi, S., Masui, S., Niwa, H., Saito, T., Shimazaki, T., Okano, H., Nishimoto, M., Muramatsu, M., Iwama, A., & Okuda, A. (2008). Consequence of the loss of Sox2 in the developing brain of the mouse. *FEBS Letters*, *582*(18), 2811-2815.

Moustakas, A., & Heldin, C.-H. (2009). The regulation of TGFβ signal transduction. *Development*, *136*(22), 3699-3714. https://doi.org/10.1242/dev.030338

Mueller, T. D., & Nickel, J. (2012). Promiscuity and specificity in BMP receptor activation [https://doi.org/10.1016/j.febslet.2012.02.043]. *FEBS Letters*, *586*(14), 1846-1859. https://doi.org/https://doi.org/10.1016/j.febslet.2012.02.043

Muñoz-Sanjuán, I., & Brivanlou, A. H. (2002). Neural induction, the default model and embryonic stem cells. *Nature Reviews Neuroscience*, *3*(4), 271-280. https://doi.org/10.1038/nrn786

Nakagomi, T., Kubo, S., Nakano-Doi, A., Sakuma, R., Lu, S., Narita, A., Kawahara, M., Taguchi, A., & Matsuyama, T. (2015). Brain vascular pericytes following ischemia have multipotential stem cell activity to differentiate into neural and vascular lineage cells. *Stem Cells*, *33*(6), 1962-1974. https://doi.org/10.1002/stem.1977

Nakatomi, H., Kuriu, T., Okabe, S., Yamamoto, S., Hatano, O., Kawahara, N., Tamura, A., Kirino, T., & Nakafuku, M. (2002). Regeneration of hippocampal pyramidal neurons after ischemic brain injury by recruitment of endogenous neural progenitors. *Cell*, *110*(4), 429-441. https://doi.org/10.1016/s0092-8674(02)00862-0

Necsulea, A., & Kaessmann, H. (2014). Evolutionary dynamics of coding and non-coding transcriptomes [Review]. *Nat Rev Genet*, *15*(11), 734-748. https://doi.org/10.1038/nrg3802

Nehls, V., Denzer, K., & Drenckhahn, D. (1992). Pericyte involvement in capillary sprouting during angiogenesis in situ. *Cell Tissue Res*, *270*(3), 469-474. https://doi.org/10.1007/bf00645048

Nehls, V., & Drenckhahn, D. (1993). The versatility of microvascular pericytes: from mesenchyme to smooth muscle? *Histochemistry*, *99*(1), 1-12. https://doi.org/10.1007/bf00268014

Nishimura, K., Weichert, R. M., Liu, W., Davis, R. L., & Dabdoub, A. (2014). Generation of induced neurons by direct reprogramming in the mammalian cochlea. *Neuroscience*, *275*, 125-135. https://doi.org/10.1016/j.neuroscience.2014.05.067

Nivet, E., Sancho-Martinez, I., & Izpisua Belmonte, J. C. (2013). Conversion of pericytes to neurons: a new guest at the reprogramming convention. *Stem Cell Res Ther*, *4*(1), 2-2. https://doi.org/10.1186/scrt150

Noack, F., Vangelisti, S., Raffl, G., Carido, M., Diwakar, J., Chong, F., & Bonev, B. (2022). Multimodal profiling of the transcriptional regulatory landscape of the developing mouse cortex identifies Neurog2 as a key epigenome remodeler. *Nat Neurosci*, *25*(2), 154-167. https://doi.org/10.1038/s41593-021-01002-4

Novak, D., Hüser, L., Elton, J. J., Umansky, V., Altevogt, P., & Utikal, J. (2020). SOX2 in development and cancer biology. *Seminars in Cancer Biology*, *67*, 74-82. https://doi.org/https://doi.org/10.1016/j.semcancer.2019.08.007

Nwadozi, E., Rudnicki, M., & Haas, T. L. (2020). Metabolic Coordination of Pericyte Phenotypes: Therapeutic Implications [Review]. *Frontiers in Cell and Developmental Biology*, *8*(77). https://doi.org/10.3389/fcell.2020.00077

Ohtsuka, T., Ishibashi, M., Gradwohl, G., Nakanishi, S., Guillemot, F., & Kageyama, R. (1999). Hes1 and Hes5 as notch effectors in mammalian neuronal differentiation. *Embo j*, *18*(8), 2196-2207. https://doi.org/10.1093/emboj/18.8.2196

Osório, J., Mueller, T., Rétaux, S., Vernier, P., & Wullimann, M. F. (2010). Phylotypic expression of the bHLH genes Neurogenin2, Neurod, and Mash1 in the mouse embryonic forebrain. *J Comp Neurol*, *518*(6), 851-871. https://doi.org/10.1002/cne.22247

Özen, I., Deierborg, T., Miharada, K., Padel, T., Englund, E., Genové, G., & Paul, G. (2014). Brain pericytes acquire a microglial phenotype after stroke. *Acta Neuropathol*, *128*(3), 381-396. https://doi.org/10.1007/s00401-014-1295-x

Ozerdem, U., Grako, K. A., Dahlin-Huppe, K., Monosov, E., & Stallcup, W. B. (2001). NG2 proteoglycan is expressed exclusively by mural cells during vascular morphogenesis. *Dev Dyn*, *222*(2), 218-227. https://doi.org/10.1002/dvdy.1200

Pang, Z. P., Yang, N., Vierbuchen, T., Ostermeier, A., Fuentes, D. R., Yang, T. Q., Citri, A., Sebastiano, V., Marro, S., Südhof, T. C., & Wernig, M. (2011). Induction of human neuronal cells by defined transcription factors. *Nature*, *476*(7359), 220-223. https://doi.org/10.1038/nature10202

Pardali, E., Goumans, M.-J., & ten Dijke, P. (2010). Signaling by members of the TGF-β family in vascular morphogenesis and disease. *Trends in Cell Biology*, *20*(9), 556-567. https://doi.org/10.1016/j.tcb.2010.06.006

Paredes, M. F., Sorrells, S. F., Cebrian-Silla, A., Sandoval, K., Qi, D., Kelley, K. W., James, D., Mayer, S., Chang, J., Auguste, K. I., Chang, E. F., Gutierrez Martin, A. J., Kriegstein, A. R., Mathern, G. W., Oldham, M. C., Huang, E. J., Garcia-Verdugo, J. M., Yang, Z., & Alvarez-Buylla, A. (2018). Does Adult Neurogenesis Persist in the Human Hippocampus? *Cell Stem Cell*, *23*(6), 780-781. https://doi.org/10.1016/j.stem.2018.11.006

Parras, C. M., Schuurmans, C., Scardigli, R., Kim, J., Anderson, D. J., & Guillemot, F. (2002). Divergent functions of the proneural genes Mash1 and Ngn2 in the specification of neuronal subtype identity. *Genes Dev*, *16*(3), 324-338. https://doi.org/10.1101/gad.940902

Pawlus, M. R., Wang, L., & Hu, C. J. (2014). STAT3 and HIF1α cooperatively activate HIF1 target genes in MDA-MB-231 and RCC4 cells. *Oncogene*, *33*(13), 1670-1679. https://doi.org/10.1038/onc.2013.115

Pawlus, M. R., Wang, L., Murakami, A., Dai, G., & Hu, C.-J. (2013). STAT3 or USF2 Contributes to HIF Target Gene Specificity. *PLoS One*, *8*(8), e72358. https://doi.org/10.1371/journal.pone.0072358

Peppiatt, C. M., Howarth, C., Mobbs, P., & Attwell, D. (2006). Bidirectional control of CNS capillary diameter by pericytes. *Nature*, *443*(7112), 700-704. https://doi.org/10.1038/nature05193

Perlow, M. J., Freed, W. J., Hoffer, B. J., Seiger, A., Olson, L., & Wyatt, R. J. (1979). Brain grafts reduce motor abnormalities produced by destruction of nigrostriatal dopamine system. *Science*, *204*(4393), 643-647. https://doi.org/10.1126/science.571147

Pertovaara, L., Kaipainen, A., Mustonen, T., Orpana, A., Ferrara, N., Saksela, O., & Alitalo, K. (1994). Vascular endothelial growth factor is induced in response to transforming growth factor-beta in fibroblastic and epithelial cells. *J Biol Chem*, *269*(9), 6271-6274.

Piao, J., Zabierowski, S., Dubose, B. N., Hill, E. J., Navare, M., Claros, N., Rosen, S., Ramnarine, K., Horn, C., Fredrickson, C., Wong, K., Safford, B., Kriks, S., El Maarouf, A., Rutishauser, U., Henchcliffe, C., Wang, Y., Riviere, I., Mann, S., Bermudez, V., Irion, S., Studer, L., Tomishima, M., & Tabar, V. (2021). Preclinical Efficacy and Safety of a Human Embryonic Stem Cell-Derived Midbrain Dopamine Progenitor Product, MSK-DA01. *Cell Stem Cell*, *28*(2), 217-229.e217. https://doi.org/10.1016/j.stem.2021.01.004

Polański, K., Young, M. D., Miao, Z., Meyer, K. B., Teichmann, S. A., & Park, J.-E. (2020). BBKNN: fast batch alignment of single cell transcriptomes. *Bioinformatics*, *36*(3), 964-965. https://doi.org/10.1093/bioinformatics/btz625

Prasad, K., Sharma, A., Garg, A., Mohanty, S., Bhatnagar, S., Johri, S., Singh, K. K., Nair, V., Sarkar, R. S., Gorthi, S. P., Hassan, K. M., Prabhakar, S., Marwaha, N., Khandelwal, N., Misra, U. K., Kalita, J., & Nityanand, S. (2014). Intravenous autologous bone marrow mononuclear stem cell therapy for ischemic stroke: a multicentric, randomized trial. *Stroke*, *45*(12), 3618-3624. https://doi.org/10.1161/strokeaha.114.007028

Reubinoff, B. E., Itsykson, P., Turetsky, T., Pera, M. F., Reinhartz, E., Itzik, A., & Ben-Hur, T. (2001). Neural progenitors from human embryonic stem cells. *Nat Biotechnol*, *19*(12), 1134-1140. https://doi.org/10.1038/nbt1201-1134

Roitbak, T., Surviladze, Z., & Cunningham, L. A. (2011). Continuous expression of HIF-1α in neural stem/progenitor cells. *Cellular and molecular neurobiology*, *31*(1), 119-133. https://doi.org/10.1007/s10571-010-9561-5

Rouget, C. (1873). Memoire sur le developpement, la structures et les proprietes des capillaires sanguins et lymphatiques. *Archs Physiol Norm Pathol. 1873; 5: 603-633*.

Rucker, H. K., Wynder, H. J., & Thomas, W. E. (2000). Cellular mechanisms of CNS pericytes. *Brain Res Bull*, *51*(5), 363-369. https://doi.org/10.1016/s0361-9230(99)00260-9

Ruiter, D., Schlingemann, R., Westphal, J., Denijn, M., Rietveld, F., & De Waal, R. (1993). Angiogenesis in wound healing and tumor metastasis. *Behring Institute Mitteilungen*(92), 258-272.

Russo, G. L., Sonsalla, G., Natarajan, P., Breunig, C. T., Bulli, G., Merl-Pham, J., Schmitt, S., Giehrl-Schwab, J., Giesert, F., & Jastroch, M. (2021). CRISPR-mediated induction of neuron-enriched mitochondrial proteins boosts direct glia-to-neuron conversion. *Cell Stem Cell*, *28*(3), 524-534. e527.

Rustenhoven, J., Jansson, D., Smyth, L. C., & Dragunow, M. (2017). Brain Pericytes As Mediators of Neuroinflammation. *Trends Pharmacol Sci*, *38*(3), 291-304. https://doi.org/10.1016/j.tips.2016.12.001

Sáez, M., Blassberg, R., Camacho-Aguilar, E., Siggia, E. D., Rand, D., & Briscoe, J. (2021). A quantitative landscape of cell fate transitions identifies principles of cellular decision-making. *bioRxiv*, 2021.2003.2011.434982. https://doi.org/10.1101/2021.03.11.434982

Satija, R., Farrell, J. A., Gennert, D., Schier, A. F., & Regev, A. (2015). Spatial reconstruction of single-cell gene expression data. *Nat Biotechnol*, *33*(5), 495-502. https://doi.org/10.1038/nbt.3192

Scardigli, R., Schuurmans, C., Gradwohl, G., & Guillemot, F. (2001). Crossregulation between Neurogenin2 and pathways specifying neuronal identity in the spinal cord. *Neuron*, *31*(2), 203-217. https://doi.org/10.1016/s0896-6273(01)00358-0

Schindelin, J. (2012). Fiji: an open-source platform for biological-image analysis. *Nat. Methods*, *9*. https://doi.org/10.1038/nmeth.2019

Semenza, G. L. (2012). Hypoxia-inducible factors in physiology and medicine. *Cell*, *148*(3), 399-408. https://doi.org/10.1016/j.cell.2012.01.021

Shepro, D., & Morel, N. M. (1993). Pericyte physiology. *Faseb j*, *7*(11), 1031-1038. https://doi.org/10.1096/fasebj.7.11.8370472

Shi, Y., & Massagué, J. (2003). Mechanisms of TGF-β Signaling from Cell Membrane to the Nucleus. *Cell*, *113*(6), 685-700. https://doi.org/https://doi.org/10.1016/S0092-8674(03)00432-X

Shimojo, H., Ohtsuka, T., & Kageyama, R. (2008). Oscillations in Notch Signaling Regulate Maintenance of Neural Progenitors. *Neuron*, *58*(1), 52-64. https://doi.org/10.1016/j.neuron.2008.02.014

Simon, C., Lickert, H., Götz, M., & Dimou, L. (2012). Sox10-iCreERT2 : a mouse line to inducibly trace the neural crest and oligodendrocyte lineage. *Genesis*, *50*(6), 506-515. https://doi.org/10.1002/dvg.22003

Smith, D. K., Yang, J., Liu, M. L., & Zhang, C. L. (2016). Small Molecules Modulate Chromatin Accessibility to Promote NEUROG2-Mediated Fibroblast-to-Neuron Reprogramming. *Stem cell reports*, *7*(5), 955-969. https://doi.org/10.1016/j.stemcr.2016.09.013

Son, E. Y., Ichida, J. K., Wainger, B. J., Toma, J. S., Rafuse, V. F., Woolf, C. J., & Eggan, K. (2011). Conversion of mouse and human fibroblasts into functional spinal motor neurons. *Cell Stem Cell*, *9*(3), 205-218. https://doi.org/10.1016/j.stem.2011.07.014

Sorrells, S. F., Paredes, M. F., Cebrian-Silla, A., Sandoval, K., Qi, D., Kelley, K. W., James, D., Mayer, S., Chang, J., Auguste, K. I., Chang, E. F., Gutierrez, A. J., Kriegstein, A. R., Mathern, G. W., Oldham, M. C., Huang, E. J., Garcia-Verdugo, J. M., Yang, Z., & Alvarez-Buylla, A. (2018). Human hippocampal neurogenesis drops sharply in children to undetectable levels in adults. *Nature*, *555*(7696), 377-381. https://doi.org/10.1038/nature25975

Spalding, K. L., Bergmann, O., Alkass, K., Bernard, S., Salehpour, M., Huttner, H. B., Boström, E., Westerlund, I., Vial, C., Buchholz, B. A., Possnert, G., Mash, D. C., Druid, H., & Frisén, J. (2013). Dynamics of hippocampal neurogenesis in adult humans. *Cell*, *153*(6), 1219-1227. https://doi.org/10.1016/j.cell.2013.05.002

Steinbeck, J. A., & Studer, L. (2015). Moving stem cells to the clinic: potential and limitations for brain repair. *Neuron*, *86*(1), 187-206. https://doi.org/10.1016/j.neuron.2015.03.002

Stern, C. D. (2006). Neural induction: 10 years on since the 'default model'. *Current Opinion in Cell Biology*, *18*(6), 692-697. https://doi.org/https://doi.org/10.1016/j.ceb.2006.09.002

Strano, A., Tuck, E., Stubbs, V. E., & Livesey, F. J. (2020). Variable Outcomes in Neural Differentiation of Human PSCs Arise from Intrinsic Differences in Developmental Signaling Pathways. *Cell Reports*, *31*(10). https://doi.org/10.1016/j.celrep.2020.107732

Stuart, T., Butler, A., Hoffman, P., Hafemeister, C., Papalexi, E., Mauck, W. M., 3rd, Hao, Y., Stoeckius, M., Smibert, P., & Satija, R. (2019). Comprehensive Integration of Single-Cell Data. *Cell*, *177*(7), 1888-1902.e1821. https://doi.org/10.1016/j.cell.2019.05.031

Sun, A. X., Yuan, Q., Tan, S., Xiao, Y., Wang, D., Khoo, A. T., Sani, L., Tran, H. D., Kim, P., Chiew, Y. S., Lee, K. J., Yen, Y. C., Ng, H. H., Lim, B., & Je, H. S. (2016). Direct Induction and Functional Maturation of Forebrain GABAergic Neurons from Human Pluripotent Stem Cells. *Cell Rep*, *16*(7), 1942-1953. https://doi.org/10.1016/j.celrep.2016.07.035

Sutter, C. H., Laughner, E., & Semenza, G. L. (2000). Hypoxia-inducible factor 1alpha protein expression is controlled by oxygen-regulated ubiquitination that is disrupted by deletions and missense mutations. *Proc Natl Acad Sci U S A*, *97*(9), 4748-4753. https://doi.org/10.1073/pnas.080072497

Takahashi, K., Tanabe, K., Ohnuki, M., Narita, M., Ichisaka, T., Tomoda, K., & Yamanaka, S. (2007). Induction of pluripotent stem cells from adult human fibroblasts by defined factors. *Cell*, *131*(5), 861-872. https://doi.org/10.1016/j.cell.2007.11.019

Takahashi, K., & Yamanaka, S. (2006). Induction of Pluripotent Stem Cells from Mouse Embryonic and Adult Fibroblast Cultures by Defined Factors. *Cell*, *126*(4), 663-676. https://doi.org/10.1016/j.cell.2006.07.024

Toresson, H., Mata de Urquiza, A., Fagerström, C., Perlmann, T., & Campbell, K. (1999). Retinoids are produced by glia in the lateral ganglionic eminence and regulate striatal neuron differentiation. *Development*, *126*(6), 1317-1326.

Torper, O., Ottosson, D. R., Pereira, M., Lau, S., Cardoso, T., Grealish, S., & Parmar, M. (2015). In Vivo Reprogramming of Striatal NG2 Glia into Functional Neurons that Integrate into Local Host Circuitry. *Cell Reports*, *12*(3), 474-481. https://doi.org/10.1016/j.celrep.2015.06.040

Traag, V. A., Waltman, L., & van Eck, N. J. (2019). From Louvain to Leiden: guaranteeing well-connected communities. *Scientific Reports*, *9*(1), 5233. https://doi.org/10.1038/s41598-019-41695-z

Trevino, A. E., Sinnott-Armstrong, N., Andersen, J., Yoon, S.-J., Huber, N., Pritchard, J. K., Chang, H. Y., Greenleaf, W. J., & Paşca, S. P. (2020). Chromatin accessibility dynamics in a model of human forebrain development. *Science*, *367*(6476), eaay1645. https://doi.org/10.1126/science.aay1645

Trost, A., Schroedl, F., Lange, S., Rivera, F. J., Tempfer, H., Korntner, S., Stolt, C. C., Wegner, M., Bogner, B., Kaser-Eichberger, A., Krefft, K., Runge, C., Aigner, L., & Reitsamer, H. A. (2013). Neural Crest Origin of Retinal and Choroidal Pericytes. *Investigative Ophthalmology & Visual Science*, *54*(13), 7910-7921. https://doi.org/10.1167/iovs.13-12946

Tsacopoulos, M., & Magistretti, P. J. (1996). Metabolic coupling between glia and neurons. *J Neurosci*, *16*(3), 877-885. https://doi.org/10.1523/JNEUROSCI.16-03-00877.1996

Tsunemoto, R., Lee, S., Szűcs, A., Chubukov, P., Sokolova, I., Blanchard, J. W., Eade, K. T., Bruggemann, J., Wu, C., Torkamani, A., Sanna, P. P., & Baldwin, K. K. (2018). Diverse reprogramming codes for neuronal identity. *Nature*. https://doi.org/10.1038/s41586-018-0103-5

Vadodaria, K. C., Mertens, J., Paquola, A., Bardy, C., Li, X., Jappelli, R., Fung, L., Marchetto, M. C., Hamm, M., Gorris, M., Koch, P., & Gage, F. H. (2016). Generation of functional human serotonergic neurons from fibroblasts. *Mol Psychiatry*, *21*(1), 49-61. https://doi.org/10.1038/mp.2015.161

van Tetering, G., van Diest, P., Verlaan, I., van der Wall, E., Kopan, R., & Vooijs, M. (2009). Metalloprotease ADAM10 is required for Notch1 site 2 cleavage. *J Biol Chem*, *284*(45), 31018-31027. https://doi.org/10.1074/jbc.M109.006775

Vasan, L., Park, E., David, L. A., Fleming, T., & Schuurmans, C. (2021). Direct Neuronal Reprogramming: Bridging the Gap Between Basic Science and Clinical Application. *Front Cell Dev Biol*, *9*, 681087. https://doi.org/10.3389/fcell.2021.681087

Vierbuchen, T., Ostermeier, A., Pang, Z. P., Kokubu, Y., Südhof, T. C., & Wernig, M. (2010). Direct conversion of fibroblasts to functional neurons by defined factors. *Nature*, *463*(7284), 1035-1041. https://doi.org/10.1038/nature08797

Vierbuchen, T., & Wernig, M. (2011). Direct lineage conversions: unnatural but useful? *Nat Biotechnol*, *29*(10), 892-907. https://doi.org/10.1038/nbt.1946

Viñals, F., Reiriz, J., Ambrosio, S., Bartrons, R., Rosa, J. L., & Ventura, F. (2004). BMP-2 decreases Mash1 stability by increasing Id1 expression. *The EMBO Journal*, *23*(17), 3527-3537. https://doi.org/https://doi.org/10.1038/sj.emboj.7600360

Wachs, F.-P., Winner, B., Couillard-Despres, S., Schiller, T., Aigner, R., Winkler, J., Bogdahn, U., & Aigner, L. (2006). Transforming Growth Factor-β1 Is a Negative Modulator of Adult Neurogenesis. *Journal of Neuropathology & Experimental Neurology*, *65*(4), 358-370. https://doi.org/10.1097/01.jnen.0000218444.53405.f0

Waddington, C. H. (1957). *The strategy of the genes; a discussion of some aspects of theoretical biology*. Allen & Unwin.

Wang, C., Liu, F., Liu, Y. Y., Zhao, C. H., You, Y., Wang, L., Zhang, J., Wei, B., Ma, T., Zhang, Q., Zhang, Y., Chen, R., Song, H., & Yang, Z. (2011). Identification and characterization of neuroblasts in the subventricular zone and rostral migratory stream of the adult human brain. *Cell Res*, *21*(11), 1534-1550. https://doi.org/10.1038/cr.2011.83

Wapinski, O. L., Vierbuchen, T., Qu, K., Lee, Q. Y., Chanda, S., Fuentes, D. R., Giresi, P. G., Ng, Y. H., Marro, S., Neff, N. F., Drechsel, D., Martynoga, B., Castro, D. S., Webb, A. E., Südhof, T. C., Brunet, A., Guillemot, F., Chang, H. Y., & Wernig, M. (2013). Hierarchical mechanisms for direct reprogramming of fibroblasts to neurons. *Cell*, *155*(3), 621-635. https://doi.org/10.1016/j.cell.2013.09.028

Wei, L., Wei, Z. Z., Jiang, M. Q., Mohamad, O., & Yu, S. P. (2017). Stem cell transplantation therapy for multifaceted therapeutic benefits after stroke. *Progress in Neurobiology*, *157*, 49-78. https://doi.org/10.1016/j.pneurobio.2017.03.003

Weinstein, D. C., & Hemmati-Brivanlou, A. (1999). Neural Induction. *Annual Review of Cell and Developmental Biology*, *15*(1), 411-433. https://doi.org/10.1146/annurev.cellbio.15.1.411

Wilmut, I., Schnieke, A. E., McWhir, J., Kind, A. J., & Campbell, K. H. (1997). Viable offspring derived from fetal and adult mammalian cells. *Nature*, *385*(6619), 810-813. https://doi.org/10.1038/385810a0

Winkler, E. A., Bell, R. D., & Zlokovic, B. V. (2010). Pericyte-specific expression of PDGF beta receptor in mouse models with normal and deficient PDGF beta receptor signaling. *Mol Neurodegener*, *5*, 32. https://doi.org/10.1186/1750-1326-5-32

Wolf, F. A., Angerer, P., & Theis, F. J. (2018). SCANPY: large-scale single-cell gene expression data analysis. *Genome Biology*, *19*(1), 15. https://doi.org/10.1186/s13059-017-1382-0

Wolf, F. A., Hamey, F. K., Plass, M., Solana, J., Dahlin, J. S., Göttgens, B., Rajewsky, N., Simon, L., & Theis, F. J. (2019). PAGA: graph abstraction reconciles clustering with trajectory inference through a topology preserving map of single cells. *Genome Biology*, *20*(1), 59. https://doi.org/10.1186/s13059-019-1663-x

Wolock, S. L., Lopez, R., & Klein, A. M. (2019). Scrublet: Computational Identification of Cell Doublets in Single-Cell Transcriptomic Data. *Cell Systems*, *8*(4), 281-291.e289. https://doi.org/https://doi.org/10.1016/j.cels.2018.11.005

Xie, B., Sun, D., Du, Y., Jia, J., Sun, S., Xu, J., Liu, Y., Xiang, C., Chen, S., Xie, H., Wang, Q., Li, G., Lyu, X., Shen, H., Li, S., Wu, M., Zhang, X., Pu, Y., Xiang, K., Lai, W., Du, P., Yuan, Z., Li, C., Shi, Y., Lu, S., & Deng, H. (2019). A two-step lineage reprogramming strategy to generate functionally competent human hepatocytes from fibroblasts. *Cell Res*, *29*(9), 696-710. https://doi.org/10.1038/s41422-019-0196-x

Yamamoto, S., Muramatsu, M., Azuma, E., Ikutani, M., Nagai, Y., Sagara, H., Koo, B.-N., Kita, S., O'Donnell, E., Osawa, T., Takahashi, H., Takano, K.-i., Dohmoto, M., Sugimori, M., Usui, I., Watanabe, Y., Hatakeyama, N., Iwamoto, T., Komuro, I., Takatsu, K., Tobe, K., Niida, S., Matsuda, N., Shibuya, M., & Sasahara, M. (2017). A subset of cerebrovascular pericytes originates from mature macrophages in the very early phase of vascular development in CNS. *Scientific Reports*, *7*(1), 3855. https://doi.org/10.1038/s41598-017-03994-1

Yamashita, M., & Emerman, M. (2006). Retroviral infection of non-dividing cells: old and new perspectives. *Virology*, *344*(1), 88-93. https://doi.org/10.1016/j.virol.2005.09.012

Yan, Y., Sabharwal, P., Rao, M., & Sockanathan, S. (2009). The antioxidant enzyme Prdx1 controls neuronal differentiation by thiol-redox-dependent activation of GDE2. *Cell*, *138*(6), 1209-1221. https://doi.org/10.1016/j.cell.2009.06.042

Yang, S., Hilton, S., Alves, J. N., Saksida, L. M., Bussey, T., Matthews, R. T., Kitagawa, H., Spillantini, M. G., Kwok, J. C. F., & Fawcett, J. W. (2017). Antibody recognizing 4-sulfated chondroitin sulfate proteoglycans restores memory in tauopathy-induced neurodegeneration. *Neurobiol Aging*, *59*, 197-209. https://doi.org/10.1016/j.neurobiolaging.2017.08.002

Yang, Y., Jiao, J., Gao, R., Yao, H., Sun, X. F., & Gao, S. (2013). Direct conversion of adipocyte progenitors into functional neurons. *Cell Reprogram*, *15*(6), 484-489. https://doi.org/10.1089/cell.2013.0013

Yokota, Y. (2001). Id and development. *Oncogene*, *20*(58), 8290-8298. https://doi.org/10.1038/sj.onc.1205090

Yu, P. B., Hong, C. C., Sachidanandan, C., Babitt, J. L., Deng, D. Y., Hoyng, S. A., Lin, H. Y., Bloch, K. D., & Peterson, R. T. (2008). Dorsomorphin inhibits BMP signals required for embryogenesis and iron metabolism. *Nat Chem Biol*, *4*(1), 33-41. https://doi.org/10.1038/nchembio.2007.54

Zalc, A., Sinha, R., Gulati, G. S., Wesche, D. J., Daszczuk, P., Swigut, T., Weissman, I. L., & Wysocka, J. (2021). Reactivation of the pluripotency program precedes formation of the cranial neural crest. *Science*, *371*(6529), eabb4776. https://doi.org/10.1126/science.abb4776

Zhang, S. C., Wernig, M., Duncan, I. D., Brüstle, O., & Thomson, J. A. (2001). In vitro differentiation of transplantable neural precursors from human embryonic stem cells. *Nat Biotechnol*, *19*(12), 1129-1133. https://doi.org/10.1038/nbt1201-1129

Zhang, Y., Pak, C., Han, Y., Ahlenius, H., Zhang, Z., Chanda, S., Marro, S., Patzke, C., Acuna, C., Covy, J., Xu, W., Yang, N., Danko, T., Chen, L., Wernig, M., & Sudhof, T. C. (2013). Rapid single-step induction of functional neurons from human pluripotent stem cells. *Neuron*, *78*(5), 785-798. https://doi.org/10.1016/j.neuron.2013.05.029

Zheng, X., Boyer, L., Jin, M., Mertens, J., Kim, Y., Ma, L., Ma, L., Hamm, M., Gage, F. H., & Hunter, T. (2016). Metabolic reprogramming during neuronal differentiation from aerobic glycolysis to neuronal oxidative phosphorylation. *Elife*, *5*, e13374. https://doi.org/10.7554/eLife.13374

Zhou, J., Su, P., Li, D., Tsang, S., Duan, E., & Wang, F. (2010). High-efficiency induction of neural conversion in human ESCs and human induced pluripotent stem cells with a single chemical inhibitor of transforming growth factor beta superfamily receptors. *Stem cells (Dayton, Ohio)*, *28*(10), 1741-1750. https://doi.org/10.1002/stem.504

Zimmermann, K. W. (1923). Der feinere Bau der Blutcapillaren. *Zeitschrift für Anatomie und Entwicklungsgeschichte*, *68*(1), 29-109. https://doi.org/10.1007/BF02593544

LIST OF FIGURES

LIST OF TABLES

LIST OF ABBREVIATIONS

A1C	primary auditory cortex (core)
AD	Alzheimer's disease
AHG	adult human gray matter
AMH	anti-Müllerian hormone
AMY	amygdaloid complex
AS	Ascl1/Sox2
ASCL1 or Ascl1	achaete-scute family BHLH transcription factor 1
BBB	blood-brain barrier
BBKNN	batch balanced k-nearest-neighbor algorithm
bHLH	basic helix–loop–helix
BMP	bone morphogenetic protein
CB	cerebellum
CBC	cerebellar cortex
CFLARE	clustering and filtering of left and right eigenvectors
CGE	caudal ganglionic eminence
ChIP-seq	chromatin immunoprecipitation DNA sequencing
CNS	central nervous system
d14	14 days after transduction
d7	7 days after transduction
DAPI	4',6-diamidino-2-phenylindole
DAPT	N-[N-(3,5-difluorophenacetyl)-L-alanyl]-S-phenylglycine t-butyl ester (γ-secretase inhibitor)
DE	differential expression
DFC	dorsolateral prefrontal cortex
DM	dorsomorphin (SMAD signaling inhibitor)
DMEM	Dulbecco's Modified Eagle's Medium
DMSO	dimethyl sulfoxide
DTH	dorsal thalamus
ESC	embryonic stem cell
FA	axial component force
FAC(S)	fluorescence-activated cell (sorting)
FCS	fetal calf serum
GAM	generalized additive model
GEM	gel bead-in-emulsion
GFP	green fluorescent protein

HBSS	Hanks' balanced salt solution
HEPES	4-(2-hydroxyethyl)-1-piperazineethanesulfonic acid
hESC	human embryonic stem cell
HIF1A	hypoxia inducible factor 1 subunit alpha
HIP	hippocampus (hippocampal formation)
hiPSC	human induced pluripotent stem cell
iN	induced neuron(al)
IPC	posteroventral (inferior) parietal cortex
iPSC	induced pluripotent stem cell
IRES	internal ribosomal entry site
ISH	*in situ* hybridization
ITC	inferolateral temporal cortex (area TEv area 20)
kNN	k-nearest neighbors algorithm
LGE	lateral ganglionic eminence
M1C	primary motor cortex (area M1 area 4)
M1C-S1C	primary motor-sensory cortex (samples)
MD	mediodorsal nucleus of thalamus
MFC	anterior (rostral) cingulate (medial prefrontal) cortex
MGE	medial ganglionic eminence
NEUROG2 or Neurog2	neurogenin 2
NOTCH	Notch receptor
NS	Neurog2/Sox2
NSC	neural stem and progenitor cell
Ocx	occipital neocortex
OFC	orbital frontal cortex
OxPhos	oxidative phosphorylation
PAGA	partition-based graph abstraction
PBS	phosphate-buffered saline
PC	principal component
pcw	postconceptional week
PCx	parietal neocortex
PD	Parkinson's disease
PDGFRB	platelet derived growth factor receptor beta
PDL	poly-D-lysine
PFA	paraformaldehyde

REST	RE1-silencing transcription factor
RFP	red fluorescent protein
RMS	rostral migratory stream
ROS	reactive oxygen species
S1C	primary somatosensory cortex (area S1 areas 312)
SB	SB431542 (SMAD signaling inhibitor)
scRNA-seq	single cell RNA sequencing
scATAC-seq	single cell Assay for Transposase Accessible Chromatin with high-throughput sequencing
SOX2 or Sox2	SRY-box transcription factor 2
STC	posterior (caudal) superior temporal cortex (area 22c)
STR	striatum
SVZ	subventricular zone
TCx	temporal neocortex
TF	transcription factor
TGF-β	transforming growth factor beta
tra	trajectory
TUBB3	tubulin beta 3 class III
UMAP	uniform manifold approximation and projection
URL	upper (rostral) rhombic lip
V1C	primary visual cortex (striate cortex area V1/17)
VFC	ventrolateral prefrontal cortex
VDR or Vdr	vitamin D receptor
WHV	woodchuck hepatitis virus
WPRE	WHV posttranscriptional regulatory element

ACKNOWLEDGMENTS

Most of all, I am extremely grateful to Prof. Marisa Karow, who infected me in 2017 with her contagious enthusiasm for the topic of direct reprogramming. Thank you for giving me the great opportunity to work in your lab, for your invaluable feedback, your constant support even during the time of your physical absence and the many, also international, opportunities for scientific exchange that you provided me with.

I could not have undertaken this project without Dr. Sven Falk, who added another very experienced perspective, from both developmental biology and computational analysis, to my project. Thank you for your assistance with data preprocessing and for the (almost) endless discussions about the data analysis that I also enjoyed very much.

I would like to express my deepest appreciation to the members of my thesis advisory committee, Prof. Marisa Karow, Prof. Moritz Rossner, Prof. Bernd Sutor and Dr. Silvia Cappello. Your feedback enabled me to focus my work towards the most promising outcomes. I am also particularly grateful to Dr. Silvia Cappello for many fruitful joint lab meetings and her co-supervision with regard to the IMPRS-TP graduate school.

Moreover, I would like to thank the chairs of our institutes in Munich and Erlangen, Prof. Magdalena Götz and Prof. Michael Wegner, for sharing their lab space and equipment. I'd like also to recognize Prof. Christian Schichor for providing us with human brain tissue samples from his patients, and Prof. Benedikt Berninger for his support.

Even though our lab was small in the beginning, several colleagues over the years have enriched my time here. I would like to extend my sincere thanks to Dr. Radhika Menon for making my start in the lab very successful and for your diverting company. Many thanks go to Elisa Gabassi for helping me out with my cells many times, Dr. Heiko Brennenstuhl for helpful discussions, and to Dr. Dandan Han for our good collaboration with the pericytes and in virus production. Additional thanks go to Doris, Sarah, Federica, Junkai and Filippo in the Karow & Falk labs and numerous helpful colleagues from both the Dept. of Phys. Genomics in Munich and the Inst. of Biochemistry in Erlangen, as well as from the UKER in Erlangen, the MPI of Psychiatry in Munich and the IMPRS-TP graduate school.

Lastly, would like to thank my family and friends for their continuous support during my studies up until my PhD, especially my parents Gerlinde and Albert, my aunt Inge, and, very importantly, my girlfriend Leonie, knowing the ups and downs from her own PhD experience, for her patience and understanding during this journey.

AFFIDAVIT

LMU LUDWIG-MAXIMILIANS-UNIVERSITÄT MÜNCHEN | Dean's Office Medical Faculty | MMRS

Affidavit

Lohrer, Benjamin
Surname, first name

Fahrstr. 17
Street

91054 Erlangen, Germany
Zip code, town, country

I hereby declare that the submitted thesis entitled:

Molecular dissection of pericyte-to-neuron reprogramming reveals cellular identity safeguarding mechanisms

is my own work. I have only used the sources indicated and have not made unauthorised use of services of a third party. Where the work of others has been quoted or reproduced, the source is always given.

I further declare that the submitted thesis or parts thereof have not been presented as part of an examination degree to any other university.

Munich, December 15th 2022
place, date

Benjamin Albert Lohrer
Signature doctoral candidate

CONFIRMATION OF CONGRUENCY

LMU LUDWIG-MAXIMILIANS-UNIVERSITÄT MÜNCHEN | Dean's Office Medical Faculty | MMRS

Confirmation of congruency between printed and electronic version of the doctoral thesis

Lohrer, Benjamin

Surname, first name

Fahrstr. 17

Street

91054 Erlangen, Germany

Zip code, town, country

I hereby declare that the submitted thesis entitled:

Molecular dissection of pericyte-to-neuron reprogramming reveals cellular identity safeguarding mechanisms

is congruent with the printed version both in content and format.

Munich, December 15th 2022

place, date

Benjamin Albert Lohrer

Signature doctoral candidate

LIST OF PUBLICATIONS

TLR5 decoy receptor as a novel anti-amyloid therapeutic for Alzheimer's disease

Chakrabarty P, Li A, Ladd T, Strickland MR, Koller EJ, Burgess JD, Funk CC, Cruz PE, Allen M, Yaroshenko M, Wang X, Younkin C, Reddy J, **Lohrer B**, Mehrke L, Moore BD, Liu X, Ceballos-Diaz C, Rosario AM, Medway C, Janus C, Hong-Dong L, Dickson DW, Giasson BI, Price ND, Younkin SG, Ertekin-Taner N & Golde TE

Published in Journal of Experimental Medicine, 2018 *10.1084/jem.20180484*

Dynamic X-chromosomal reactivation enhances female brain resilience

Käseberg S, Bertin M, Menon R, Gabassi E, Todorov H, Frank S, Brennenstuhl H, **Lohrer B**, Winter J, Krummeich J, Winkler J, Winner B, Weis E, Hartwich D, Diederich S, Luck K, Gerber S, Berninger B, Falk S, Schweiger S & Karow M

Submitted to Cell, 2022

Cross-species ectopic expression of a primate RNA in mouse neurons promotes neuronal activity and CREB function

Pruunsild P, Bengtson CP, Loss I, **Lohrer B** & Bading H

Submitted to Journal of Biological Chemistry, 2022

Using human iPS cell-derived pericytes as renewable and editable source to study direct lineage reprogramming into induced neurons

Menon R, Petrucci L, **Lohrer B**, Schichor C, Winner B, Schulze M, Riemenschneider MJ, Zhang J, Kühn R, Falk S & Karow M

Submitted to Journal of Cellular Reprogramming, 2022

Counteracting cellular safeguarding mechanisms during direct lineage reprogramming into human induced neurons

Lohrer B, Schichor C, Berninger B, Karow M & Falk S

Manuscript in preparation, 2022